

10

AD-A144 797



REPRODUCTION OF THIS DOCUMENT IS UNLIMITED

DTIC FILE COPY

A PARAMETRIC STUDY OF  
 HIGH ALTITUDE NUCLEAR EMP  
 THESIS  
 Randy J. Lavigne  
 First Lieutenant, USAF  
 AFIT/GNE/PH/84M-10

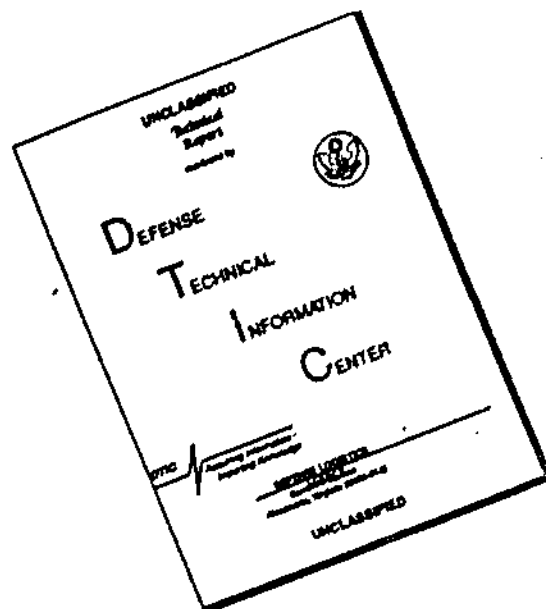
*[Handwritten signature]*

DEPARTMENT OF THE AIR FORCE  
 AIR UNIVERSITY (ATC)  
**AIR FORCE INSTITUTE OF TECHNOLOGY**

Wright-Patterson Air Force Base, Ohio

84 03 0 086

# DISCLAIMER NOTICE



**THIS DOCUMENT IS BEST QUALITY AVAILABLE. THE COPY FURNISHED TO DTIC CONTAINED A SIGNIFICANT NUMBER OF PAGES WHICH DO NOT REPRODUCE LEGIBLY.**

AFIT/GNE/PH/84M-10

①

A PARAMETRIC STUDY OF  
HIGH ALTITUDE NUCLEAR EMP  
THESIS

Randy J. Lavigne  
First Lieutenant, USAF

AFIT/GNE/PH/84M-10

Approved for public release; distribution unlimited.

AFIT/GNE/PH/84M-10

A PARAMETRIC STUDY OF  
HIGH ALTITUDE NUCLEAR EMP FIELDS

THESIS

Presented to the Faculty of the School of Engineering  
of the Air Force Institute of Technology  
Air University  
in Partial Fulfillment of the  
Requirements for the Degree of  
Master of Science

by

Randy J. Lavigne, B.S.

1Lt                      USAF

Graduate Nuclear Engineering

March 1984

Approved for public release; distribution unlimited.

## Preface

The purpose of this investigation is to determine the energy associated with the electromagnetic spectrum between 100 kilohertz and 100 megahertz from high altitude nuclear EMP. The computer code developed to generate simulated EMP fields (EMPFRE) is designed to be flexible. The gamma ray pulse can be represented as a collection of functions or can be adapted to read and interpolate between a set of data points. Other physical parameters such as Compton electron characteristics are easily identified and changed. A parametric study is conducted to determine cause and effect relationships between burst parameters and the frequency characteristics of the EMP.

I would like to thank my faculty advisor Lt. Col. John Erkkila for his patience and understanding. He applied his experience in this field to guide me away from fruitless endeavors but allowed me to do my own work. The insight I gained from his advice is appreciated.

Finally, I would like to thank my wife, [REDACTED], for her endless reserves of patience. This thesis would not have been possible without her support.

Randy J. Lavigne



A-1

## Contents

	Page
Preface . . . . .	ii
List of Figures . . . . .	v
List of Tables . . . . .	vii
Abstract . . . . .	viii
I. Introduction	
Background . . . . .	1
Scope . . . . .	2
Assumptions and Limitations . . . . .	2
Overview . . . . .	3
II. Theory	
Gamma Ray Deposition . . . . .	4
Compton Electron Dynamics . . . . .	13
Retarded Time . . . . .	14
Compton Currents and Secondary Electron Density . . . . .	15
Air Chemistry . . . . .	19
Air Conductivity . . . . .	22
Electromagnetic Fields . . . . .	23
III. Numerical Methods	
Burst Geometry . . . . .	26
Gamma Ray Yield Function . . . . .	28
Initial Electron Velocity . . . . .	29
Mean Free Path . . . . .	29
Compton Dynamics . . . . .	33
Electron Range . . . . .	36
Compton Electron Time of Flight . . . . .	37
Compton Electron Production Rate . . . . .	38
Compton Current and Secondary Electron Source . . . . .	40
Air Chemistry . . . . .	43
Electron Mobility and Conductivity . . . . .	47
Solving for the Electric Fields . . . . .	48
Fourier Transform . . . . .	70
IV. Analysis of Numerical Technique	
Compton Electron Range . . . . .	64
Spatial and Time Increments . . . . .	67
Lorentz Model . . . . .	70
Truncation of Electric Field . . . . .	73

V. Parametric Studies	
Gamma Pulse History . . . . .	77
Gamma Ray Energy . . . . .	86
Yield . . . . .	92
Height of Burst . . . . .	95
Dip Angle . . . . .	98
VI. Conclusions and Recommendations	
Conclusions . . . . .	101
Recommendations . . . . .	102
Bibliography . . . . .	104
Appendix A: Verification of EMPFRE . . . . .	106
Appendix B: Program Description . . . . .	112
Vita	

## List of Figures

<u>Figure</u>	<u>Page</u>
2.1 Gamma Ray Deposition, HOB=75 Km, 1.5 MeV . . . . .	6
2.2 Gamma Ray Deposition, HOB=100 Km, 1.5 MeV . . . . .	7
2.3 Gamma Ray Deposition, HOB=200 Km, 1.5 MeV . . . . .	8
2.4 Gamma Ray Deposition, HOB=300 Km, 1.5 MeV . . . . .	9
2.5 Gamma Ray Deposition, HOB=100 Km, Along Vertical . . . . .	10
2.6 Gamma Ray Deposition, HOB=100 Km, 30 <sup>o</sup> Off Vertical . . . . .	11
2.7 Gamma Ray Deposition, HOB=100 Km, 60 <sup>o</sup> Off Vertical . . . . .	12
2.8 Polar Coordinate System . . . . .	18
3.1 Burst Geometry and Key Variables . . . . .	27
3.2 Gamma Ray Attenuation Cross Sections . . . . .	30
3.3 Stepwise Procedure in the Solution of the Differential Equations . . . . .	58
4.1 Electric Field, Compton Electron Range . . . . .	65
4.2 Frequency Profile, Compton Electron Range . . . . .	66
4.3 Electric Field, Time Step . . . . .	68
4.4 Frequency Profile, Time Step . . . . .	69
4.5 Electric Field, Spatial Step . . . . .	71
4.6 Frequency Profile, Spatial Step . . . . .	72
4.7 Electric Field, Mobility Limit . . . . .	74
4.8 Frequency Profile, Mobility Limit . . . . .	75
5.1 Electric Field, TP=2.0 Shakes, Beta=1.5 Alpha Alpha=5.0E7, 1.0E8 and 2.5E8 (sec <sup>-1</sup> ) . . . . .	78
5.2 Frequency Profile, TP=2.0 Shakes, Beta=1.5 Alpha Alpha=5.0E7, 1.0E8 and 2.5E8 (sec <sup>-1</sup> ) . . . . .	79
5.3 Electric Field, TP=1.5 Shakes, Beta=1.5 Alpha Alpha=2.5E8 and 5.0E8 (sec <sup>-1</sup> ) . . . . .	80



List of Figures (continued)

<u>Figure</u>	<u>Page</u>
5.4 Frequency Profile, TP=1.5 Shakes, Beta=1.5 Alpha Alpha=2.5E8 and 5.0E8 (sec <sup>-1</sup> ) . . . . .	81
5.5 Electric Field, TP=1.0 Shakes, Beta=1.5 Alpha Alpha=5.0E8, 1.0E9 and 2.5E9 (sec <sup>-1</sup> ) . . . . .	82
5.6 Frequency Profile, TP=1.0 Shakes, Beta=1.5 Alpha Alpha=5.0E8, 1.0E9 and 2.5E9 (sec <sup>-1</sup> ) . . . . .	83
5.7 Electric Field, TP=0.5 Shakes, Beta=1.2 Alpha Alpha=2.5E9 and 5.0E9 (sec <sup>-1</sup> ) . . . . .	84
5.8 Frequency Profile, TP=0.5 Shakes, Beta=1.2 Alpha Alpha=2.5E9 and 5.0E9 (sec <sup>-1</sup> ) . . . . .	85
5.9 Electric Field, Gamma Ray Energy, Yield =0.1 Kilotons . . . . .	88
5.10 Frequency Profile, Gamma Ray Energy, Yield =0.1 Kilotons . . . . .	89
5.11 Electric Field, Gamma Ray Energy, Yield =E (MeV) 0.0667 Kilotons . . . . .	90
5.12 Frequency Profile, Gamma Ray Energy, Yield =E (MeV) 0.0667 Kilotons . . . . .	91
5.13 Electric Field, Gamma Ray Yield . . . . .	93
5.14 Frequency Profile, Gamma Ray Yield . . . . .	94
5.15 Electric Field, Height of Burst . . . . .	96
5.16 Frequency Profile, Height of Burst . . . . .	97
5.17 Electric Field, Geomagnetic Field Dip Angle . . . . .	99
5.18 Frequency Profile, Geomagnetic Field Dip Angle . . . . .	100
A.1 Electric Field, Verification . . . . .	107
A.2 Frequency Profile, Verification . . . . .	109
B.1 Flow Diagram For Program EMPFRE . . . . .	113
B.2 Flow Diagram For Subroutine EFIELD . . . . .	114

Tables

<u>Tables</u>	<u>Page</u>
3.1 Data Used in EMPFRE . . . . .	32
3.2 Empirical Fit to COMP Results . . . . .	35
3.3 Electron Mobility . . . . .	49
3.4 Runge-Kutta Without Automatic Step Reduction . . . . .	53
3.5 Runge-Kutta With Automatic Step Reduction . . . . .	53
A.1 Maximum Electric Fields From HEMPB . . . . .	111

### Abstract

A program is developed to model the electromagnetic pulse from a high altitude nuclear detonation. A Runge-Kutta numerical technique is used to solve for the electric fields. A continuous Fourier Transform of the EMP is used to determine the frequency profile of the EMP. Parametric studies are performed to determine cause and effect relationships between burst parameters and the EMP frequency profile from 100 KHz to 100 MHz. Burst parameters studied are: gamma pulse time history, gamma ray energies from 1 MeV to 10 MeV, gamma ray yield, height of burst from 75 Km to 200 Km and intersection angle of the slant range with the geomagnetic field from 90 degrees to 30 degrees.

## I. INTRODUCTION

### BACKGROUND

EMP (electromagnetic pulse) is a prompt effect of a nuclear explosion, consisting of a broad spectrum of radio waves. These radio waves can induce electric currents into unprotected systems. The currents cause resistive heating that can melt electrical contacts or damage electrical components. Estimates of the shape and magnitude of the EMP are based on sparse experimental data and computer simulations of the physical processes which generate the EMP.

Studies conducted in the late 1950's concluded that the EMP from a high altitude nuclear explosion would be confined to the upper atmosphere and would not be a threat to systems near the ground; therefore, little attention was paid to the subject. EMP resurfaced as a problem in 1962 when a 1.4 megaton bomb detonated 248 miles above Johnson Island was believed responsible for the failure of street lights in Hawaii (800 miles away) (Ref 3). A subsequent experiment to characterize the EMP was inconclusive because the magnitude was still underestimated and the equipment used was saturated by the EMP. In late 1963, scientists at Los Alamos Corporation and the RAND Corporation were the first to explain the physical processes which generated the EMP. The limited test ban treaty precluded the experiments that could be used to verify the theory of EMP generation (Ref 3:1009).

"Defense strategists today assume that a single Soviet warhead detonated 200 miles above Nebraska would knock out unprotected communications equipment all across the United States" (Ref 4:1248).

The projected damage to military systems are based on two assumptions. First, the EMP will have peak fields on the order of 50,000 volts per meter. Second, the high frequency end of the electromagnetic spectrum has sufficient energy to induce large electrical currents into exposed lengths of wire. The amount of energy in the high frequency end of the electromagnetic spectrum depends on the peak electric field and shape parameters such as the rise time (time required to reach the peak of the pulse). The damage potential is sensitive to the EMP spectral characteristics.

#### SCOPE

This investigation determines the energy associated with the frequency components of the EMP from a high altitude nuclear detonation. This goal is achieved in two stages. First, a computer code (EMPFRE) is developed to model the processes that create the EMP. Second, a continuous Fourier transform is found for the simulated EMP and Parseval's theorem is used to calculate the energy associated with the frequencies between 100 kilohertz and 100 megahertz.

#### ASSUMPTIONS AND LIMITATIONS

EMPFRE calculates the electrical field strength at discrete values of time up to 4 shakes (1 shake= $1E-8$  seconds). The late time electric fields will not have significant impact on the frequency range of interest. The energy distributions are based on this time range.

EMPFRE relies on approximations developed by Karzas and Latter (Ref 9) for the currents and secondary electron density. Discrete numerical methods are used extensively including a fourth order Runge-Kutta

technique to solve for the electric fields. Discussions of the impacts from these approximations are presented in Chapter IV.

#### OVERVIEW

The background theory for high altitude EMP is presented in Chapter II. The methods used to model the processes that generate EMP are presented in Chapter III. Sample results are presented in Chapter IV to characterize the errors due to program parameters. Parametric studies relate burst parameters to frequency characteristics in Chapter V. Conclusions and recommendations are made in Chapter VI.

## II. THEORY

This chapter is a distillation of theoretical work done by W. J. Karzas and R. Latter (Ref 9), J. H. Erkkila (Ref 5,6,7) and C. L. Longmire (Ref 12). Information from these sources form the theoretical foundation needed to understand the processes that lead to the generation of high altitude, nuclear EMP. The primary source of EMP from high altitude detonation is the result of the gamma rays. Gamma rays account for 0.1 to 0.5% of the total yield. Gamma rays entering the atmosphere produce Compton electron currents. Maxwell's equations predict the electromagnetic fields resulting from these currents. The electromagnetic fields that are transverse to the gamma ray direction propagate from the absorption region to the ground. Processes relating to this phenomenon are described and references are provided for further detail.

### GAMMA RAY DEPOSITION

The number of gamma rays emitted from a nuclear detonation as a function of time is written as:

$$S_Y(t) = \frac{Y}{E} f(t) \quad (2.1)$$

where    Y    -total energy of gamma ray yield  
          E    -mean energy of the gamma rays emitted  
          f(t) -time dependence of the pulse

The time dependence of the pulse is normalized:

$$\int_{-\infty}^{\infty} f(t) dt = 1 \quad (2.2)$$

The prompt gamma ray emission rate is proportional to the neutron population in the device. The gamma ray pulse from a fission device will rise exponentially with the neutron population. Prompt gamma rays are generated by inelastic collisions between neutrons and the device materials and by fission reactions.

The density of Compton recoil electrons produced per gamma ray emitted from the burst as a function of position is written as

$$g(r) = \frac{\exp \int_0^r \frac{dr'}{\lambda_T(r')}}{4\pi r^2 \lambda_C(r)} \quad (2.3)$$

where  $\lambda_T(r)$  -gamma ray mean free path  
 $\lambda_C(r)$  -mean free path due to Compton interactions  
 $r$  -distance from burst

This expression assumes the gamma ray is absorbed by its first interaction. Multiple scatters are not accounted for. The scattered gamma ray will lag behind the pulse due to the deflection.

Gamma ray deposition profiles are a function of height of burst (HOB) and gamma ray energy. Figures 2.1, 2.2, 2.3 and 2.4 are contour plots of Compton electron generation density which are used to demonstrate the dependence on HOB for 1.5 MeV gamma rays. Figures 2.5, 2.6 and 2.7 are plots of Compton electron generation density along discrete slant ranges which are used to demonstrate the dependence on gamma ray energy for an exponential atmosphere. The impact of these parameters on the EMP is a topic of the parametric studies in Chapter V.



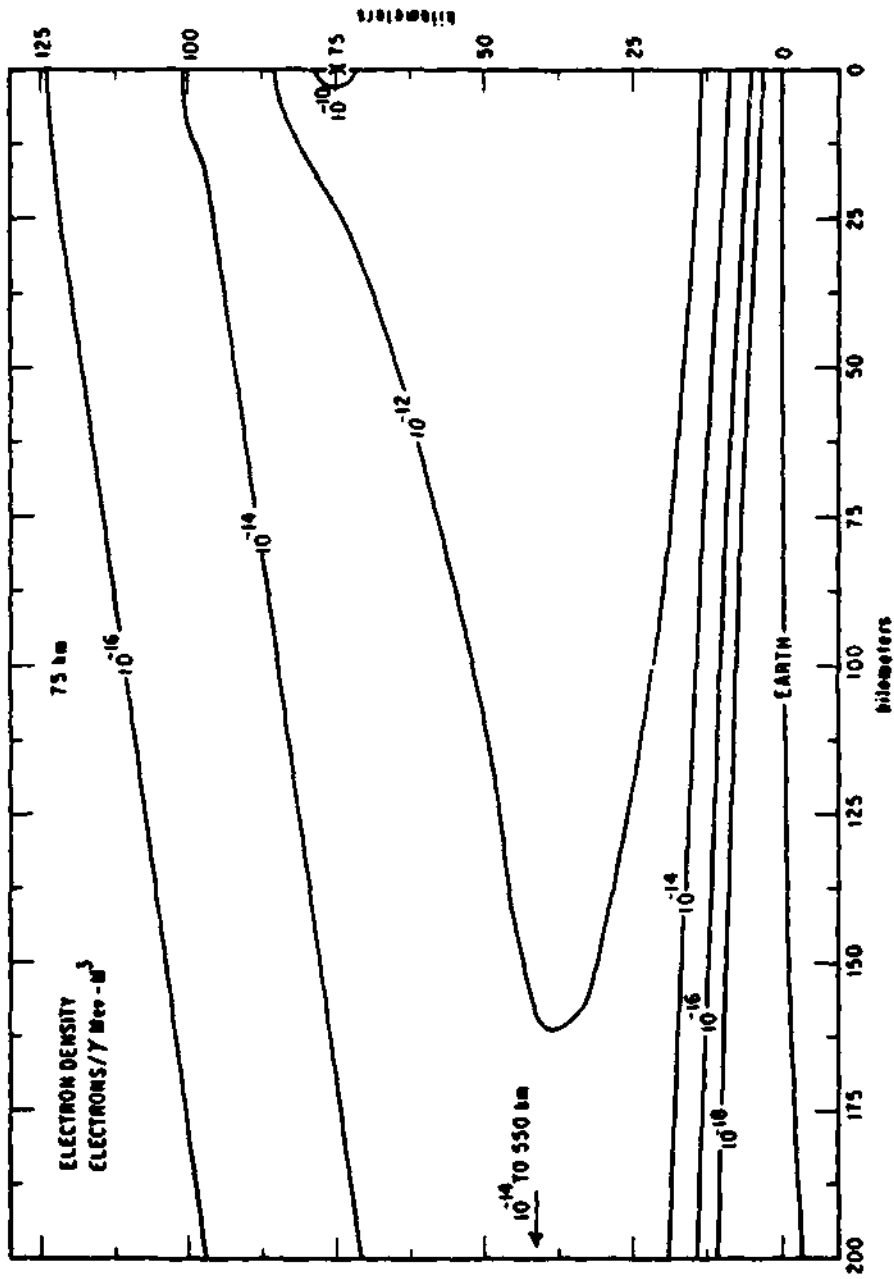


Figure 2.1 Gamma Ray Deposition, HOB=75 Km, 1.5 MeV (Ref 6)

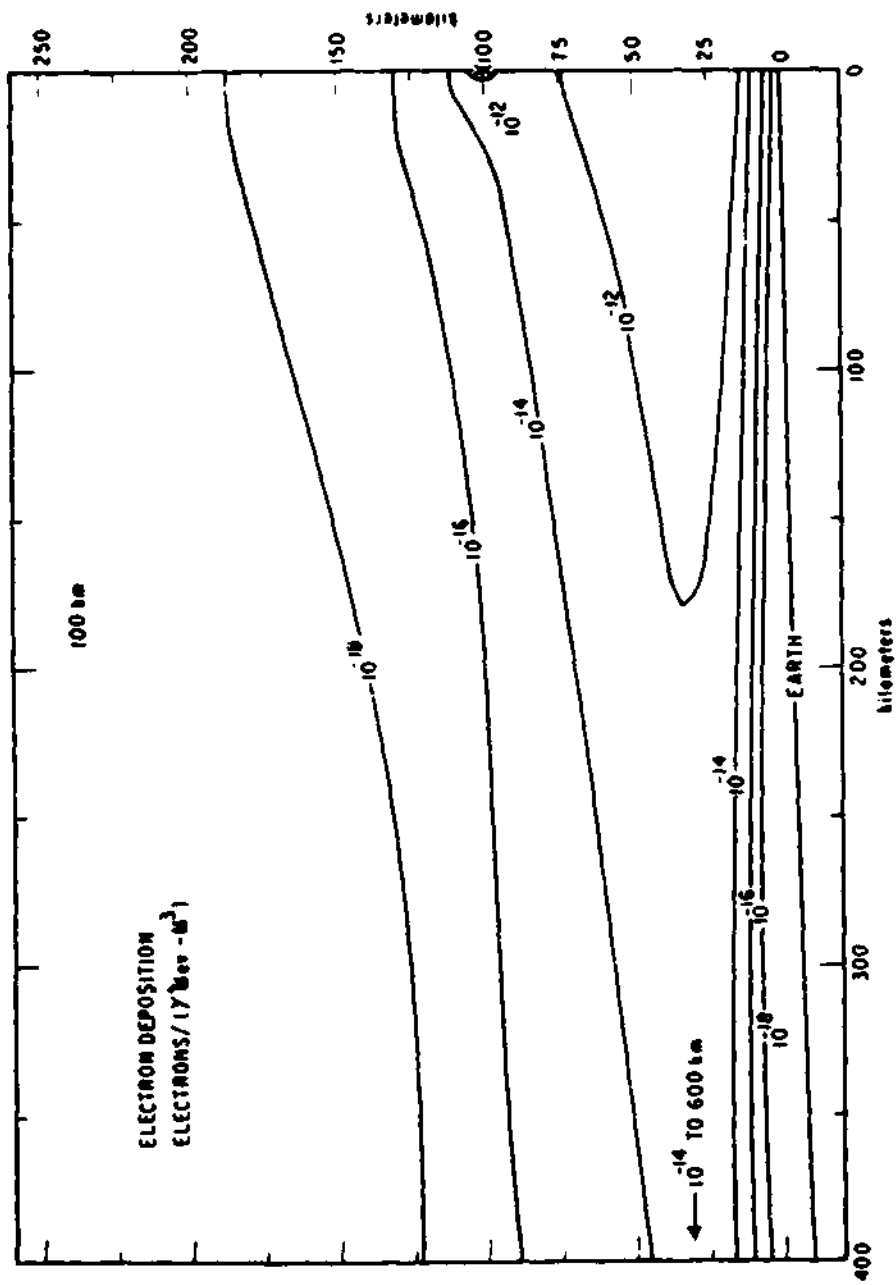


Figure 2.2 Gamma Ray Deposition, HOH=100 km, 1.5 MeV (Ref 5)

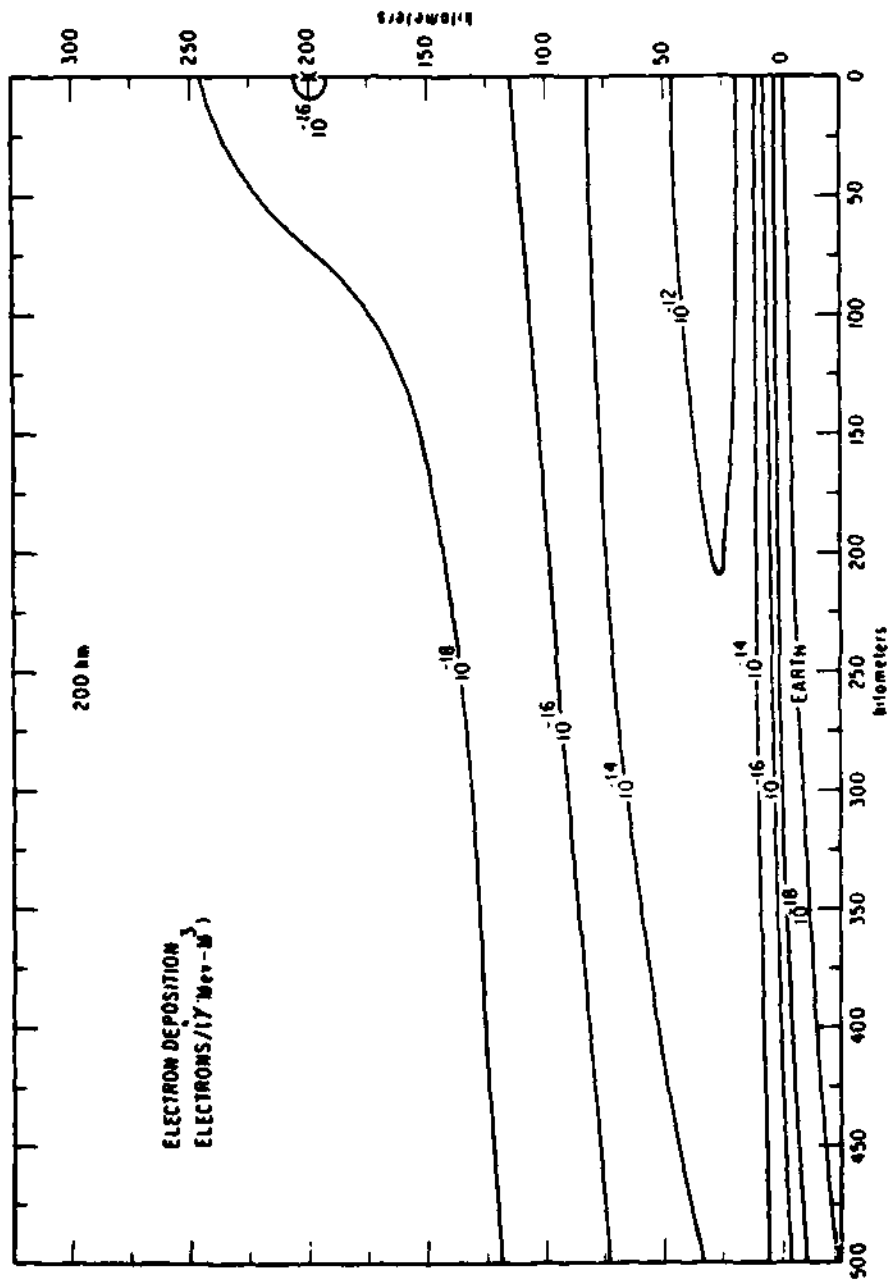


Figure 2.3 Gamma Ray Deposition, HOB=200 Km, 1.5 MeV (Ref 6)

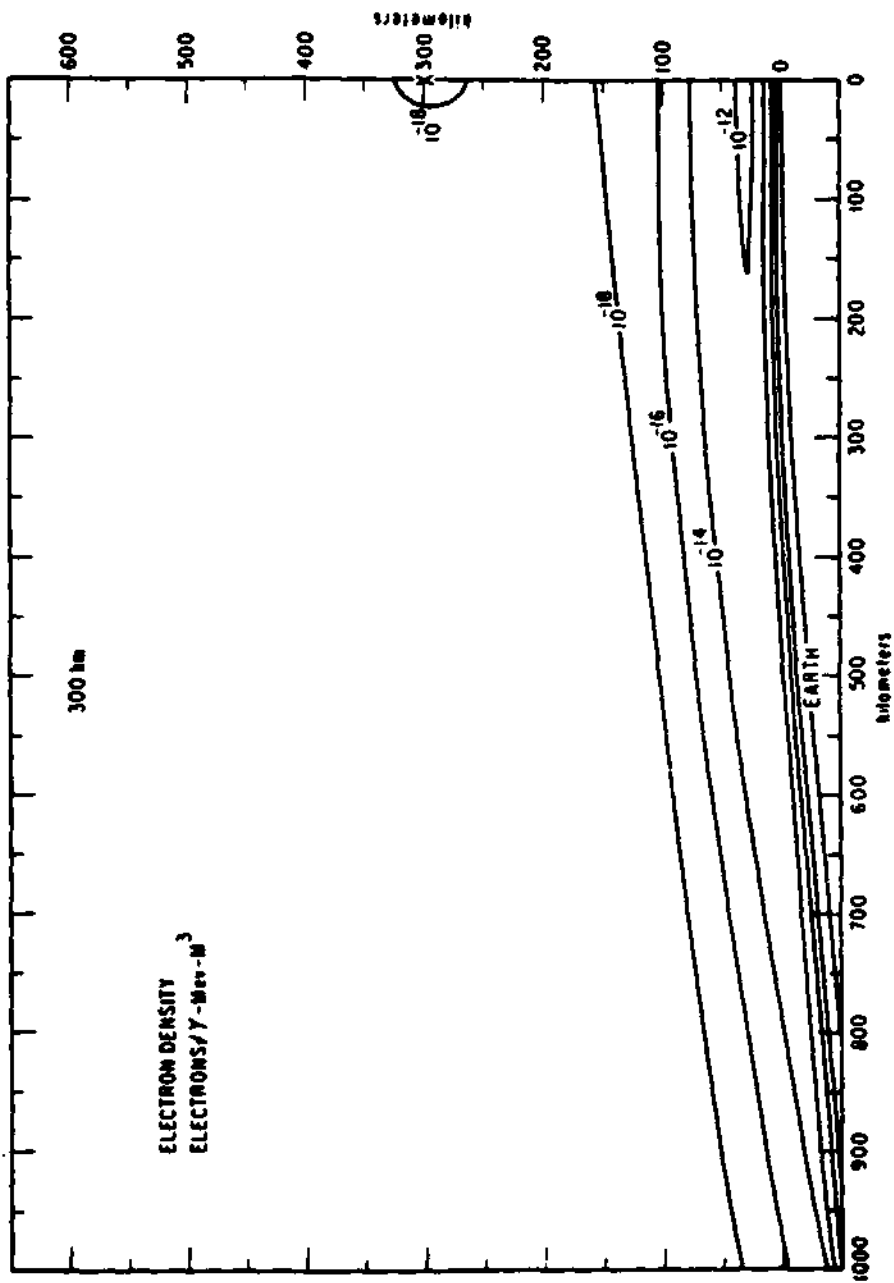


Figure 2.4 Gamma Ray Deposition, HOB=300 Km, 1.5 MeV (Ref 6)

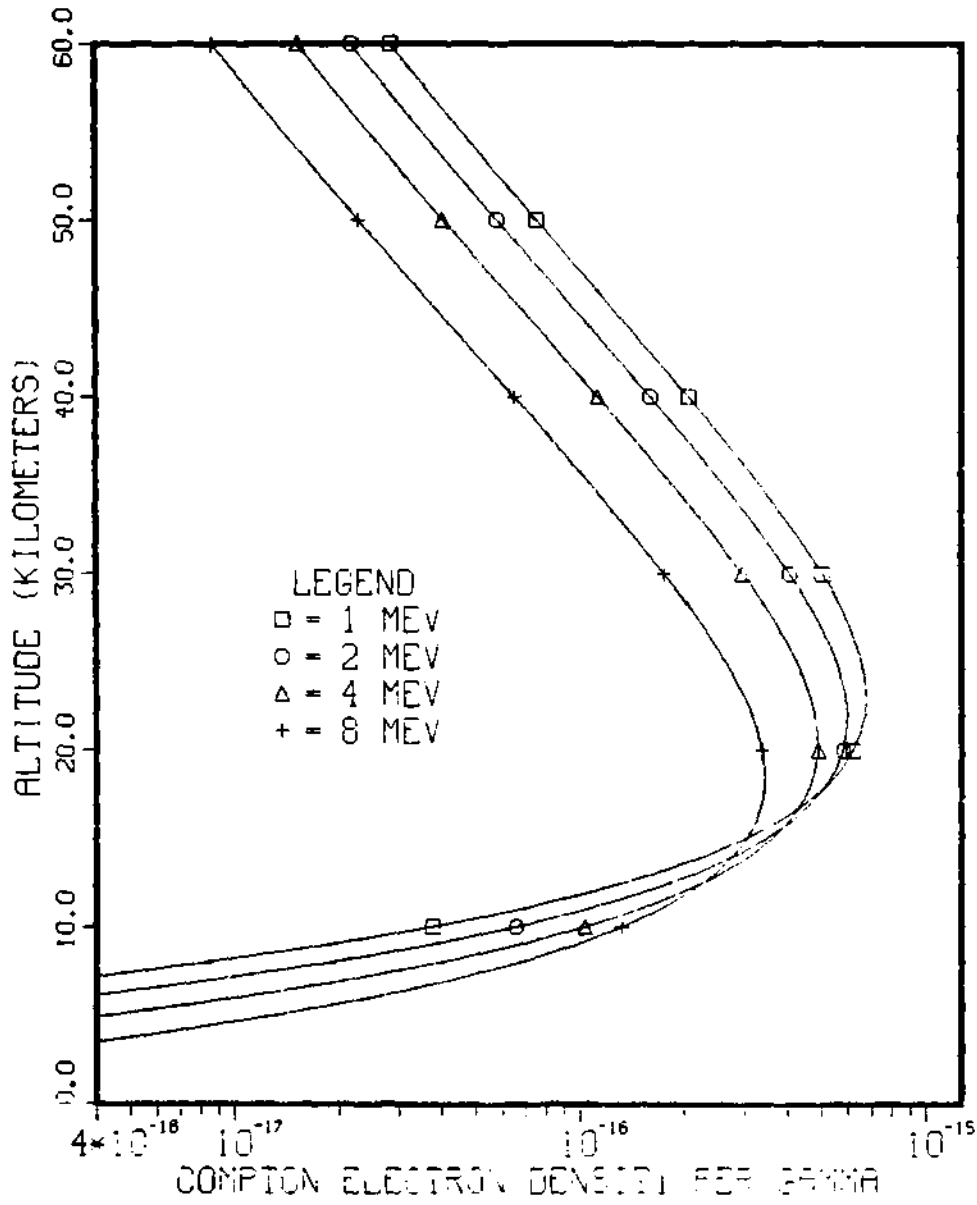


Figure 2.5 Gamma Ray Deposition, HOB=100 Km, Along Vertical

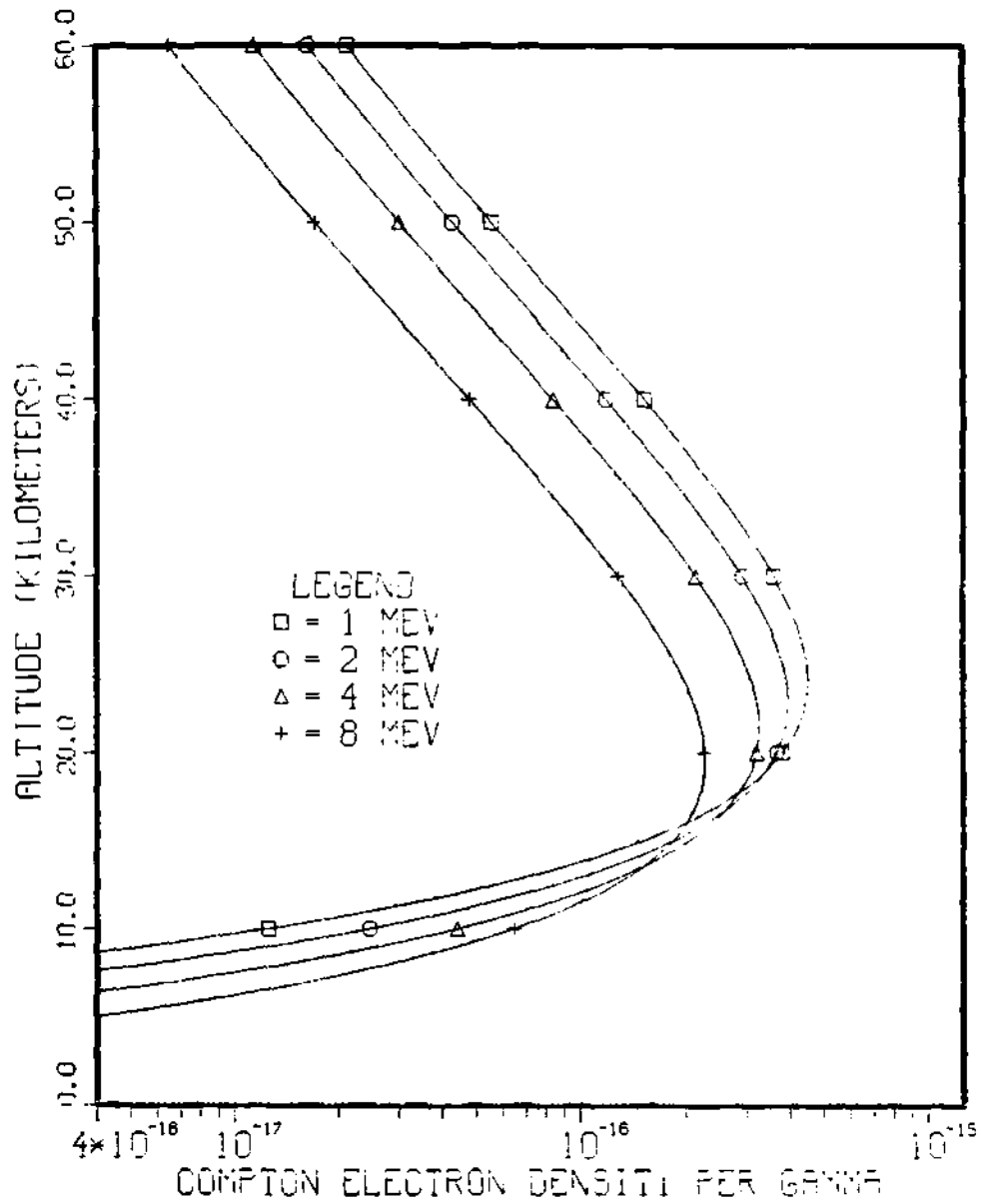


Figure 2.6 Gamma Ray Deposition, HOB=100 Km, 30° Off Vertical

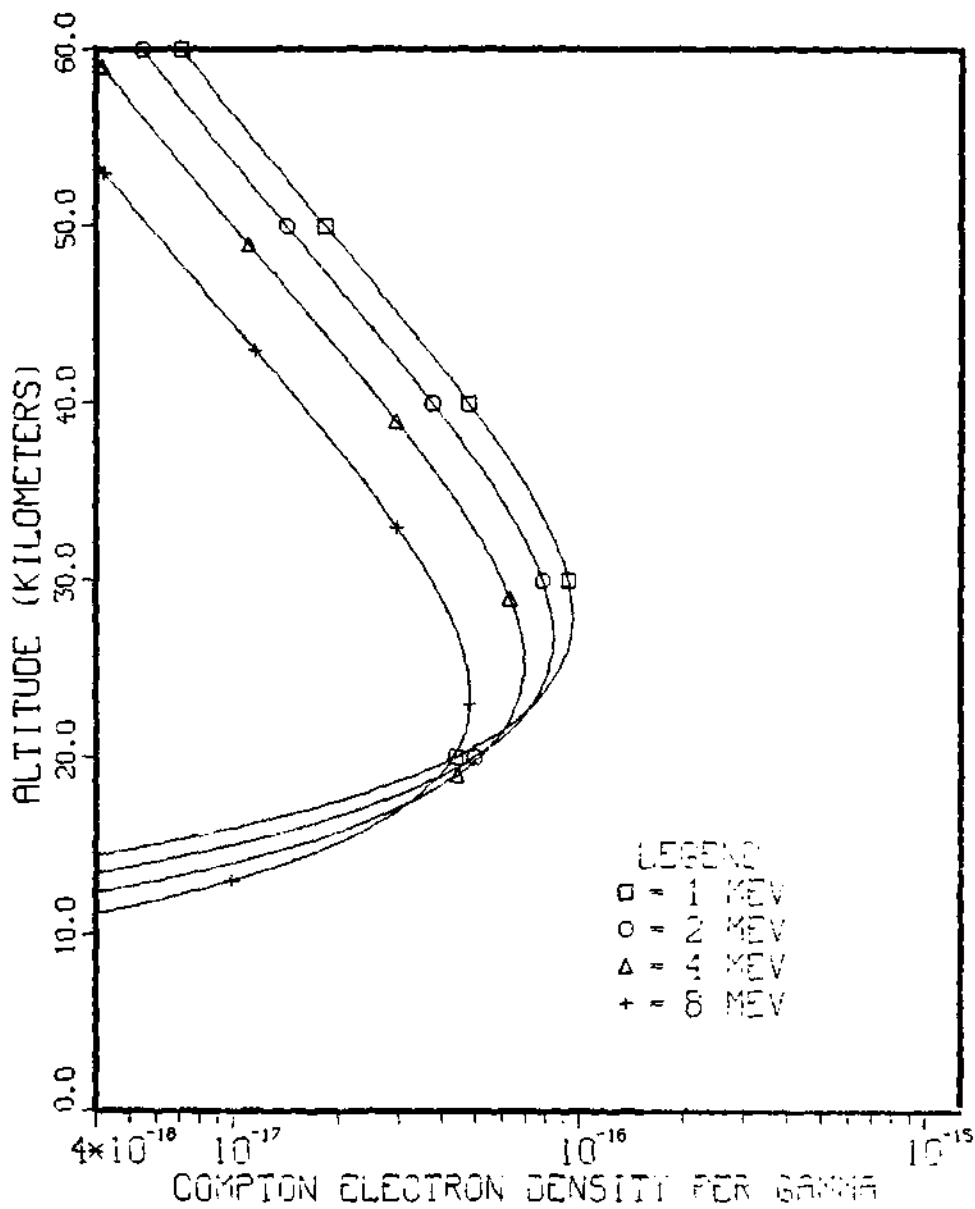


Figure 2.7 Gamma Ray Deposition, HOB=100 Km, 60° Off Vertical

### COMPTON ELECTRON DYNAMICS

The Compton interaction can be visualized as a billiard ball collision between a gamma ray and a molecular electron. Conservation of energy and momentum is used to derive the following relationships.

Kinetic energy of the Compton recoil electron

$$KE = E_{\gamma} \frac{p}{1+p} \quad (2.4)$$

where  $E_{\gamma}$  -incident gamma ray energy  
 $p = \alpha(1 - \cos\theta)$   
 $\alpha = E_{\gamma}/E_0$   
 $E_0$  -rest mass energy of the electron (0.511MeV)  
 $\theta$  -photon deflection angle

Compton recoil electron and photon deflection angles

$$\cot(\phi) = (1+\alpha)\tan\left(\frac{\theta}{2}\right) \quad (2.5)$$

where  $\phi$  -Compton recoil electron deflection angle

The Kline-Nishina cross sections for Compton scattering describe the scattering probability verses angle (Ref 5). The Compton electron is generally relativistic; therefore, the energy is expressed as

$$E = KE + m_0c^2 = \frac{m_0c^2}{\sqrt{1 - v^2/c^2}} \quad (2.6)$$

where  $KE$  -kinetic energy  
 $m_0c^2$  -rest mass energy of an electron  
 $v$  -velocity of Compton recoil electron



Solving for the velocity

$$v = c \sqrt{1 - \left( \frac{m_0 c^2}{KE + m_0 c^2} \right)^2} \quad (2.7)$$

The primary energy loss mechanism for Compton electrons is coulomb collisions with molecular electrons. The collisions result in the ionization of air molecules. Experiments show that one electron-ion pair is produced per 34 electron volts of energy deposited by a Compton electron. A 1MeV Compton electron will create 30,000 electron-ion pairs during its time of flight. For highly relativistic electrons, these collisions have little effect on the Compton electron velocity. As the Compton electron loses energy, the deflections from coulomb collisions become large. As a result, the Compton electron has a forward component of velocity close to the speed of light over most of its forward range. The Compton electron reaches its effective range when the deflections become large and the net current produced goes to zero. A Compton electron traveling at the initial velocity over the effective range is a convenient approximation when modeling the Compton currents.

#### RETARDED TIME

The gamma ray pulse from a nuclear detonation can be visualized as an expanding spherical shell with a thickness of a few meters. In a standard time frame of reference, the arrival time of the pulse will be a function of distance from the burst. A transformation is made to a frame of reference where a given phase of the gamma pulse will arrive at any location at the same time. The modified frame of reference is

called retarded time ( $\tau$ ). Retarded time is defined as

$$\tau = t - \frac{r}{c} \quad (2.8)$$

where  $t$  -standard time  
 $r$  -distance from burst  
 $c$  -speed of light

The retarded time frame is convenient because the phase of the gamma pulse does not shift with position.

#### COMPTON CURRENTS AND SECONDARY ELECTRON DENSITY

Approximations for the Compton currents and secondary electron density were developed by Karzas and Latter (Ref 9). These expressions are based on two assumptions. First, the Compton electrons travel at the initial velocity over the entire range. Second, the Compton electron production rate is constant over the range of a Compton electron. The range of Compton electrons at the peak of the deposition region is on the order of tens of meters. Figures 2.1 thru 2.7 show that Compton electron production rates vary slowly over these distances.

The expressions are best understood by writing them down as they would be in the absence of a magnetic field.

Compton electron density

$$n_c(r, \tau) = g(r) Y_\gamma \int_0^{R/v_0} f(\tau, \tau') d\tau' \quad (2.9)$$

where  $n_c(r, \tau)$  -density of Compton recoil electrons  
 $Y_\gamma$  -gamma yield  
 $R$  -Compton electron range  
 $v_0$  -initial Compton electron velocity

$f(\tau, \tau')$  -time dependence of the gamma flux accounting  
for the electron's progression through  
retarded time

$$f(\tau, \tau') = f[\tau - \tau'(1-v_0/c)] \quad (2.10)$$

The gamma ray pulse travels at the speed of light. A phase of the gamma pulse will have a fixed value of retarded time. The Compton electrons are traveling at  $v_0 < C$ ; therefore, the electron will progress through retarded time at a rate of  $(1-v_0/C)$ . During the Compton electron's time of flight  $(R/v_0)$ , the electron will contribute to the Compton electron density in the retarded time range of  $\tau$  (birth) to  $\tau + (1-v_0/C)R/v_0$ . Equation 2.9 is the expression for the Compton electron density at  $r$  and  $\tau$  where the integral sums the contribution from earlier retarded time. Expressions for the secondary electron production rate and Compton current are based on the Compton electron density.

The secondary electron production rate ( $n_s$ ) from one Compton electron is assumed to be constant over the Compton electrons range. The secondary electron production rate is expressed as

$$n_s(r, \tau) \approx Q \frac{v}{R} g(r) \int_0^{R/v} f(\tau, \tau') d\tau' \quad (2.11)$$

where  $Q$  -number of secondary electrons created per Compton  
electron

The net Compton current would be in the radial direction.

$$J_r(r, \tau) \approx -ev_0 g(r) \epsilon \int_0^{R/v_0} f(\tau, \tau') d\tau' \quad (2.12)$$

where  $\epsilon$  -average cosine of the initial Compton recoil  
 electron deflection angle  
 $e$  -charge of an electron

The earth's geomagnetic field impacts the results in two ways. First, the curvature of the Compton electron's path causes an acceleration of its movement through retarded time. The expression for the time dependence of the gamma flux accounting for the electron's progression through retarded time becomes

$$f(\tau, r) = f\left[\tau - \left(1 - \frac{v}{c} \cos^2(\theta)\right)\tau' + \frac{v}{\omega c} \sin^2(\theta) \sin(\omega\tau')\right] \quad (2.13)$$

where  $\theta$  -angle between the earth's geomagnetic field and the  
 direction of gamma ray motion  
 $\omega$  -Larmor frequency for the Compton electrons in the  
 earth's geomagnetic field

Second, transverse currents are produced. Polar coordinates with the axis along the earth's geomagnetic field (Figure 2.8) are used to describe these currents.

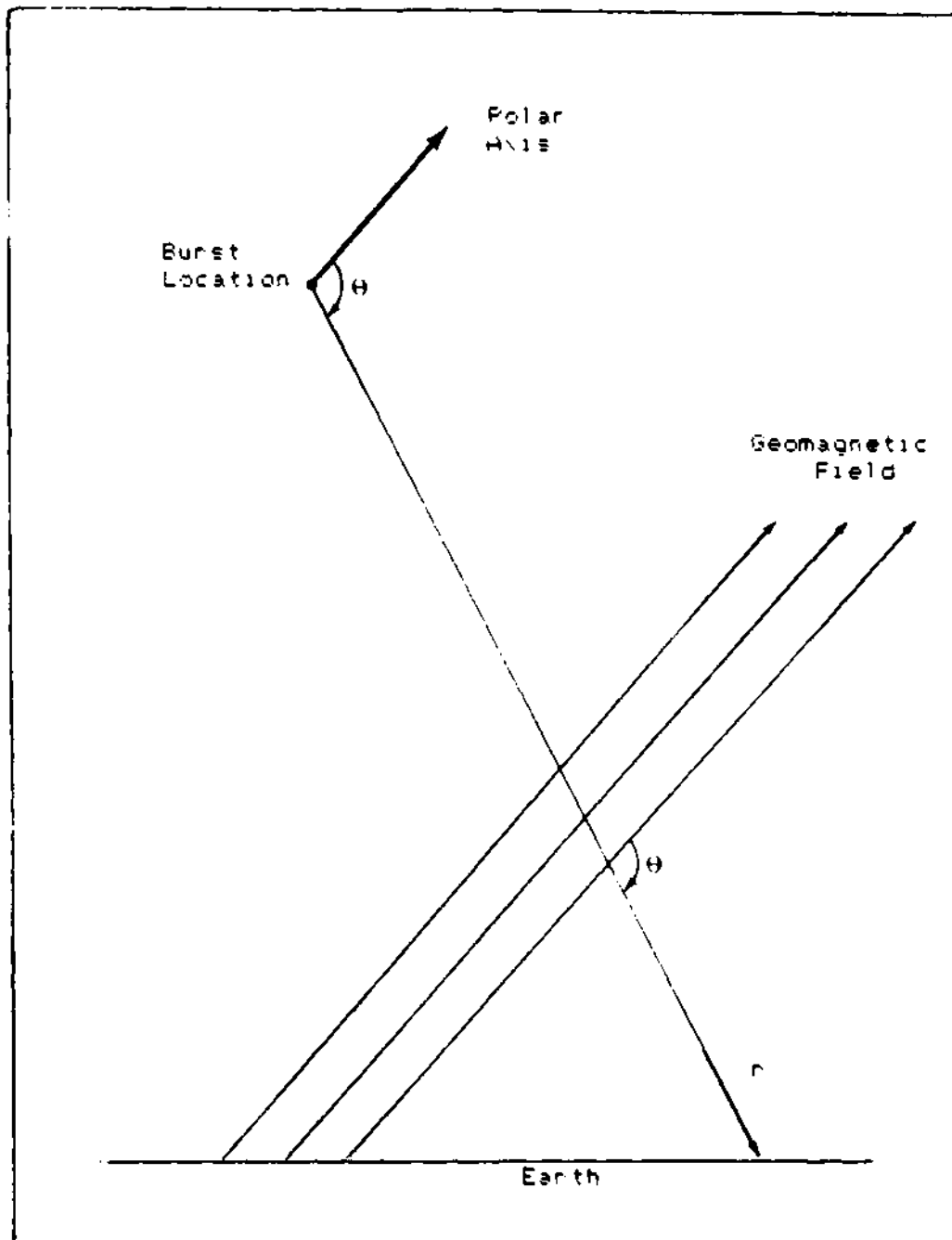


Figure 2.8 Polar Coordinate System

### Radial Compton Current

$$J_r(r, \tau) = -e\varepsilon v_0 g(r) \int_0^{R/v_0} f(\tau, \tau') [\cos^2(\theta) + \sin^2(\theta) \cos(\omega\tau')] dt' \quad (2.14)$$

### Theta Compton Current

$$J_\theta(r, \tau) = -e\varepsilon v_0 g(r) \int_0^{R/v_0} f(\tau, \tau') \sin(\theta) \cos(\theta) \cdot [\cos(\omega\tau') - 1] dt' \quad (2.15)$$

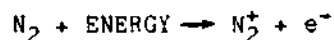
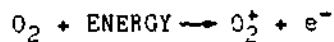
### Phi Compton Current

$$J_\phi(r, \tau) = -e\varepsilon v_0 g(r) \int_0^{R/v_0} f(\tau, \tau') \sin(\theta) \cdot \sin(\omega\tau') dt' \quad (2.16)$$

## AIR CHEMISTRY

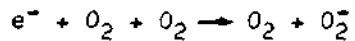
Air chemistry refers to the processes that govern the secondary electron and ion densities (Ref 7). The processes are described here in order of dominance in early time for high altitude EMP.

IONIZATION. Compton electrons ionized oxygen and nitrogen in the air. Ionization is the source for secondary electrons and positive ions. On the average, 34 electron volts of energy are lost by the Compton electron per electron-ion pair created.



ELECTRON ATTACHMENT. Secondary electrons attach to oxygen molecules to form a negative ion. The primary mode for attachment requires the simultaneous collision of the secondary electron and two

oxygen molecules:



Electron attachment removes secondary electrons and creates negative ions. The rate equations describing this process are

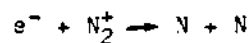
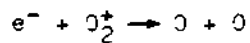
$$\frac{d}{dt} N_e(r, \tau) = -K_1(r, \tau) N_e(r, \tau) \quad (2.17)$$

$$\frac{d}{dt} N_-(r, \tau) = K_1(r, \tau) N_e(r, \tau) \quad (2.18)$$

where  $N_e(r, \tau)$  -secondary electron density  
 $N_-(r, \tau)$  -negative ion density  
 $K_1(r, \tau)$  -electron attachment rate constant

The electron attachment rate constant is proportional to air density squared and is a function of humidity and electric field strength. For high altitude EMP, the humidity is close to zero.

DISSOCIATIVE RECOMBINATION. Secondary electrons attach to positive ions. The electron binding energy dissociates the molecule:



Dissociative recombination removes secondary electrons and positive ions. The rate equations describing this process are

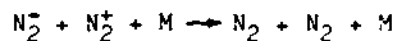
$$\frac{d}{dt} N_e(r, \tau) = -k_2 N_e(r, \tau) N_+(r, \tau) \quad (2.19)$$

$$\frac{d}{dt} N_+(r, \tau) = -k_2 N_e(r, \tau) N_+(r, \tau) \quad (2.20)$$

where  $k_2$  -dissociative rate constant

The dissociative recombination rate is approximately equal to  $2 \times 10^3 \text{ m}^3/\text{sec}$  and is independent of air density.

NEUTRALIZATION. Negative ions attach to positive ions. The process requires a three body collision:



where  $M$  -third molecule

Neutralization removes positive and negative ions. The rate equations describing the process are

$$\frac{d}{dt} N_+(r, \tau) = -k_3(r) N_+(r, \tau) N_-(r, \tau) \quad (2.21)$$

$$\frac{d}{dt} N_-(r, \tau) = -k_3(r) N_+(r, \tau) N_-(r, \tau) \quad (2.22)$$

where  $k_3(r)$ -neutralization rate constant

The neutralization rate constant is proportional to air density and is approximately equal to  $1 \text{ m}^3/\text{sec}$  at sea level.

The approximate values for the dissociative recombination rate constant and the neutralization rate constant are adequate because these processes have little effect on early time secondary electron and ion densities. The rate equations of these processes are combined to form a



set of coupled differential equations that govern the secondary electron and ion densities.

$$\begin{aligned} \frac{d}{dt} N_e(r, \tau) &= n_s(r, \tau) - k_1(r, \tau) N_e(r, \tau) \\ &\quad - k_2 N_e(r, \tau) N_+(r, \tau) \end{aligned} \quad (2.23)$$

$$\begin{aligned} \frac{d}{dt} N_+(r, \tau) &= n_s(r, \tau) - k_2 N_e(r, \tau) N_+(r, \tau) \\ &\quad - k_3(r) N_+(r, \tau) N_-(r, \tau) \end{aligned} \quad (2.24)$$

$$\begin{aligned} \frac{d}{dt} N_-(r, \tau) &= -k_1(r, \tau) N_e(r, \tau) \\ &\quad - k_3(r) N_+(r, \tau) N_-(r, \tau) \end{aligned} \quad (2.25)$$

#### AIR CONDUCTIVITY

The secondary electrons and ions drift in response to the electric field (E). Air conductivity ( $\sigma$ ) relates the displacement current density (J) to the electric field strength:

$$\vec{J} = \sigma \vec{E} \quad (2.26)$$

Mobility ( $\mu$ ) is used to relate the drift velocities to the electric field strength. The mobility for ions is approximately equal to  $2.5 \times 10^{-4} \text{ m}^2/(\text{volt sec})$  for STP (standard temperature and pressure) air and is inversely proportional to air density. The electron mobility is larger than the ion mobility and is a function of field strength and humidity as well as being inversely proportional to air density. The conductivity expressed in terms of charge density and mobility is

$$\sigma(r, \tau) = [N_e(r, \tau) \mu_e(r, \tau) + (N_+(r, \tau) + N_-(r, \tau)) \mu_i(r)] q \quad (2.27)$$

where  $\mu_e(r, \tau), \mu_1(r)$  -electron and ion mobilities

$q$  -charge of an electron

Air conductivity is primarily dependent on electron mobility and density.

### ELECTROMAGNETIC FIELDS

The electromagnetic fields are described by Maxwell's equations. Maxwell's equations expressed in rationalized MKS units are

$$\nabla \cdot \vec{E} = \frac{\rho}{\epsilon_0} \quad (2.28)$$

$$\nabla \times \vec{E} = -\frac{\partial \vec{B}}{\partial t} \quad (2.29)$$

$$\nabla \cdot \vec{B} = 0 \quad (2.30)$$

$$\nabla \times \vec{B} = \mu_0 \vec{j} + \frac{1}{c^2} \frac{\partial \vec{E}}{\partial t} \quad (2.31)$$

where  $\vec{E}$  -electric field vector

$\vec{B}$  -magnetic field vector

$\rho$  -charge density

$\epsilon_0$  -permittivity of free space

$\mu_0$  -permeability of free space

$\vec{j}$  -current density vector

$c$  -speed of light

Maxwell's equations are expressed in polar coordinates and retarded time by making the following transformations:

$$\frac{\partial}{\partial t} \rightarrow \frac{\partial}{\partial \tau}$$

$$\nabla \rightarrow \nabla - \hat{e}_r \frac{1}{c} \frac{\partial}{\partial \tau}$$

where  $\hat{e}_r$  -unit vector in the radial direction

Maxwell's equations expressed in polar coordinates and retarded time are written as

$$\nabla \cdot \vec{E} - \hat{e}_r \cdot \frac{1}{c} \frac{\partial \vec{E}}{\partial \tau} = \frac{\sigma}{\epsilon} \quad (2.32)$$

$$\nabla \times \vec{E} - \hat{e}_r \times \frac{1}{c} \frac{\partial \vec{E}}{\partial \tau} = -\frac{\partial \vec{B}}{\partial \tau} \quad (2.33)$$

$$\nabla \cdot \vec{B} - \hat{e}_r \cdot \frac{1}{c} \frac{\partial \vec{B}}{\partial \tau} = 0 \quad (2.34)$$

$$\nabla \times \vec{B} - \hat{e}_r \times \frac{1}{c} \frac{\partial \vec{B}}{\partial \tau} = \mu \vec{J} + \frac{1}{c^2} \frac{\partial \vec{E}}{\partial \tau} \quad (2.35)$$

Karzas and Latter (Ref 9) derived differential equations that describe the transverse and radial electric fields. Terms involving spatial derivatives are neglected when compared to derivatives with respect to  $\tau$ . This is known as the high frequency approximation. The differential equations resulting from the high frequency approximation are written as

### Radial Electric Field

$$\frac{\partial}{\partial t} E_r + \frac{J}{\epsilon} = 0 \quad (2.36)$$

### Transverse Electric Fields

$$\frac{\partial}{\partial r} r E_\theta + \frac{\mu c}{2} j_\theta = 0 \quad (2.37)$$

$$\frac{\partial}{\partial r} r E_\phi + \frac{\mu c}{2} j_\phi = 0 \quad (2.38)$$

where

$E_\theta, E_\phi, E_r$  -components of electric field vector

$J_\theta, J_\phi, J_r$  -components of current density vector

The current density is the vector sum of the Compton current density and the conduction current density. The conduction current is the current from electrons and ions drifting in the local electric field.

The differential equation for the radial electric field (EQ 2.36) describes the time variation of the radial electric field in terms of the local current density. The differential equations for the transverse electric field (EQS 2.37 and 2.38) describe the spatial variation of the transverse electric fields in terms of the local current density and conductivity. The transverse electric fields are generated in the absorption region and are able to propagate to the ground.

### III. NUMERICAL METHODS

Chapter III discusses the numerical methods used in EMPFRE to model the processes discussed in Chapter II. The approach used to solve for the electric fields was developed by J. H. Erkkila (Ref 5). Many of the approximations made to model the phenomenon were proposed by W. J. Karzas and R. Latter (Ref 9). The details of the methods used are presented in the following sections.

#### BURST GEOMETRY

The geometry and coordinate system used for EMPFRE are shown in Figure 3.1. ZRMIN and ZRMAX are the upper and lower bounds of the gamma ray absorption region. RMIN and RMAX are the distances from the burst point to ZRMIN and ZRMAX along R. EMPFRE calculates the electric fields along R from RMIN to RMAX. The transverse components of the electric field propagate from RMAX to the target with a loss due to spherical divergence.

If the height of burst is less than the default value for ZRMIN (50 kilometers), ZRMIN is set equal to the height of burst and ZRMAX is set equal to the target altitude. If the target altitude is greater than the default value for ZRMAX (10 kilometers), ZRMAX is set equal to the target altitude. If ZRMAX is set to the target altitude, the radial component of the electric field is included.

Polar coordinates centered at the burst point are used to compute the electric fields. The polar axis is parallel to the earth's magnetic field.

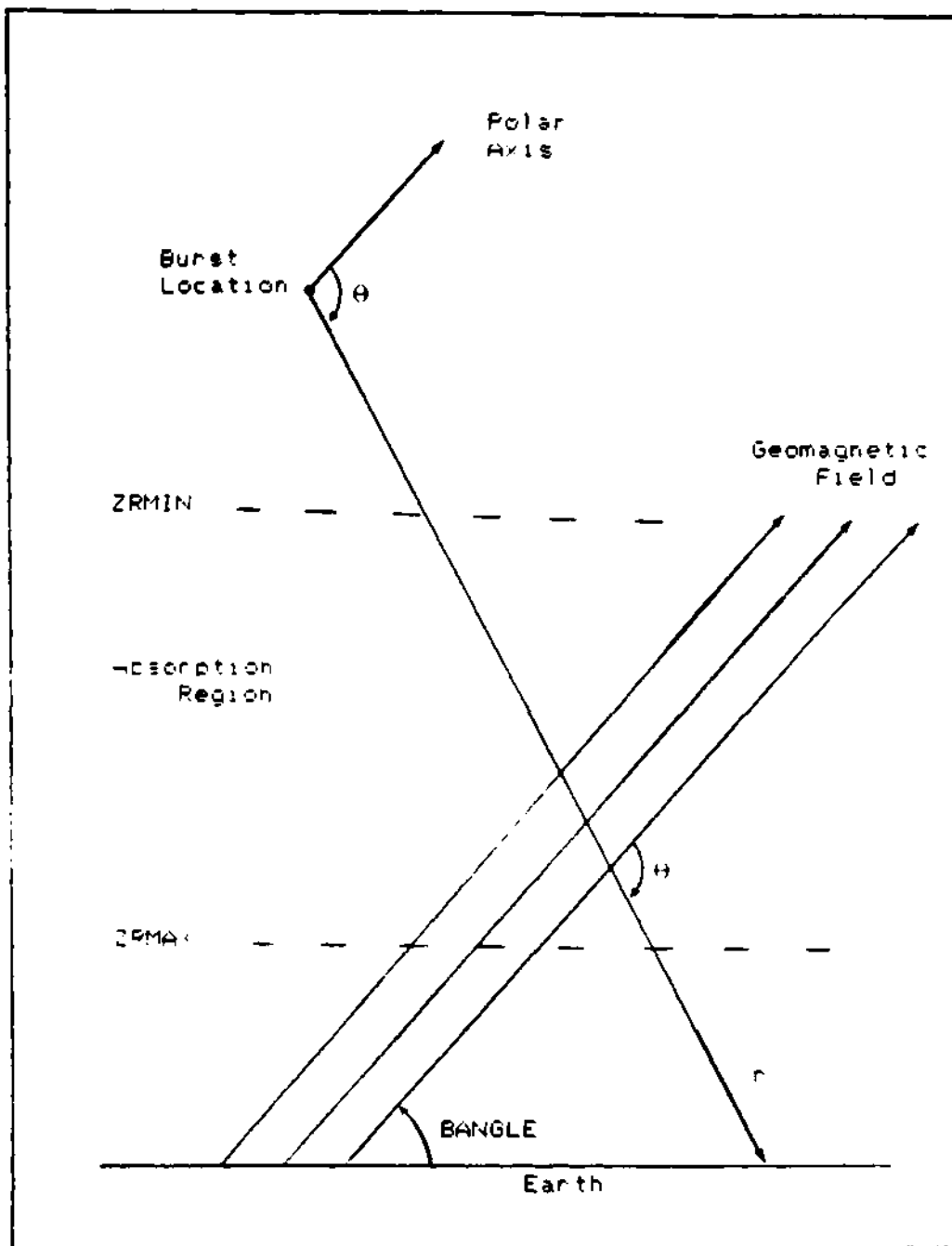


Figure 3.1 Burst Geometry and Key Variables

The target location is designated by the rectangular coordinates x, y and z in meters. The earth is assumed to be flat and z is the target altitude. The x-axis points to magnetic west. The y-axis points to magnetic south.

BANGLE (the geomagnetic field dip angle) is specified in degrees.

The angle theta ( $\theta$ ) is found by taking the dot product of a unit vector in the direction of the earth's magnetic field ( $\hat{B}$ ) and a unit vector in the radial direction ( $\hat{r}$ ):

$$\theta = \text{ARC COS}(\hat{B} \cdot \hat{r}) \quad (3.1)$$

$$\text{where } \hat{B} = \text{COS}(\text{BANGLE}) \hat{j} + \text{SIN}(\text{BANGLE}) \hat{k}$$

$$\hat{r} = x \hat{i} + y \hat{j} + (HOB - z) \hat{k}$$

#### GAMMA RAY YIELD FUNCTION

EMPFHE is designed to analyze the electro magnetic pulse from an arbitrary mono-energetic gamma pulse. The total gamma ray yield (kilotons), gamma ray energy and a function ( $F(r)$ ) that is proportional to the gamma ray yield as a function of time are required as input parameters. The yield in kilotons is converted to MeV. The gamma ray energy is used to calculate the yield as number of gamma rays emitted. Finally, a proportionality constant is found to convert the value of the function to the gamma ray emission rate. The proportionality constant is derived by integrating the function using the trapezoidal rule:

$$\int_0^{\infty} F(r) dt = \Delta t \cdot [F(r_0)/2 + F(r_1) + F(r_2) + \dots + F(r_{n-1}) + F(r_n)/2] \quad (3.2)$$

where  $F(r)$  - gamma function

$\Delta t$  - retarded time step

$t_n = n \cdot \Delta t$

The integral of the chosen function multiplied by the proportionality constant must be equal to the total gamma ray yield:

$$\int_0^{\infty} C \cdot F(\tau) d\tau = \text{YIELD} \quad (3.3)$$

The constant can be taken out of the integral and solved for with the integral approximated by the trapezoidal rule.

$$C \approx \frac{\text{YIELD}}{\Delta\tau \cdot [F(\tau_1)/2 + F(\tau_2) + \dots + F(\tau_n)/2]} \quad (3.4)$$

The function  $F(\tau)$  can be in the form of a mathematical expression or a set of data points where interpolation is used.

#### INITIAL ELECTRON VELOCITY

The initial relativistic energy of the Compton electron is given by

$$E = KE_0 + m_0 c^2 \quad (3.5)$$

$$E = m_0 c^2 / (1 - v_0^2/c^2) \quad (3.6)$$

where  $KE_0$  - initial kinetic energy

$v_0$  - initial velocity

Solving for the initial velocity, the equation is

$$v_0 = 2.99E8 \cdot \text{SQRT}(1 - (0.511 / (KE_0 + 0.511))^2) \quad (3.7)$$

where  $KE_0$  - initial kinetic energy (MeV)

$v_0$  - initial velocity (meters/second)

#### MEAN FREE PATH

The absorption coefficients ( $\mu$ ) for  $\gamma$ -ray interactions in air are shown in Figure 3.2. The mean free path is given by

$$\text{MFP} = \frac{1}{\mu \rho} \quad (3.8)$$

where  $\rho$  - the density of air



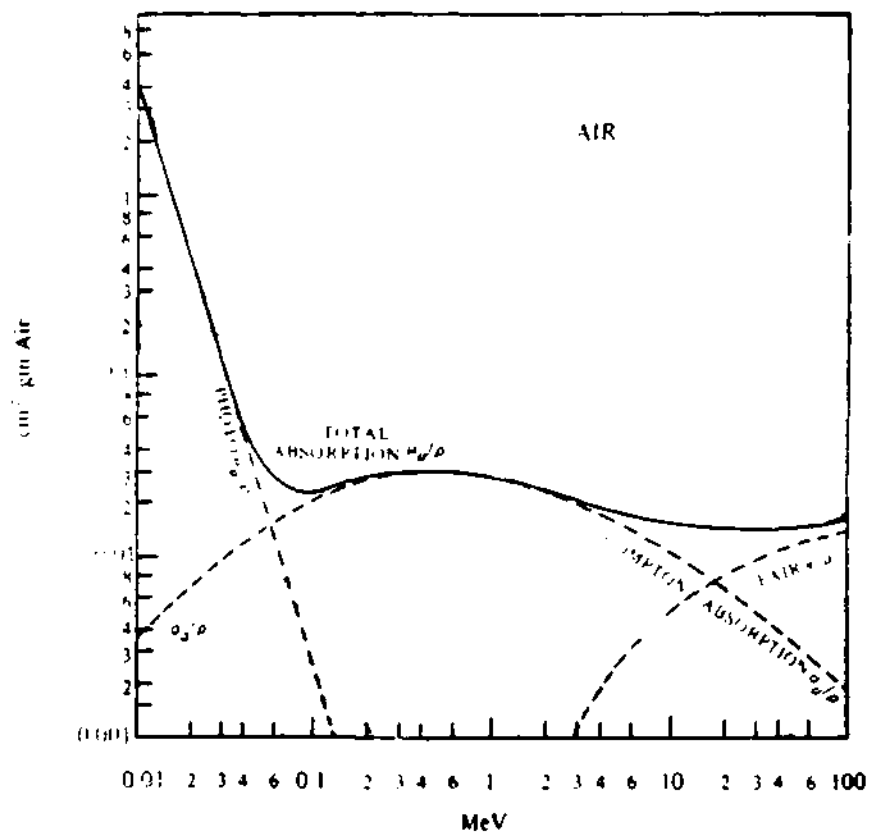


Figure 3.2 Gamma Ray Attenuation Cross Sections

The mean free path for Compton interaction and total absorption is found using an empirical approximation to Figure 3.2. The equations used to approximate the mean free path in STP air as a function of energy are

For  $0.2 \text{ MeV} < E < 0.5 \text{ MeV}$

$$\text{MFP}_c = \text{MFP}_t = 1/[0.0035 + (\ln(E) + 1.609)/3271] \quad (3.9)$$

For  $0.5 \text{ MeV} < E < 1.5 \text{ MeV}$

$$\text{MFP}_c = \text{MFP}_t = 1/[0.0038 - (\ln(E) + 0.6931)/1927] \quad (3.10)$$

For  $1.5 \text{ MeV} < E < 10. \text{ MeV}$

$$\text{MFP}_c = 1/[0.0033 + (0.4055 - \ln(E))/983] \quad (3.11)$$

$$\text{MFP}_t = 1/[0.0033 + (0.4055 - \ln(E))/1423] \quad (3.12)$$

where  $E$  - gamma ray energy (MeV)

$\text{MFP}_c$  - mean free path for Compton interaction

$\text{MFP}_t$  - mean free path for all interactions

The MFP is inversely proportional to air density, therefore; MFP as a function of altitude is

$$\text{MFP}(\text{ALT}) = \text{MFP}_{\text{STP}} \text{EXP}(\text{ALTITUDE}/7000 \text{ Meters}) \quad (3.13)$$

The MFP for Compton interaction and total absorption (where different) as a function of gamma-ray energy in STP air is generated from an empirical fit of Figure 3.2. Values for the MFP in STP air are provided in Table 3.1.

Gamma Energy (MeV)	Compton MFP (m)	Total MFP (m)	Compton Electron Range (m)	Initial Electron Velocity (v/c)
0.2	285.7		0.021	0.37
0.3	275.9		0.073	0.50
0.4	269.4		0.16	0.59
0.5	264.6		0.28	0.67
0.75	282.5		0.68	0.78
1.0	295.0		1.21	0.85
2.0	329.2	319.7	4.06	0.95
3.0	380.9	351.8	7.49	0.98
4.0	428.8	378.7	11.2	0.99
5.0	475.0	402.6	15.0	0.992
7.5	590.7	454.8	24.9	0.997
10.0	714.2	500.8	34.0	0.998

Table 3.1 Data Used in EMPFRE

## COMPTON DYNAMICS

Values for the median Compton electron energy, Compton electron deflection angle and gamma ray deflection angle were found by using the Kline-Nishina cross sections for Compton scattering. First, the median Compton electron deflection angle is determined. The corresponding Compton electron energy and gamma ray deflection angle are calculated. COMP is a program written by LTC J. Erkkila that performs this task. Empirical fits of the results are used in EMPFRE and are given below:

### Compton Electron Energy

For  $E_e < 4$  MeV

$$E = E_e \cdot (0.195 + (\ln(E_e) + 1.609) / 5.992) \quad (3.14)$$

For  $E_\gamma > 4$  MeV

$$E = E_e \cdot (0.695 + (\ln(E_\gamma) - 1.386) / 9.153) \quad (3.15)$$

### Compton Electron Deflection Angle

For  $0.2 \text{ MeV} < E_\gamma < 0.5 \text{ MeV}$

$$\theta = 1.2488 - 0.18 \cdot (\ln(E_\gamma) + 1.6094) \quad (3.16)$$

For  $0.5 \text{ MeV} < E_\gamma < 1.5 \text{ MeV}$

$$\theta = 1.0383 - 0.1422 \cdot (\ln(E_\gamma) + 0.6931) \quad (3.17)$$

For  $1.5 \text{ MeV} < E_\gamma < 10. \text{ MeV}$

$$\theta = 0.9163 + 0.1371(0.4055 - \ln(E_\gamma)) \quad (3.18)$$

### Gamma Ray Deflection Angle

For  $0.2 \text{ MeV} < E_\gamma < 0.5 \text{ MeV}$

$$\phi = 0.7054 - 0.09527 \cdot (\ln(E_\gamma) + 1.6094) \quad (3.19)$$

For  $0.5 \text{ MeV} < E_\gamma < 10. \text{ MeV}$

$$\phi = 0.6981 - 0.6861 \cdot (\ln(E_\gamma) + 0.6931) \quad (3.20)$$

where  $E$  - Compton electron energy (MeV)

$E_\gamma$  - gamma energy (MeV)

$\Theta$  - Compton electron deflection (radians)

$\phi$  - gamma deflection angle (radians)

Values of Compton electron energy, Compton electron deflection angle and gamma ray deflection angle from the empirical fits are provided in Table 3.2 along with the results from COMP.

Gamma Energy (MeV)	COS $\theta$ [Ref] (Rad)	Error (%)	COS $\phi$ [Ref] (Rad)	Error (%)	Energy [Ref] (MeV)	Error (%)
0.2	0.3165 [0.3160]	0.16	0.7071 [0.7082]	0.15	0.0390 [0.0422]	7.5
0.3	0.3848 [0.3849]	0.03	0.7338 [0.7267]	0.98	0.0788 [0.0796]	1.0
0.4	0.4320 [0.4313]	0.16	0.7522 [0.7671]	0.68	0.1242 [0.1232]	0.81
0.5	0.4679 [0.4650]	0.62	0.7660 [0.7671]	0.14	0.1739 [0.1718]	1.2
0.75	0.5181 [0.5213]	0.61	0.8179 [0.8107]	0.89	0.3116 [0.3095]	0.67
1.0	0.5527 [0.5576]	0.88	0.8511 [0.8443]	0.81	0.4635 [0.4640]	0.11
2.0	0.6396 [0.6370]	0.41	0.9182 [0.9180]	0.02	1.158 [1.174]	1.4
3.0	0.6813 [0.6797]	0.24	0.9485 [0.9487]	0.02	1.941 [1.959]	0.92
4.0	0.7096 [0.7086]	0.14	0.9659 [0.9644]	0.16	2.780 [2.781]	0.004
5.0	0.7308 [0.7300]	0.11	0.9769 [0.9735]	0.35	3.597 [3.677]	2.2
7.5	0.7676 [0.7668]	0.10	0.9915 [0.9849]	0.67	5.727 [5.804]	1.3
10.0	0.7923 [0.7909]	0.18	0.9976 [0.9900]	0.77	7.950 [8.036]	1.1

Table 3.2 Empirical Fit to COMP Results

### ELECTRON RANGE

Range equations are from Radiological Health Handbook (Ref 16).

For  $0.01 \text{ MeV} < E < 2.5 \text{ MeV}$

$$R = 412 \cdot E^{(1.265 - 0.0954 \cdot \ln(E))} \quad (3.21)$$

For  $E > 2.5 \text{ MeV}$

$$R = 530 \cdot E^{-106} \quad (3.22)$$

where  $R$  -range (mg/cm)

$E$  -energy (MeV)

The range in STP air is found by dividing the range (above) by the density of STP air ( $\rho_{\text{STP}} = 1.293 \text{ mg/cm}^3$ ). Converting to meters and correcting for altitude, the final equations are

For  $0.01 \text{ MeV} < E < 2.5 \text{ MeV}$

$$R = 3.19 \cdot E^{(1.265 - 0.0954 \cdot \ln(E))} \cdot \text{EXP}(ALT/7000) \quad (3.23)$$

For  $E > 2.5 \text{ MeV}$

$$R = 4.10 \cdot E^{-0.82} \cdot \text{EXP}(ALT/7000) \quad (3.24)$$

where  $R$  -range (meters)

$ALT$  -altitude (meters)

Electron range as a function of energy in STP air is provided in Table

3.2. The electron range includes the effects of straggling; therefore, the range is the forward component of the electron's path:

$$R = \sum_{n=1}^N \text{PATH} \cdot \cos(\theta_n) \quad (3.25)$$

where PATH -distance traveled between collisions  $n-1$  and  $n$

$N$  -total number of collisions to thermalize the electron

$\theta$  -deflection angle from original path

The average  $\cos(\theta_n)$  term approaches 1 for high energy electrons early in TOF (time of flight) and goes to zero for low energy electrons after many collisions.

#### COMPTON ELECTRON TIME OF FLIGHT

The Compton electron time of flight is approximated by assuming the Compton electron travels at its initial velocity over its entire range. Therefore, the Compton electron time of flight is written as

$$\text{TOF} = \text{RANGE}(R) / v_0 \quad (3.26)$$

$$\text{TOF} = \text{RANGE}_0 \cdot \text{EXP}(\text{ALT}/7000) / v_0 \quad (3.27)$$

where RANGE(R) -Compton electron range at R

$v_0$  -initial velocity

RANGE<sub>0</sub> -range in STP air (meters)

ALT -altitude (meters)

Assuming a constant velocity over the entire range is justified for relativistic Compton electrons at high altitudes because energy loss in early TOF primarily reduces the electron's mass. Later in the electron



lifetime, the electron will have lagged behind the pulse in retarded time primarily due to its curved trajectory. Electrons lagging behind the gamma ray pulse become unimportant due to the increase in conductivity.

#### COMPTON ELECTRON PRODUCTION RATE

The Compton electron production rate is calculated with the assumption that scattered gamma rays are ignored. The gamma ray flux is expressed as

$$F_{\gamma}(R, \tau) = S_{\gamma}(\tau) \frac{\int_0^R \text{EXP}[-\int_0^{r'} \frac{dr''}{\lambda_{\gamma}(r'')}]}{4\pi R^2} \quad (3.28)$$

where  $\lambda(r)$  - gamma ray MFP at  $r$  (meters)

$R$  - position along slant range (meters)

$s_{\gamma}(\tau)$  - gamma ray emission rate at  $\tau$  ( $\text{sec}^{-1}$ )

Assuming an exponential atmosphere, the MFP as a function of  $r$  can be related to the MFP in STP air as

$$\text{MFP}(R) = \text{MFP}_0 \cdot \text{EXP} \left[ \frac{\text{HOB} - R \cdot \text{COS}(A)}{7000} \right] \quad (3.29)$$

where  $\text{MFP}_0$  - mean free path for STP air (meters)

$\text{HOB}$  - height of burst (meters)

$A$  - angle between vertical and slant range

The Compton electron production rate is found by

$$\dot{N}_C(R, \tau) = S_Y(\tau) \left[ \frac{\text{EXP}[-dr/\text{MFP}_t(R)]}{4\pi R^2 \cdot \text{MFP}_C(R)} \right] \quad (\text{m}^{-3}\text{sec}^{-1}) \quad (3.30)$$

where  $\text{MFP}_t(r)$  -mean free path for total absorption

$\text{MFP}_C(r)$  -mean free path for Compton interaction

For an exponential atmosphere, the formula for Compton electron production rate as a function of R is expressed as

$$\dot{N}_C(R, \tau) = S_Y(\tau) \frac{\text{EXP}\left[\frac{-7000}{\text{COS}(A) \cdot \text{MFP}_C}\right] \left( \text{EXP}\left[\frac{R \cdot \text{COS}(A) - \text{HOB}}{7000}\right] - \text{EXP}\left[\frac{-\text{HOB}}{7000}\right] \right)}{4\pi R^2 \cdot \text{MFP}_C \cdot \text{EXP}\left[\frac{\text{HOB} - R \cdot \text{COS}(A)}{7000}\right]} \quad (3.31)$$

where  $\text{MFP}_t, \text{MFP}_C$  -mean free path for STP air (meters)

The gamma rays are assumed to be in a collimated beam. A scattered gamma ray changes direction and lags behind the pulse. Compton electrons produced by these gamma rays will not contribute to the EMP because of the increase in conductivity at late times. Therefore, scattering removes the gamma ray from the pulse.

## COMPTON CURRENT AND SECONDARY ELECTRON SOURCE

Integral equations for the Compton current density and the secondary electron source density developed by Karzas and Latter are solved numerically (Ref 9).

Secondary Electron Production Rate

$$N_s(r, \tau) \approx Q \frac{v_0}{R(r)} G(r) \int_0^{\text{TOF}} f(\tau, \tau') d\tau' \quad (3.32)$$

Radial Compton Current Density

$$J_r(r, \tau) \approx -ev_0 G(r) \int_0^{\text{TOF}} f(\tau, \tau') [\cos^2(\theta) + \sin^2(\theta) \cos(\omega\tau')] d\tau' \quad (3.33)$$

Theta Compton Current Density

$$J_\theta(r, \tau) \approx -ev_0 G(r) \int_0^{\text{TOF}} f(\tau, \tau') [\sin(\theta) \cos(\theta) (\cos(\omega\tau') - 1)] d\tau' \quad (3.34)$$

Phi Compton Current Density

$$J_\phi(r, \tau) \approx -ev_0 G(r) \int_0^{\text{TOF}} f(\tau, \tau') [\sin(\theta) \sin(\omega\tau')] d\tau' \quad (3.35)$$

where TOF -Compton electron time of flight

$f(\tau, \tau')$  -time variation of gamma emission ( $\text{sec}^{-1}$ )

$$f(\tau, \tau') = f[\tau - (1 - \beta \cdot \cos^2(\theta)) \cdot \tau' + \beta \cdot \sin^2(\theta) \frac{\sin(\omega\tau')}{\omega}] \quad (3.36)$$

$\tau$  -retarded time(sec)

$r$  -position along the slant range (m)

$Q$  -number of secondary electrons produced per

Compton electron

$v_0$  -initial Compton electron velocity (m/sec)

$R(r)$  -Compton electron range (m)

$G(r)$  -Compton electron source density per  
yield ( $m^{-3}$ )

$e$  -electron charge (coulombs)

$\omega$  -Larmor frequency for a Compton electron ( $sec^{-1}$ )

$\theta$  -the angle between the slant range and the geomagnetic field

$\beta$  -initial velocity (fraction of  $c$ )

The integral equations were solved numerically. The equations used to solve for Compton current density and the secondary electron source density are listed below:

Secondary Electron Production Rate

$$N_c(r, \tau) \approx Q \frac{v_0}{R(r)} G(r) \sum_{n=1}^n f(\tau, \tau_n') \Delta \tau' \quad (3.37)$$

Radial Compton Current Density

$$J_r(r, \tau) \approx -ev' G(r) \sum_{n=1}^n f(\tau, \tau_n') [\cos^2(\theta) + \sin^2(\theta) \cos(\omega \tau_n')] \Delta \tau' \quad (3.38)$$

Theta Compton Current Density

$$J_\theta(r, \tau) \approx -ev' G(r) \sum_{n=1}^n f(\tau, \tau_n') [\sin(\theta) \cos(\theta) (\cos(\omega \tau_n') - 1)] \Delta \tau' \quad (3.39)$$

Phi Compton Current Density

$$J_{\phi}(r, \tau) \approx -ev'G(r) \sum_{n=1}^N f(\tau, \tau_n') \text{SIN}(\theta) \text{SIN}(\omega\tau_n') \Delta\tau' \quad (3.40)$$

where  $\Delta\tau'$  -retarded time step size (0.05 Shakes)

$$\tau_n' = n \cdot \Delta\tau'$$

$$N = R(r)/v_c/\Delta\tau'$$

$v'$  -component of the initial velocity

in the radial direction

These computations are performed in subroutine current. The retarded time step used to approximate the integrals is 0.05 shakes. The gamma output of the device will change slowly over this time for most gamma histories. This subroutine drives the computation time. The program uses about 4 seconds of cpu time per electric field evaluation on the CDC CYBER 750 at this time increment. Decreasing the step-size becomes very expensive.

## AIR CHEMISTRY

The set of differential equations which govern the electron and ion densities as a function of time are written as

Electron Density

$$\frac{d}{dt}N_e(r,\tau) = S(r,\tau) - K_1(r) \cdot N_e(r,\tau) - K_2 \cdot N_e(r,\tau) \cdot N_+(r,\tau) \quad (3.41)$$

Positive Ion Density

$$\frac{d}{dt}N_+(r,\tau) = S(r,\tau) - K_2 \cdot N_e(r,\tau) \cdot N_+(r,\tau) - K_3(r) \cdot N_+(r,\tau) \cdot N_-(r,\tau) \quad (3.42)$$

Negative Ion Density

$$\frac{d}{dt}N_-(r,\tau) = K_1(r) \cdot N_e(r,\tau) - K_3(r) \cdot N_+(r,\tau) \cdot N_-(r,\tau) \quad (3.43)$$

where  $N_e(r,\tau)$  -electron density ( $m^{-3}$ )

$N_+(r,\tau)$  -positive ion density ( $m^{-3}$ )

$N_-(r,\tau)$  -negative ion density ( $m^{-3}$ )

$S(r,\tau)$  -secondary electron source density ( $m^{-3} \cdot sec^{-1}$ )

$K_1(r)$  -attachment rate constant ( $sec^{-1}$ )

(proportional to air density squared)

$k_2$  -dissociative recombination rate constant ( $m^3/sec$ )

$K_3(r)$  -neutralization rate constant ( $m^3/sec$ )

(proportional to air density)

The secondary electron source density is calculated at intervals equal to the electric field retarded time step. Its value is assumed to be a linear function of time between evaluations. The first derivatives

with respect to retarded time are replaced by a forward difference approximation. The numerical method used to solve the air chemistry differential equations are written as

Electron Density

$$N_e(r, \tau_{n+1}) = N_e(r, \tau_n) + [S(r, \tau_n) - K_1(r) \cdot N_e(r, \tau_n) - K_2 \cdot N_e(r, \tau_n) \cdot N_+(r, \tau_n)] \cdot \Delta\tau \quad (3.44)$$

Positive Ion Density

$$N_+(r, \tau_{n+1}) = N_+(r, \tau_n) + [S(r, \tau_n) - K_2 \cdot N_e(r, \tau_n) \cdot N_+(r, \tau_n) - K_3(r) \cdot N_+(r, \tau_n) \cdot N_-(r, \tau_n)] \cdot \Delta\tau \quad (3.45)$$

Negative Ion Density

$$N_-(r, \tau_{n+1}) = N_-(r, \tau_n) + [K_1(r) \cdot N_e(r, \tau_n) - K_3(r) \cdot N_+(r, \tau_n) \cdot N_-(r, \tau_n)] \cdot \Delta\tau \quad (3.46)$$

where  $\Delta\tau$  -retarded time increment

$$\tau_n = n \cdot \Delta\tau$$

The retarded time increment is one hundredth the size of the increment used for the electric field.

The rate constant for electron attachment is a function of the air density, the electric field strength and the water vapor. The empirical fit for the rate constant was developed by Longley and Longmire (Ref 11) and employs cgs units. The electric field (volts/meter) is converted to electrostatic units per atmosphere. The equations were modified to take

advantage of an exponential atmosphere. The equations for the empirical fit are written as

$$\epsilon = 3.331 \times 10^{-5} \cdot E \cdot \text{EXP}(\text{ALT}/7000) \quad (3.47)$$

where E -electric field (volts/meter)  
 ALT -altitude (meters)  
 $\epsilon$  -electric field (esu/atmosphere)

For  $\epsilon < \epsilon_1$

$$\epsilon_0 = \sqrt{(1+2.457 \cdot p^{0.834})} \quad (3.48)$$

For  $\epsilon_1 < \epsilon < \epsilon_2$

$$\epsilon_0 = [(0.1185 \cdot p^{1.668} + \epsilon)^{0.5} - 0.3442 \cdot p^{0.834}]^2 \quad (3.49)$$

For  $\epsilon_2 < \epsilon$

$$\epsilon_0 = -1.195 \cdot p^{0.834} \quad (3.50)$$

where

$$\epsilon_1 = 0.07853 \cdot (1+2.457 \cdot p^{0.834}) \quad (\text{esu/atmosphere}) \quad (3.51)$$

$$\epsilon_2 = 3.015 + 1.195 \cdot p^{0.834} \quad (\text{esu/atmosphere}) \quad (3.52)$$

p -percent of water vapor

Rate constant for electron attachment ( $\text{sec}^{-1}$ )

$$K = (1-0.01 p)[1+0.344 \cdot p] A_3 + A_2 \quad (3.53)$$

where  $A_2$  -two body attachment rate ( $\text{sec}^{-1}$ )

$$A_2 = 1.22 \times 10^8 \cdot \text{EXP}(-\text{ALT}/7000) \cdot \text{EXP}(-21.15/\epsilon_0) \quad (3.54)$$



$A_3$  -three body attachment rate ( $\text{sec}^{-1}$ )

$$A_3 = \frac{1 \times 10^8 \cdot \text{EXP}(-2 \text{ ALT}/7000) \cdot (0.62 + 800 \epsilon_0^2)}{1 + 1 \times 10^3 \cdot \epsilon^2 \cdot [\epsilon_0 \cdot (1 + 0.03 \cdot \epsilon_0^2)]^{0.33}} \quad (3.55)$$

The rate constant for dissociative recombination is independent of air density and has a value

$$K_2 = 2 \times 10^{-13} \text{ (m}^3/\text{sec)} \quad (3.56)$$

The rate constant for neutralization is proportional to air density. The equation for the rate constant is written as

$$K_3 = \text{EXP}(-\text{ALT}/7000) \text{ (m}^3/\text{sec)} \quad (3.57)$$

The time scale that EMPFRE works with is of the order of  $1 \times 10^{-7}$  seconds. For this time scale, electron attachment is the key process; therefore, more effort is concerned with modeling this process.

### ELECTRON MOBILITY AND CONDUCTIVITY

The electron mobility is a function of air density, electric field strength and water vapor. The empirical fit for electron mobility was developed by Longley and Longmire (Ref 16). The electron mobility is written as

$$\mu_e = \frac{3.331 \times 10^{-7} \cdot \mu_a}{1 - 0.01 p + 0.01 \cdot p \cdot R} \quad (3.58)$$

where

$$\mu_a = 1 \times 10^6 \cdot \text{EXP}(\text{ALT}/7000) \cdot \frac{16.8 + \epsilon_0}{0.63 + 26.7 \cdot \epsilon_0} \quad (3.59)$$

$$R = 1.55 + 210 / (1 + 11.8 \cdot \epsilon_0 + 7.2 \cdot \epsilon_0^2) \quad (3.60)$$

p - percent of water vapor

The parameter ( $\epsilon_0$ ) is defined in the section on air chemistry. Table 3.3 provides values of the electron mobility as a function of altitude and electric field strength with no water vapor.

The positive and negative ion mobility is approximated by

$$\mu_i = 2.5 \times 10^{-4} \cdot \text{EXP}(\text{ALT}/7000) \text{ (m}^2/\text{volt/sec)} \quad (3.61)$$

The conductivity (amps/m/volt) is written as

$$\delta(r, \tau) = [N_e(r, \tau) \cdot \mu_e(r, \tau) + (N_+(r, \tau) + N_-(r, \tau)) \cdot \mu_i(r)] \cdot q \quad (3.62)$$

where  $N_e(r, \tau)$  - secondary electron density ( $\text{m}^{-3}$ )

$N_+(r, \tau)$  - positive ion density ( $\text{m}^{-3}$ )

$N_-(r, \tau)$  - negative ion density ( $\text{m}^{-3}$ )

q - electron charge ( $1.6 \times 10^{-19}$  coulombs)

For early time, the conductivity is primarily a function of secondary electron density and mobility; therefore, more effort is used to model electron mobility than for ion mobility.

SOLVING FOR THE ELECTRIC FIELDS

Three differential equations are solved to find the components of the electric field:

For the radial electric field ( $E_r$ )

$$\frac{\delta E_r}{\delta \tau} = - \frac{J_r + \sigma \cdot E_r}{\epsilon_0} \quad (3.63)$$

For the theta electric field ( $E_\theta$ )

$$\frac{\delta E_\theta}{\delta r} = - \frac{E_\theta}{r} - \frac{\mu_0 \cdot c}{2} \cdot (J_\theta + \mu \cdot E_\theta) \quad (3.64)$$

For the phi electric field ( $E_\phi$ )

$$\frac{\delta E_\phi}{\delta r} = - \frac{E_\phi}{r} - \frac{\mu_0 \cdot c}{2} \cdot (J_\phi + \mu \cdot E_\phi) \quad (3.65)$$

where  $\tau$  -retarded time in seconds

$J$  -radial Compton current density

$\epsilon_0$  -permittivity of vacuum

( $8.854 \times 10^{-12}$  farad/m)

$\sigma$  -conductivity

$\mu_0$  -permeability of vacuum ( $4\pi \times 10^{-7}$  Henry/m)

$c$  -speed of light ( $2.99 \times 10^8$  m/sec)

E-field (V/m)	ALTITUDE					
	0 Km	1 Km	10 Km	20 Km	40 Km	60 Km
0	2.389	2.756	9.968	41.59	724.2	12609
0.5	2.388	2.754	9.950	41.29	644.8	4981.
5	2.379	2.742	9.796	38.80	365.2	1460.
50	2.293	2.629	8.539	25.74	114.1	464.4
500	1.735	1.929	4.385	8.899	33.80	272.1
5K	0.687	0.735	1.315	2.539	16.71	247.8
50K	0.195	0.208	0.404	1.062	14.35	145.3

Table 3.3 Electron Mobility

These differential equations were solved numerically with a fourth order Runge-Kutta technique. The differential equations are of the form

$$\frac{\delta E}{\delta x} = f(x, E) \quad (3.66)$$

The Runge-Kutta method solves equation 3.66 for  $E_1$  at  $x_0 + \Delta x$  when the value of  $E_0$  is known at  $x_0$  (Ref 5). The fourth order Runge-Kutta technique generates 4 estimates of the change in  $E$  over the interval  $\Delta x$ :

$$K1 = \Delta x \cdot f(x_0, E_0) \quad (3.67)$$

$$K2 = \Delta x \cdot f(x_0 + \Delta x/2, E_0 + K1/2) \quad (3.68)$$

$$K3 = \Delta x \cdot f(x_0 + \Delta x/2, E_0 + K2/2) \quad (3.69)$$

$$K4 = \Delta x \cdot f(x_0 + \Delta x, E_0 + K3) \quad (3.70)$$

The value of  $E_1 = E(x_0 + \Delta x)$  is approximated by

$$E_1 = E_0 + (\Delta x/6) \cdot (K1 + 2 \cdot (K2 + K3) + K4) \quad (3.71)$$

The Runge-Kutta method is convenient for two reasons. First, the method requires one value of the electric field to start the computation. Second, the independent variable increment can be varied during the computation. The drawback is that the error is difficult to estimate (Ref 13:74). When the second derivative of the electric field with respect to the independent variable ( $x$ ) becomes large, the independent variable increment must be reduced to avoid instabilities and reduce error.

Two scenarios lead to instabilities in the Runge-Kutta technique for this application.

1) Solving for the radial electric field differential equation in early time, the second derivative with respect to time will be positive and can become large. An instability occurs when the initial time increment causes a large error in  $K_1$  (too small). The value of  $K_2$  (too large) over corrects for  $K_1$ . The value of  $K_3$  (too small) over corrects for  $K_2$  and becomes even smaller than  $K_1$ . Finally  $K_4$  (too large) over corrects for  $K_3$  and becomes larger than  $K_2$ . The estimates of the increase in the radial electric field ( $K_1$ - $K_4$ ) will oscillate when the second derivative is not equal to zero. These oscillations are reduced by decreasing the increment when the second derivative becomes large.

2) Solving for the transverse electric field as saturation is reached, the second derivative with respect to position will be negative and can become large. An instability occurs when the initial position increment causes a large error in  $K_1$  (too large). The value of  $K_2$  (too small) over corrects for  $K_1$ . The value of  $K_3$  (too large) over corrects for  $K_2$  and becomes even larger than  $K_1$ . Finally  $K_4$  (too small) over corrects for  $K_3$  and becomes smaller than  $K_2$ . The estimates of the increase in the transverse electric field ( $K_1$ - $K_4$ ) will oscillate when the second derivative is not equal to zero. These oscillations are reduced by decreasing the position increment when the second derivative becomes large.

Initial development of EMPFRE used as a fixed independent variable increment to solve the differential equations. This method was unstable

for gamma yields that drove the electric field to saturation because the second derivative with respect to the independent variable becomes large at that point. Instabilities are forecasted by monitoring the behavior of K1 thru K4.

When the oscillations grow, the independent variable increment is reduced and the procedure is repeated. Three tests were used to forecast instabilities. When one of the following conditions were met, the independent variable increment was halved:

$$1) \quad K1^2 > 2 K2^2 \quad (3.72)$$

$$2) \quad K2^2 > 2 K1^2 \quad (3.73)$$

$$3) \quad K1 K4 < 0 \quad (3.74)$$

An instability observed without these checks is modeled with a program designed to study the behavior of K1-K4 and the results are presented in Table 3.4. The effectiveness of these checks is demonstrated with Table 3.5 by observing K1-K4, before and after the checks are implemented.

SOLVING FOR THE RADIAL FIELD. The radial electric field is solved by applying a fourth order Runge-Kutta technique to the differential equation for the radial electric field (Eq 3.63). The independent variable is retarded time. Equation 3.66 becomes

$$\frac{dE_r}{dt} = f(\tau, E_r) \quad \text{with } r = \text{const} \quad (3.75)$$

R (Km)	K1	K2	K3 (Volts/Meter)	K4	J/SIGMA	E-FIELD
64					9524.	9394.
66	28.7	25.6	29.9	11.8	9524.	9418.
68	25.7	16.5	31.5	-20.5	9524.	9435.
70	31.4	0.61	59.6	-155.	9524.	9435.
72	92.2	-81.4	299.	-1245.	9524.	9315.
74	707.	-969.	3126.	-1.5E4	9525.	7622.
76	9476.	-1.5E4	4.9E4	-2.5E5	9525.	-2.2E4
78	1.7E5	-2.8E5	9.3E5	-4.8E6	9527.	-5.8E5

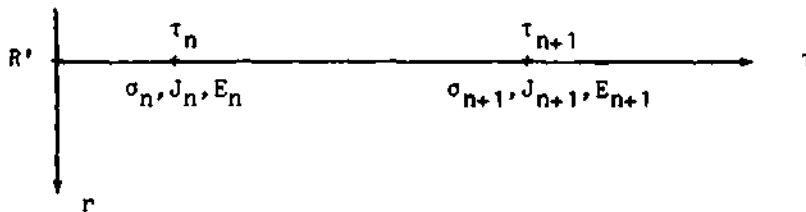
Table 3.4 Runge-Kutta Without Automatic Step Reduction

R (Km)	K1	K2	K3 (Volts/Meter)	K4	J/SIGMA	E-FIELD
64					9524.	9394.
66	28.7	25.6	29.9	11.8	9524.	9418.
68	10.6	8.97	10.3	7.08	9524.	9440.
70	7.60	6.52	7.60	4.90	9524.	9455.
72	5.67	4.69	5.80	3.00	9524.	9465.
74	4.35	3.21	4.63	1.09	9525.	9472.
76	1.13	1.10	1.12	1.07	9525.	9478.
78	0.54	0.53	0.54	0.52	9526.	9480

Table 3.5 Runge-Kutta With Automatic Step Reduction



The radial electric field is solved by stepping along retarded time with position held constant. The ray below symbolizes this displacement.



where  $J_n, J_{n+1}$  -radial Compton current for  $\tau_n, \tau_{n+1}$  at  $R'$   
 $\sigma_n, \sigma_{n+1}$  -conductivity for positions  $\tau_n, \tau_{n+1}$  at  $R'$   
 $E_n$  -radial electric field for position  $\tau_n$   
 $E_{n+1}$  -unknown radial electric field for position  $\tau_{n+1}$

EMPFRE generates values of the current and conductivity for positions  $\tau_n$  and  $\tau_{n+1}$  but the Runge-Kutta method requires an additional value at the mid point. The current and conductivity are assumed to be linear across  $\Delta\tau$ ; therefore, the mid point values are the linear averages of the values for positions  $\tau_n$  and  $\tau_{n+1}$ . If the retarded time step is reduced, additional values are generated. Equations that generate the estimates of the change in  $E_r$  over the interval become

$$K1 = - \frac{\Delta\tau}{\epsilon_0} (J_n + \sigma_n \cdot E_n) \quad (3.76)$$

$$K2 = - \frac{\Delta\tau}{\epsilon_0} \left[ \frac{(J_n + J_{n+1})}{2} + \frac{(\sigma_n + \sigma_{n+1})}{2} \right] \cdot (E_n + K1/2) \quad (3.77)$$

$$K3 = - \frac{\Delta\tau}{\epsilon_0} \left[ \frac{(J_n + J_{n+1})}{2} + \frac{(\sigma_n + \sigma_{n+1})}{2} \right] \cdot (E_n + K2/2) \quad (3.78)$$

$$K4 = - \frac{\Delta \tau}{\epsilon_0} [J_{n+1} + \sigma_{n+1} \cdot (E_n + K3)] \quad (3.79)$$

The unknown radial electric field at  $r_{n+1}$  is approximated by

$$E_{n+1} = E_n + [K1 + 2(K2 + K3) + K4] / 6 \quad (3.80)$$

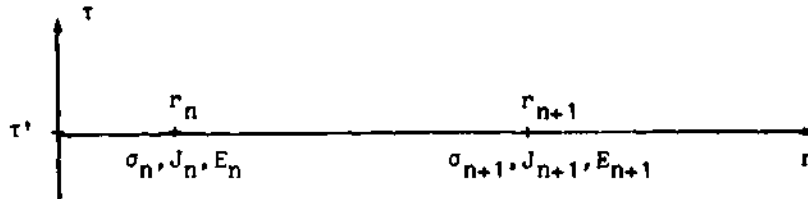
The radial electric field is assumed to be zero for all  $R'$  at  $r=0$ .

SOLVING FOR THE TRANSVERSE ELECTRIC FIELD. The transverse electric fields are solved by applying a fourth order Runge-Kutta technique to the differential equation for the theta or phi electric fields (Eqs 3.64 or 3.65). The theta and phi electric fields are considered together in this section because the differential equations are identical in form and the method outlined in this section applies to either.

The independent variable is the spatial position  $R$ . Equation 3.66 becomes

$$\frac{\delta E_T}{\delta r} = f(r, E_T) \quad (3.81)$$

A transverse electric field is solved by stepping along the slant range with retarded time held constant. The ray below symbolizes this displacement:



where

$J_n, J_{n+1}$  - a transverse Compton current for  $r_n, r_{n+1}$  at  $\tau'$

$\sigma_n, \sigma_{n+1}$  - conductivity for  $r_n, r_{n+1}$  at  $\tau'$

$E_n$  - a transverse electric field for  $r_n$

$E_{n+1}$  - unknown transverse electric field for  $r_{n+1}$

EMPFRE generates values of the current and conductivity for positions  $r_n$  and  $r_{n+1}$ , but the Runge-Kutta method requires an additional value at the mid point. The current and conductivity are assumed to be linear across  $\Delta r$ ; therefore, the midpoint values are the linear averages of the values for the positions  $r_n$  and  $r_{n+1}$ . If the spatial step is reduced, additional values are generated. Equations that generate the estimates of the change in  $E_T$  over the integral  $\Delta r$  become

$$K1 = -\Delta r \cdot \frac{1}{r} + \frac{\mu_0 \cdot c \cdot \sigma_n}{2} \cdot E_n + \frac{\mu_0 \cdot c}{2} \cdot J_n \quad (3.82)$$

$$K2 = -\Delta r \cdot \frac{1}{r_n + \Delta r / 2} + \frac{\mu_0 \cdot c \cdot (\sigma_n + \sigma_{n+1})}{4} \cdot (E_n + K1/2) + \frac{\mu_0 \cdot c}{4} \cdot (J_n + J_{n+1}) \quad (3.83)$$

$$K3 = -\Delta r \cdot \frac{1}{r_n + \Delta r/2} + \frac{\mu_0 \cdot c \cdot (\sigma_n + \sigma_{n+1})}{4} \cdot (E_n + K2/2) + \frac{\mu_0 \cdot c}{4} (J_n + J_{n+1}) \quad (3.84)$$

$$K4 = -\Delta r \cdot \frac{1}{r_{n+1}} + \frac{\mu_0 \cdot c \cdot \sigma_{n+1}}{2} (E_n + K3) + \frac{\mu_0 \cdot c}{2} J_{n+1} \quad (3.85)$$

The unknown transverse electric field for  $R_{n+1}$  is approximated by

$$E_{n+1} = E_n + (K1 + 2 \cdot (K2 + K3) + K4) / 6 \quad (3.86)$$

The transverse electric field is assumed to be zero above the absorption region for all  $\tau$ .

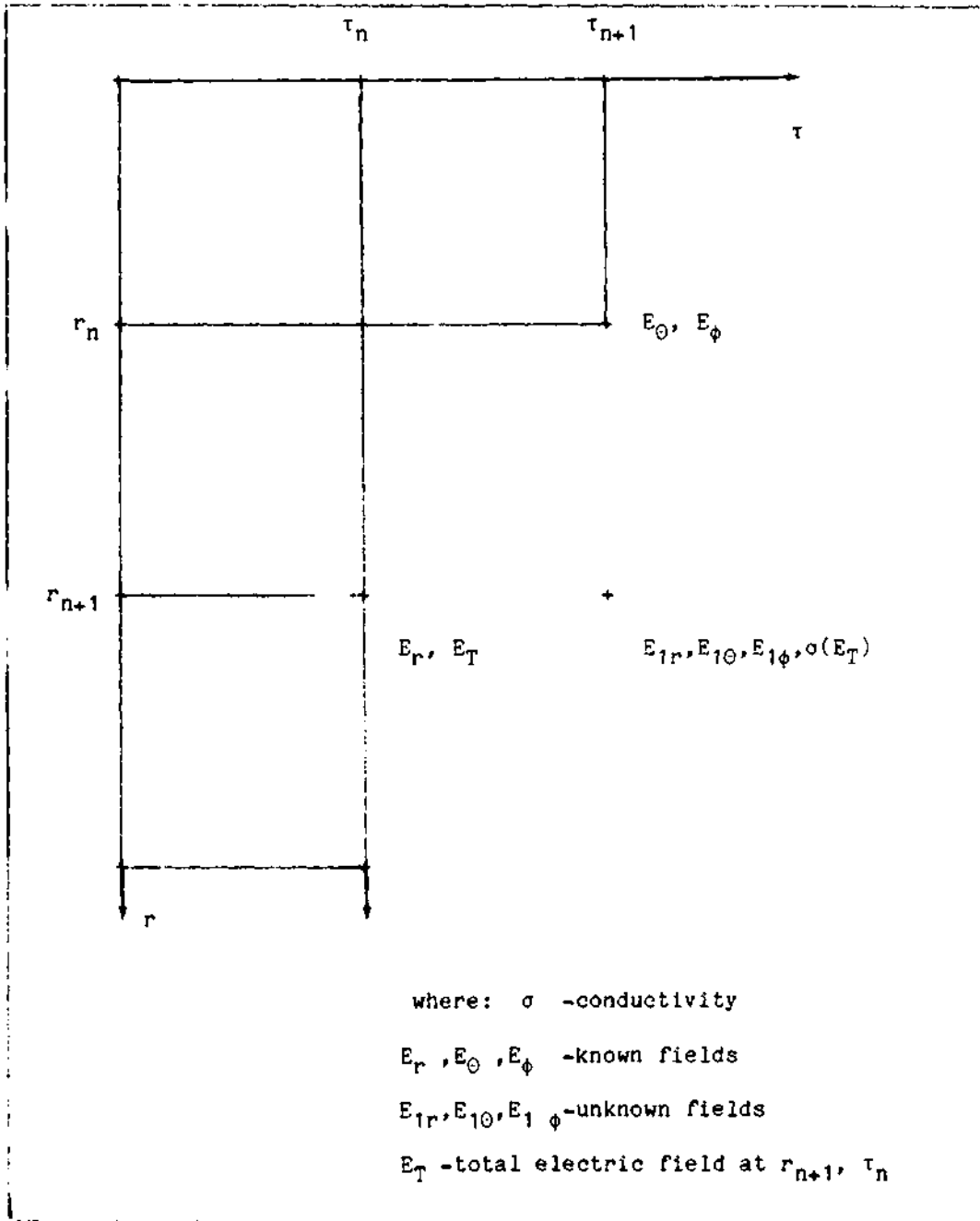


Figure 3.3 Stepwise Procedure in the Solution of the Differential Equations (Ref 5)

COMPUTATIONAL PROCEDURE. The electron mobility is a function of the total electric field. The conductivity is a function of electron mobility; therefore, the three differential equations for the electric field are dependent and must be solved simultaneously. The procedure for solving for the electric field is symbolized in Figure 3.3. An estimate of the electric field at  $r_{n+1}, \tau_{n+1}$  must be made to calculate the conductivity. The conductivity at  $r_{n+1}, \tau_{n+1}$  is based on the total electric field ( $E_T$ ) from  $r_{n+1}, \tau_n$ . This direction was chosen because the number of retarded time steps is large compared to the number of positional steps.

The fields along  $\tau_n$  are solved for all  $r$ . The fields along  $\tau_{n+1}$  have been solved from the top of the absorption region down to  $r_n$ . The transverse fields at  $r_{n+1}, \tau_{n+1}$  are solved from the fields at  $r_n, \tau_{n+1}$ . The radial field at  $r_{n+1}, \tau_{n+1}$  are solved from the radial field at  $r_{n+1}, \tau_n$ . This procedure is repeated until the lower limit of the absorption region is reached. The transverse components of the EMP will attenuate as  $1/r$  as it propagates to the ground.

## FOURIER TRANSFORM

The formula for the Fourier transform is written as

$$g(\alpha) = \frac{1}{\sqrt{2\pi}} \int_{-\infty}^{\infty} E(\tau) \cdot \text{EXP}(-i\alpha\tau) d\tau \quad (3.87)$$

or

$$g(\alpha) = \frac{1}{\sqrt{2\pi}} \int_{-\infty}^{\infty} E(\tau) \cdot [\text{COS}(\alpha\tau) - i \cdot \text{SIN}(\alpha\tau)] d\tau \quad (3.88)$$

where  $g(\alpha)$  - Fourier transform  
 $\alpha$  - angular frequency ( $\text{sec}^{-1}$ )

The Fourier transform subroutine solves the following integrals using Simpson's rule:

$$g(\alpha) = \int_{-\infty}^{\infty} \frac{E(\tau)}{\sqrt{2\pi}} \cdot \text{COS}(\alpha\tau) d\tau - i \int_{-\infty}^{\infty} \frac{E(\tau)}{\sqrt{2\pi}} \cdot \text{SIN}(\alpha\tau) d\tau \quad (3.89)$$

The magnitude of the Fourier transform is found by multiplying by its complex conjugate and taking the square root of the product:

$$|g(\alpha)| = [g(\alpha) \cdot g(\alpha)]^{0.5} \quad (3.90)$$

A relationship between the energy associated with a frequency band and the Fourier transform is found by applying Parseval's theorem:

$$\int_0^{\infty} |g(\alpha)|^2 d\alpha = \int_0^{\infty} |E(\tau)|^2 d\tau \quad (3.91)$$

The energy ( $\epsilon$ ) associated with the electromagnetic pulse is equal to

$$\epsilon = \int_0^{\infty} \frac{|E(\tau)|^2}{\eta} d\tau \quad (3.92)$$

where  $\eta = (\mu_0/\epsilon_0)$

Substituting this expression of energy into Parseval's theorem relates the Fourier transform to energy:

$$\epsilon = \int_0^{\infty} \frac{|g(\alpha)|^2}{\eta} d\alpha \quad (3.93)$$

The continuous Fourier transform is evaluated at 30 discrete values of angular frequency. The energy associated with a frequency is found by

$$\text{Energy (J-sec/m}^2) = \frac{|g(\alpha)|^2}{\eta} \quad (3.94)$$

To save execution time, the late time electric fields are not calculated. Terminating the integral for the Fourier transform at the last value for the electric field  $E(\tau_N)$ , would produce an artificial transient. The abrupt termination would effect the frequency content. The Fourier transform subroutine fits a sine function for the electric field from  $E(\tau_N)$  to an artificial termination at  $E(\tau_E)=0$ . The slope of



the sine function is matched to the slope the electric field at  $\tau_n$ . The angular frequency for the sine function ( $\omega$ ) is found by

$$\omega = \frac{E(\tau_{n-1}) - E(\tau_n)}{A \cdot \Delta\tau} \quad (3.95)$$

where  $\Delta\tau$  -retarded time step

$A$  -amplitude of the sine function

For  $\tau > \tau_n$ , the electric field is set to

$$E(\tau) = A[1 - \text{SIN}(\omega \cdot (\tau - \tau_n))] \quad (3.96)$$

The upper limit of the integral becomes

$$\tau = \tau_n + \pi / (2\omega) \quad (3.97)$$

where  $E(\tau_E) = 0$  and  $\left. \frac{dE(\tau)}{d\tau} \right|_{\tau_E} = 0$

#### IV. ANALYSIS OF NUMERICAL TECHNIQUE

The solution of Maxwell's equations for high altitude EMP in EMPFRE involves several trade-offs between accuracy and computer resources. The purpose of EMPFRE is to show the effects burst, parameters such as geometry and gamma output, on the frequency content of the EMP. A small accumulative error is accepted because the basic cause and effect relationships will be insensitive to the accumulative error associated with EMPFRE. An effort is made to identify exceptions to this rule. Parametric studies are made to determine optimum compromises for each trade-off. A review of these studies is made here to provide insight about the error accepted in EMPFRE. The input parameters for the base case are listed below:

$$X=0 \text{ Meters} \quad (4.1)$$

$$Y=0 \text{ Meters} \quad (4.2)$$

$$Z=0 \text{ Meters} \quad (4.3)$$

$$HOB=100 \text{ Kilometers} \quad (4.4)$$

$$Y_{\gamma}=0.1 \text{ Kilotons} \quad (4.5)$$

$$E_{\gamma}=2 \text{ MeV} \quad (4.6)$$

$$B=5.5 \times 10^{-5} \text{ Webers/Meter} \quad (4.7)$$

$$\text{Dip Angle}=0 \text{ Degrees} \quad (4.8)$$

$$NDEL R=50 \quad (4.9)$$

$$DEL T=5 \times 10^{-10} \text{ Seconds} \quad (4.10)$$

These parameters are held constant while the parameter in question is varied. The accumulative error is estimated by using a sample HEMPB (High Altitude EMP Program used at the Air Force Weapons Lab) solution as a

test case. The comparison to HEMPB is made in Appendix A.

#### COMPTON ELECTRON RANGE

The Compton electron range determines the secondary electron production rate in EMPFRE. The program assumes a linear energy loss over the life of the Compton electron. Therefore, the secondary electron production rate is proportional to the total local Compton current. With this model, changing the effective electron range for a fixed Compton electron energy will impact the secondary electron production rate. The physical effect being observed by varying the Compton electron range is changing the secondary electron production rate.

The mean forward range for the Compton electrons is approximated by a relationship from the Radiological Health Handbook (Ref 16:29). The estimate of the electron range for a 2 MeV gamma ray is 4.06 meters at sea level. The Compton electron range is varied from 2.03 to 6.09 meters. Figure 4.1 shows the variation in the resulting EMP. Figure 4.2 shows the variation introduced into the frequency content.

The estimate of the mean forward range of the Compton electron impacts the secondary electron density and the conductivity. The lifetime of the Compton electron is calculated from the initial electron velocity and the forward range; therefore, an increase in the forward range will increase the Compton electron lifetime. The number of secondary electrons produced per Compton electron is fixed at  $1/33eV$ . The secondary electron production rate is inversely proportional to the Compton electron life-time. An increase in the Compton electron life-time will decrease the secondary electron production rate and density at

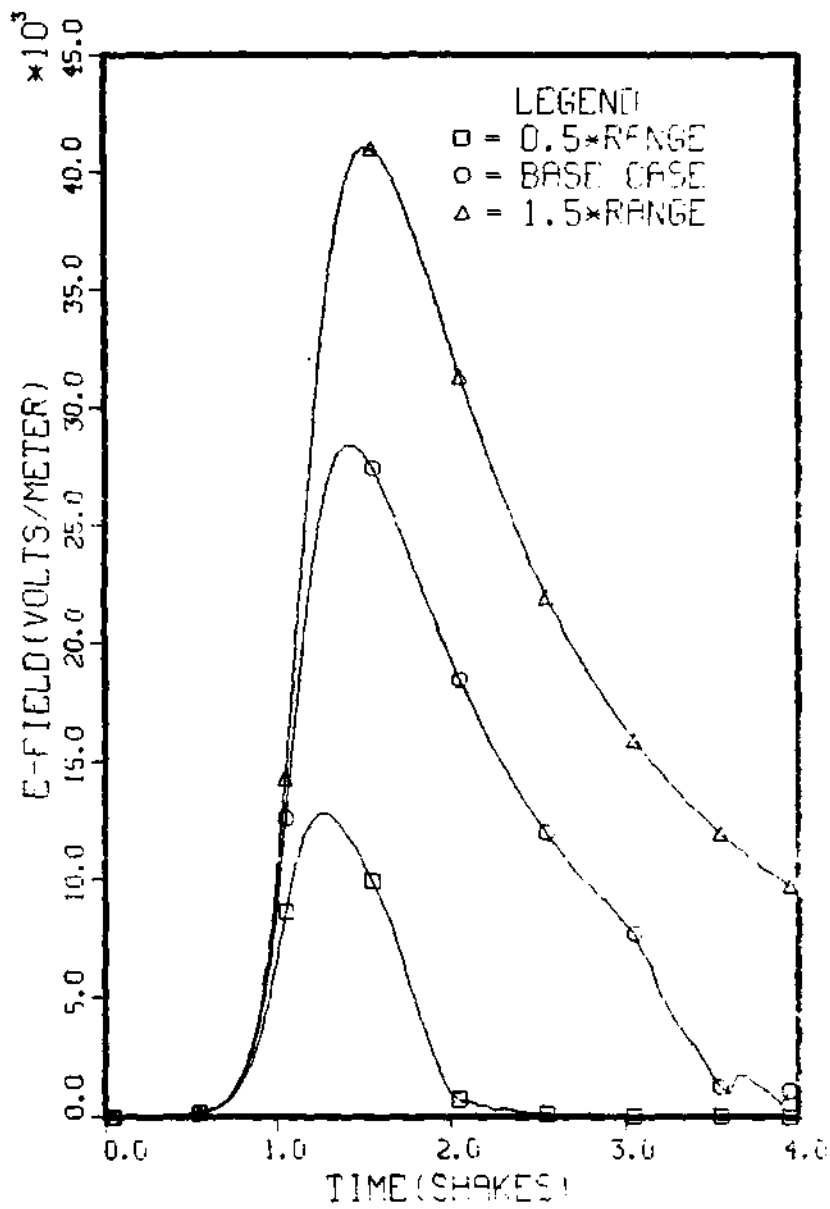


Figure 4.1 Electric Field, Compton Electron Range

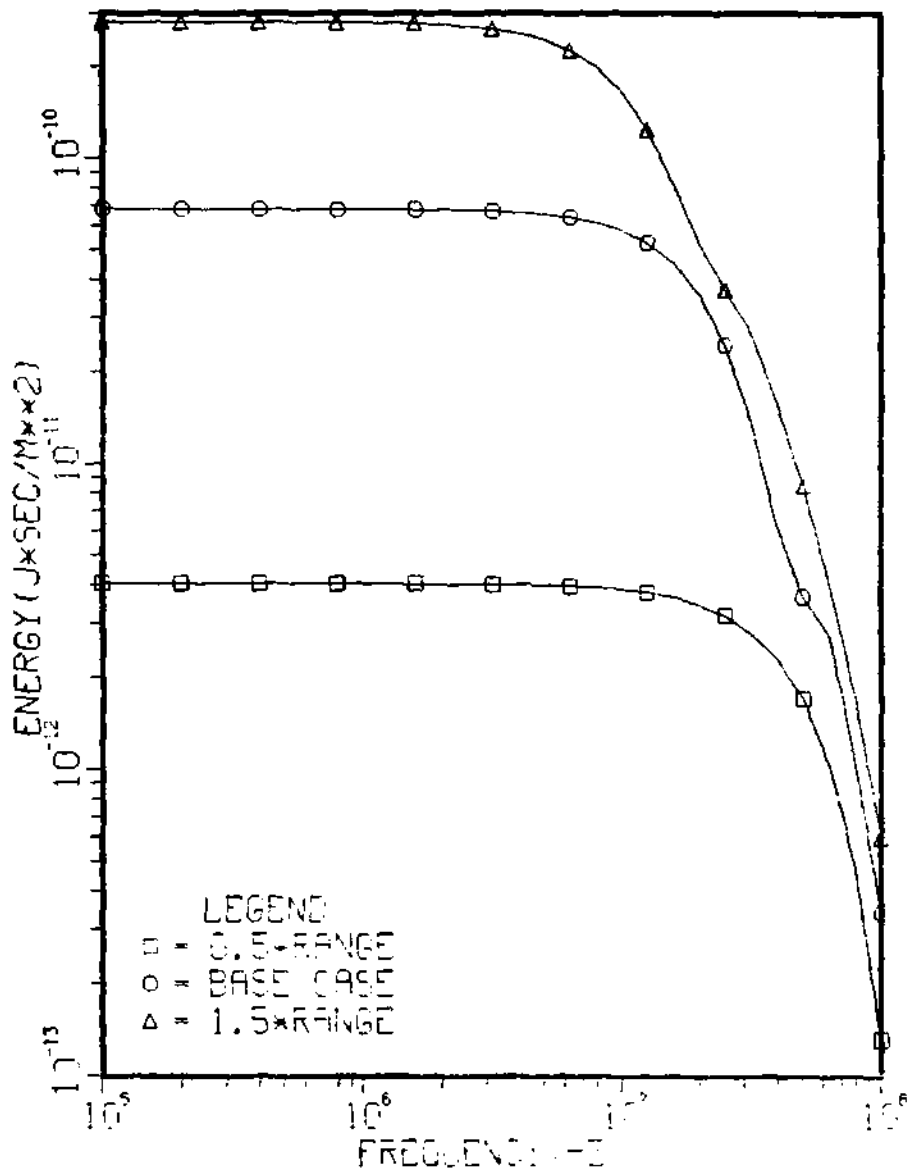


Figure 4.2 Frequency Profile, Compton Electron Range

early times. The resulting decrease in conductivity will cause the EMP to rise faster and decay slower. The resulting electric fields are larger and the pulse is broadened.

The change in the electric fields has an impact on the frequency profile of the EMP. The threshold frequency is defined as the frequency where the energy begins to drop from its constant value for low frequencies. The energy increases with Compton range but the threshold frequency decreases due to broadening of the pulse. An error in the Compton electron range has a large impact on the resulting EMP.

#### SPATIAL AND TIME INCREMENTS

A fourth order Runge-Kutta numerical technique is used to solve the differential equations for the electric fields. The application of this method is discussed in Chapter III. The solution becomes unstable when the spatial (for the transverse field) or time (for the radial field) increments become large. This problem is corrected by internal checks that halve the increment if instabilities are predicted. The remaining error is due to the discrete parameter updates.

The key parameter is the electron mobility. The electron mobility is a function of the electric field and altitude. The electric field is approximated by the electric field from the last time step at that position. See Figure 3.6 for a stepwise procedure in the solution of the electric field. The variation in the EMP associated with increasing the time increment is demonstrated by Figure 4.3. The time increment is varied between  $2.5 \times 10^{-10}$  and  $2 \times 10^{-9}$  seconds. Figure 4.4 shows the associated variation in the frequency content.

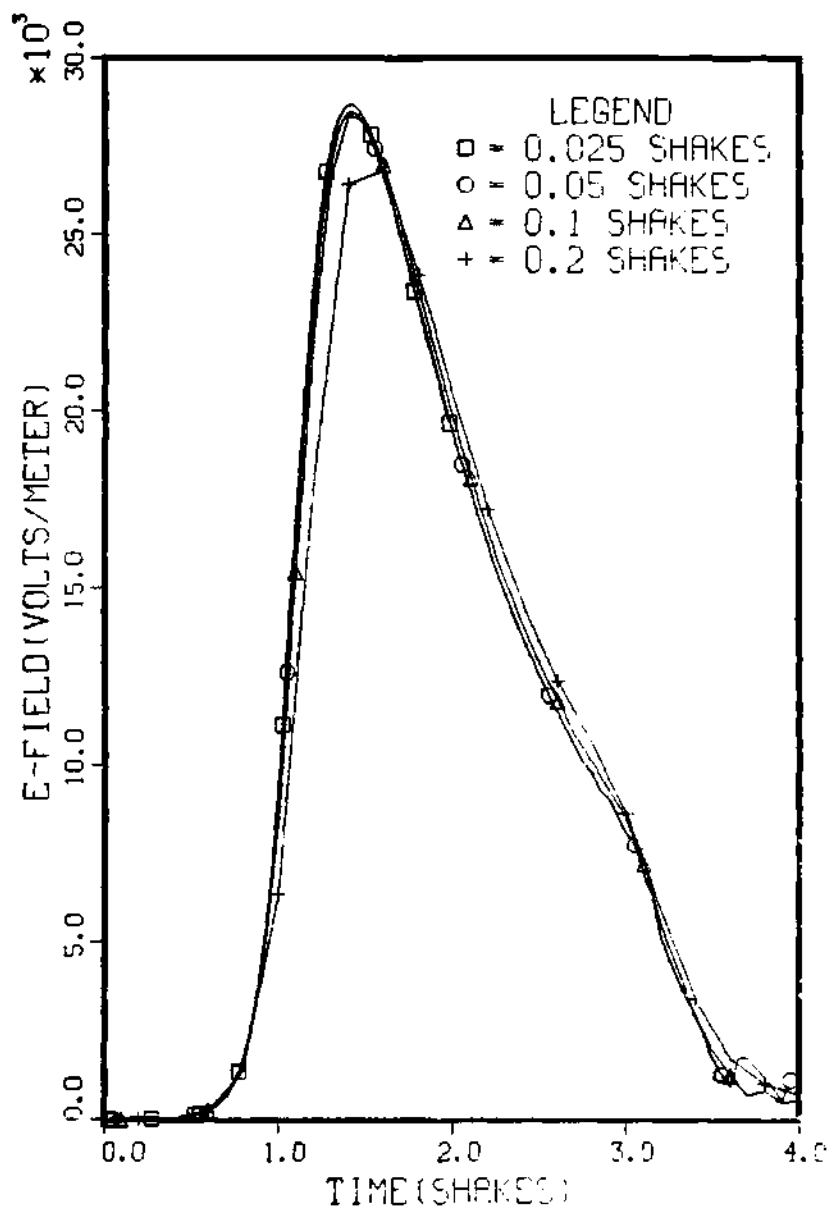


Figure 4.3 Electric Field, Time Step

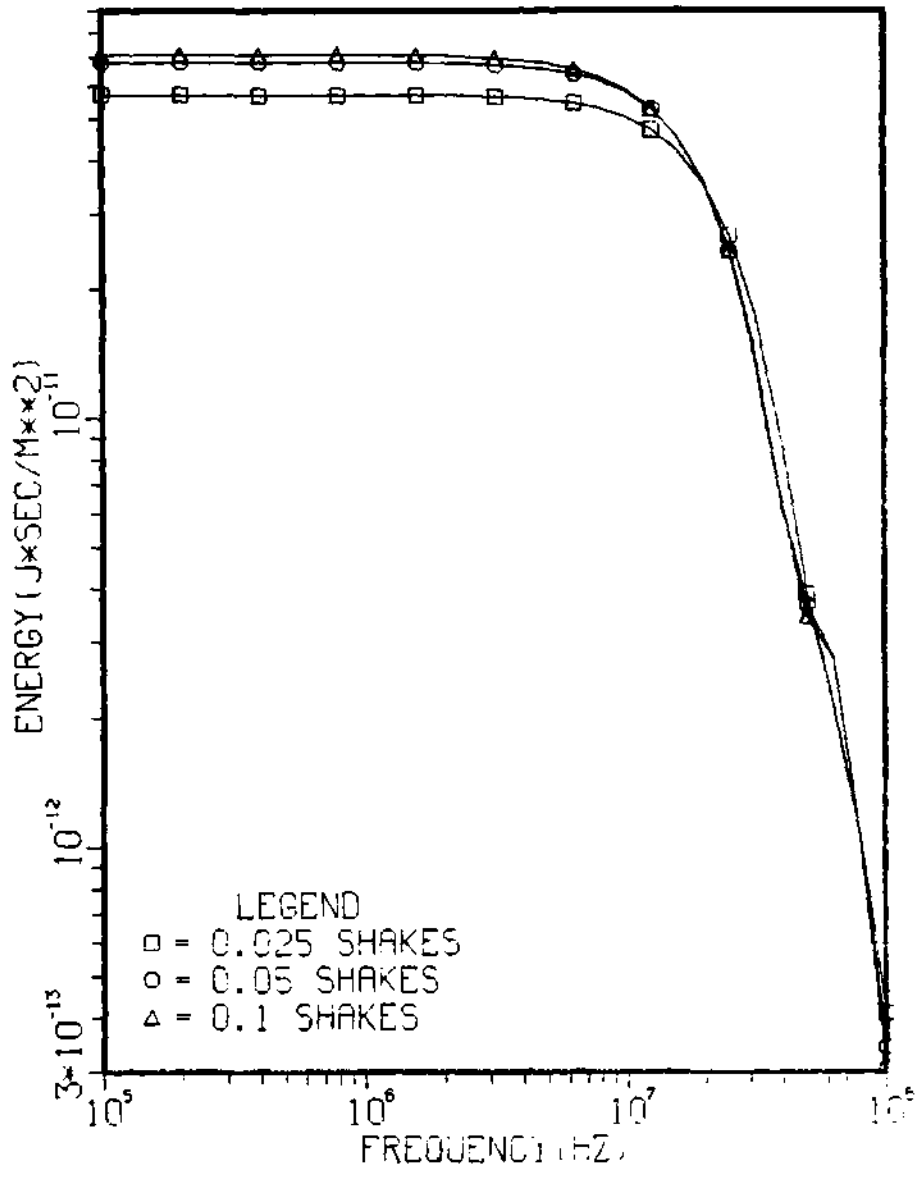


Figure 4.4 Frequency Profile, Time Step



Increases in the spatial increment produce an error because parameters such as Compton currents, secondary electron density and electron mobility will vary across the spatial increment. The variation in the EMP associated with increasing the spatial increment is demonstrated by Figure 4.5. The spatial increment is varied between 25 and 100 steps. Figure 4.6 shows the associated variation in the frequency profile.

#### LORENTZ MODEL

The Lorentz model assumes the secondary electrons are born at thermal equilibrium with the electrons drifting in the local electric field. This approximation is imposed to simplify the calculations but causes EMPRE to underestimate the rise time and peak of the EMP. As a result, the energy associated with the high frequencies are underestimated.

The secondary electrons are born at about 10 eV (Ref 2) and take more than  $1 \times 10^{-8}$  seconds to thermalize from this energy at an altitude of 20 kilometers. By assuming the velocities are isotropic, the secondary electrons are effectively at a higher temperature than proposed by the Lorentz model. A more detailed discussion of this issue is presented in Chapter VI. The lower temperature predicted by the Lorentz model over-estimates the electron mobility because the collision cross sections vary with electron energy. In the Lorentz model, the secondary electron mobility ranges from 2.39 to 0.195  $\text{m}^2/(\text{sec-volt})$  at sea level. A crude way to demonstrate the variation in the EMP associated with the depressed secondary electron temperature is to set an upper limit on electron mobility. The base case uses the Lorentz

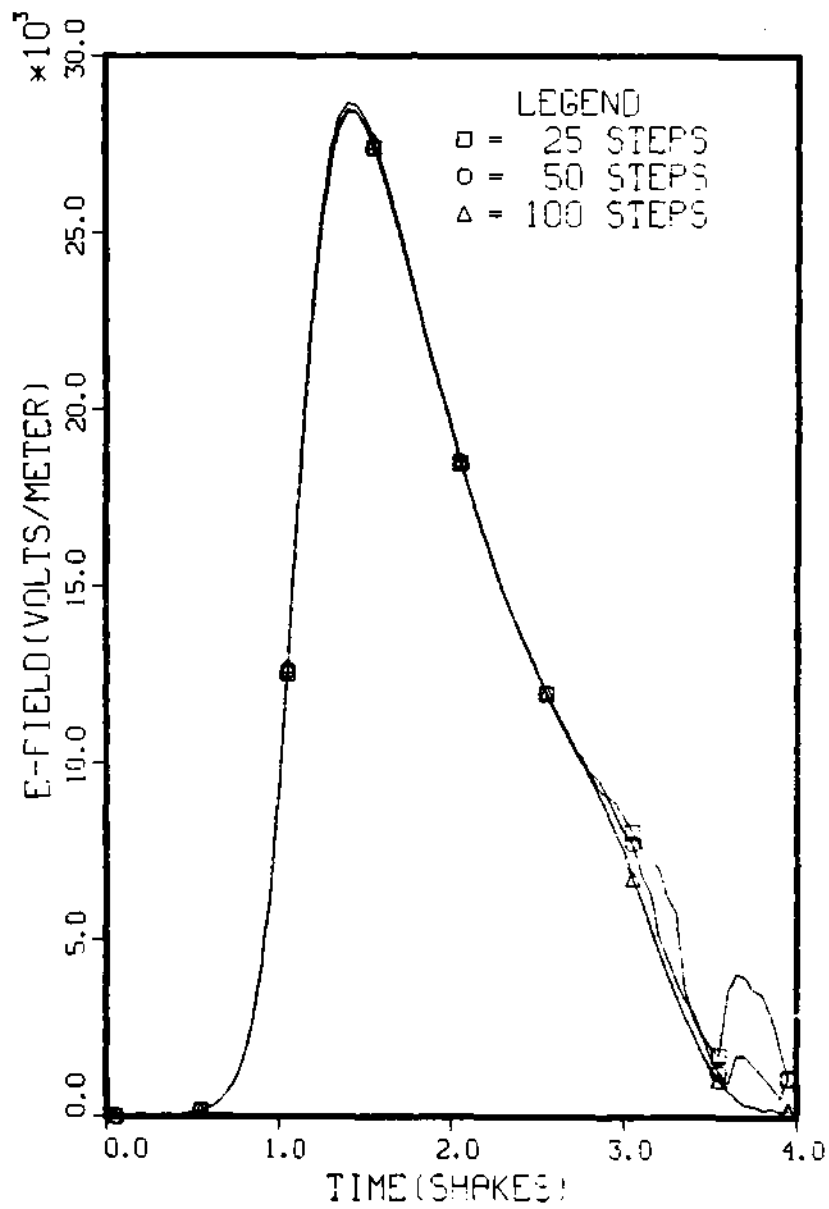


Figure 4.5 Electric Field, Spatial Step

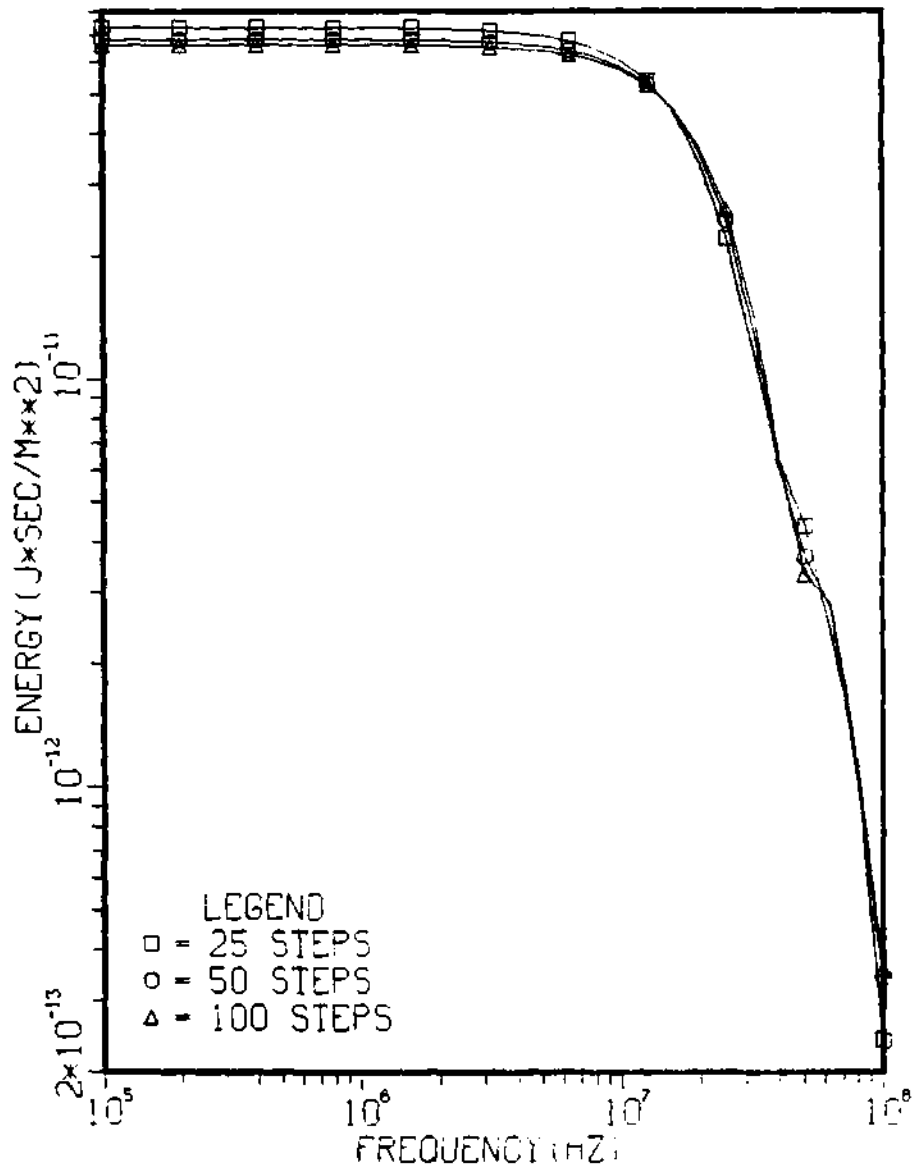


Figure 4.6 Frequency Profile, Spatial Step

Model and the maximum mobility at sea level is varied from the Lorentz model to a maximum mobility of  $0.02 \text{ m}^2/(\text{sec-volt})$  and adjusted for altitude. The variation in the EMP associated with the increase in secondary electron temperature is demonstrated in Figure 4.7. Figure 4.8 shows the associated variation in the frequency content.

#### TRUNCATION OF ELECTRIC FIELD

EMPFRE calculates the electric field for several shakes and then terminates the calculation. Test runs indicate the time step size could be increased after the first few shakes without introducing excessive error. This approach would be appropriate for examining the electric field but not for studying the high frequency characteristics. A decrease in the sampling rate would cause aliasing in an unpredictable manner. Termination of the pulse is accomplished by merging a sine function to it as discussed in Chapter III.

The angular frequency of the sine function is chosen to match the slope of the pulse at termination. The impact of this technique on the Fourier transform is discussed in Appendix A.

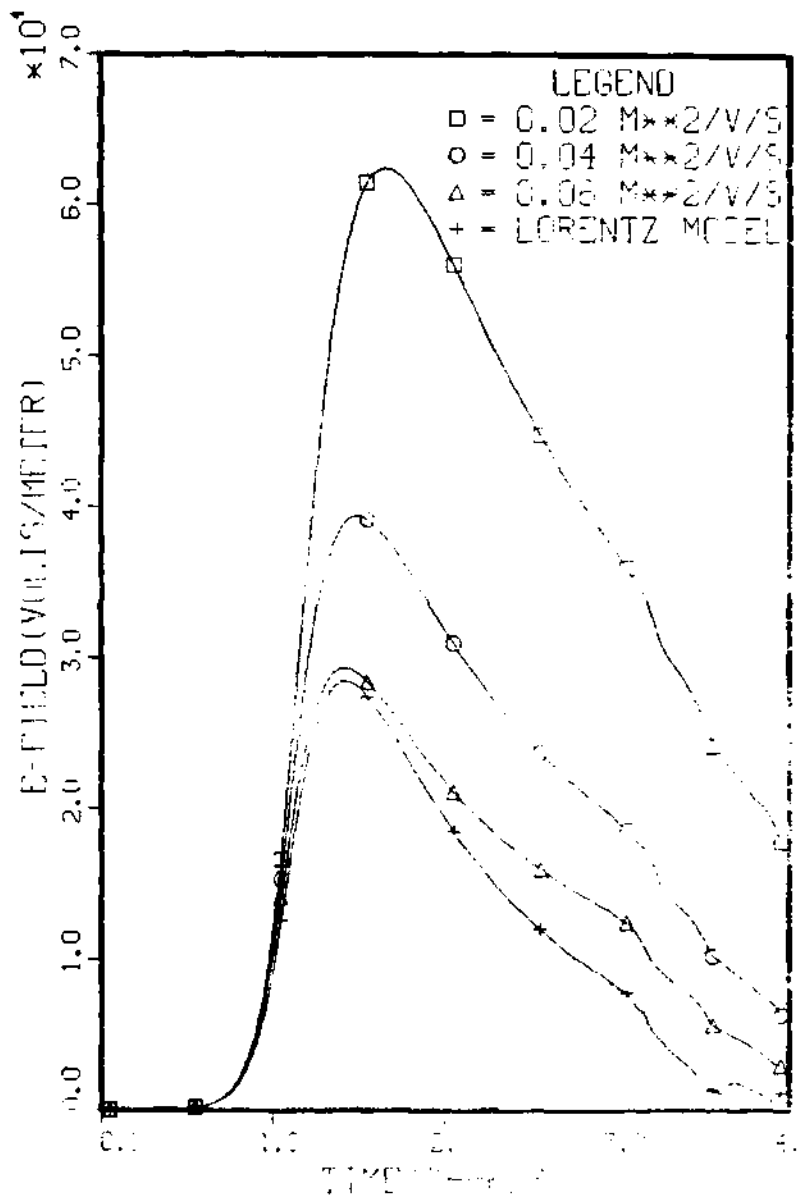


Figure 4.7 Electric Field, Mobility Limit

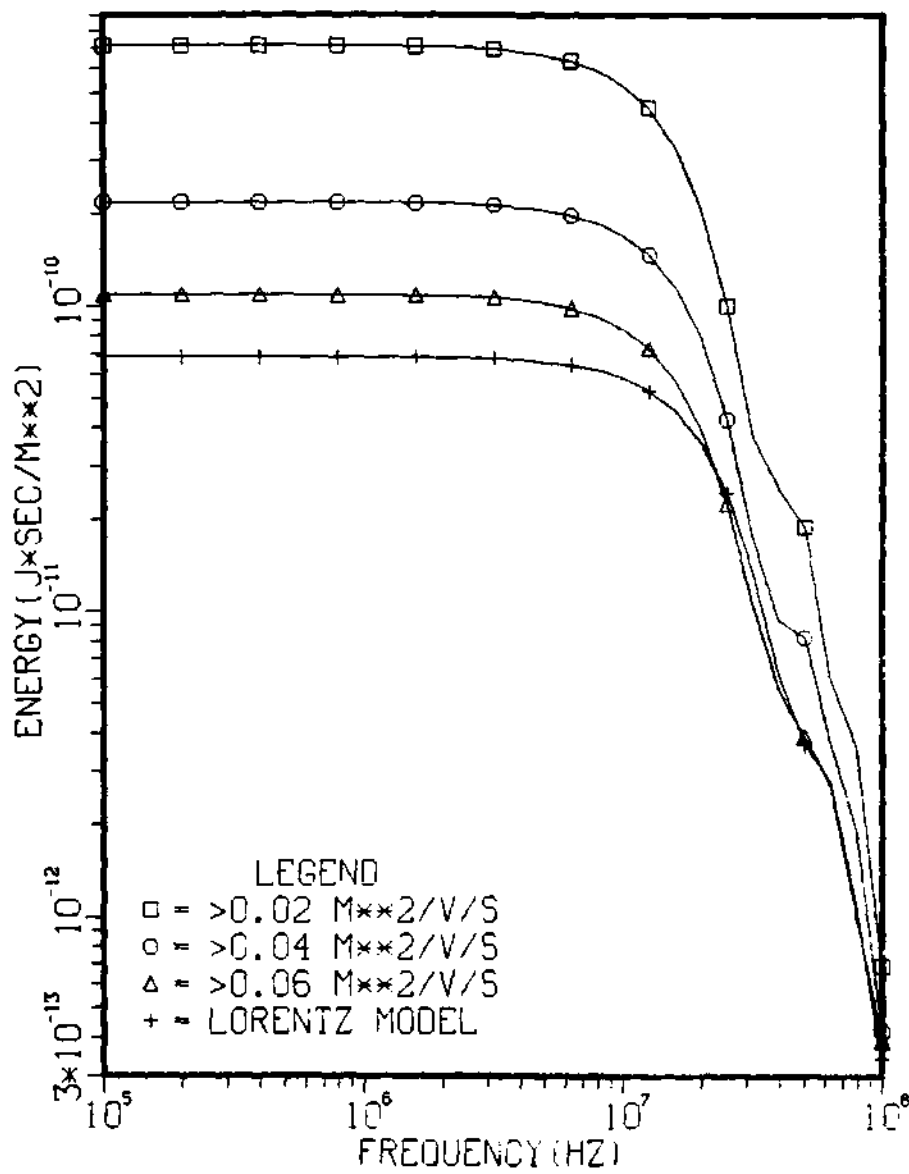


Figure 4.8 Frequency Profile, Mobility Limit

## V. PARAMETRIC STUDIES

The gamma ray pulse from a device rises exponentially. The parameter for characterizing the rise will vary due to changes in compression and boosting. The details of the gamma ray pulse history are not modeled due to classification. EMPFRE approximates the gamma ray pulse history with a single parameter for exponential rise and a second parameter for decay.

$$Y_{\gamma}(\tau) = c \cdot \left[ \frac{\text{EXP}(\alpha\tau)}{1 + \text{EXP}(\beta \cdot (\tau - TP))} \right] \quad (5.1)$$

where  $\alpha$  -parameter to characterize exponential rise  
 $\beta$  -parameter to characterize exponential decay  
TP -time of peak  
C -yield normalization constant

For retarded time less than TP, the gamma output of the device rises exponentially.

$$Y_{\gamma}(\tau) = C \cdot \text{EXP}(\alpha\tau) \quad (5.2)$$

For retarded time greater than TP, the gamma output of the device decays exponentially.

$$Y_{\gamma}(\tau) = K \cdot \text{EXP}((\alpha - \beta) \cdot \tau) \quad (5.3)$$

This pulse shape is used for the parametric studies. Unless specified, the parameters for the burst are:

$$\alpha = 1.0E9/\text{second} \quad (5.4)$$

$$\beta = 1.5E9/\text{second} \quad (5.5)$$

$$TP = 1.0E-8 \text{ second} \quad (5.6)$$

$$E_{\gamma} = 1.5 \text{ MeV} \quad (5.7)$$

$$Y_{\gamma} = 0.1 \text{ kiloton} \quad (5.8)$$

$$HOB = 100 \text{ kilometers} \quad (5.9)$$

$$BANGLE = 0 \text{ degrees} \quad (5.10)$$

TARGET LOCATION:

$$X = 0 \text{ meters} \quad (5.11)$$

$$Y = 0 \text{ meters} \quad (5.12)$$

$$Z = 0 \text{ meters} \quad (5.13)$$

GAMMA PULSE HISTORY

The alpha ( $\alpha$ ) of the gamma pulse impacts the EMP rise time and peak field. The gamma ray rise time determines the Compton current history which directly impacts the EMP. Another mechanism involves the phasing between the Compton current and conductivity. The EMP rises with the Compton currents until the air conductivity becomes large. The Compton electrons have a time of flight greater than 10 shakes; therefore, the Compton currents continue to rise while the gamma ray pulse decays. The decay of the EMP is due to the increase in conductivity. The rise characteristics of the gamma pulse determines how far the electric field rises before being choked off by the build-up of conductivity.

The impact of a change in the parameter alpha [Eq. 5.1] on the electric field is demonstrated by Figures 5.1, 5.3, 5.5 and 5.7. The impact on the spectral characteristics are indicated by Figures 5.2, 5.4, 5.6 and 5.8. The examples are grouped with equal values of TP. The TP is chosen to reduce the effects of the function starting at a non-zero value.



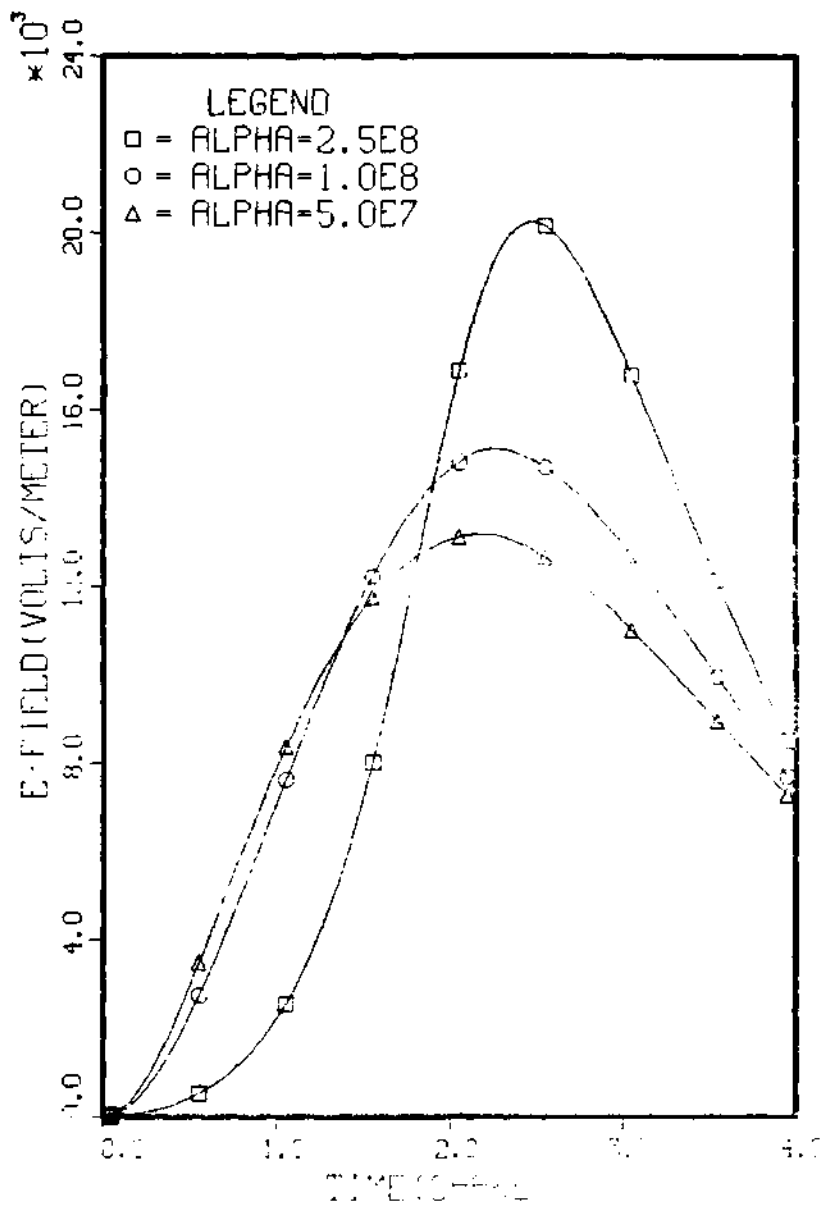


Figure 5.1 Electric Field, TP=2.0 Shake, Beta=1.5·Alpha  
 Alpha=5.0x10<sup>7</sup>, 1.0x10<sup>8</sup> and 2.5x10<sup>8</sup> (sec<sup>-1</sup>)

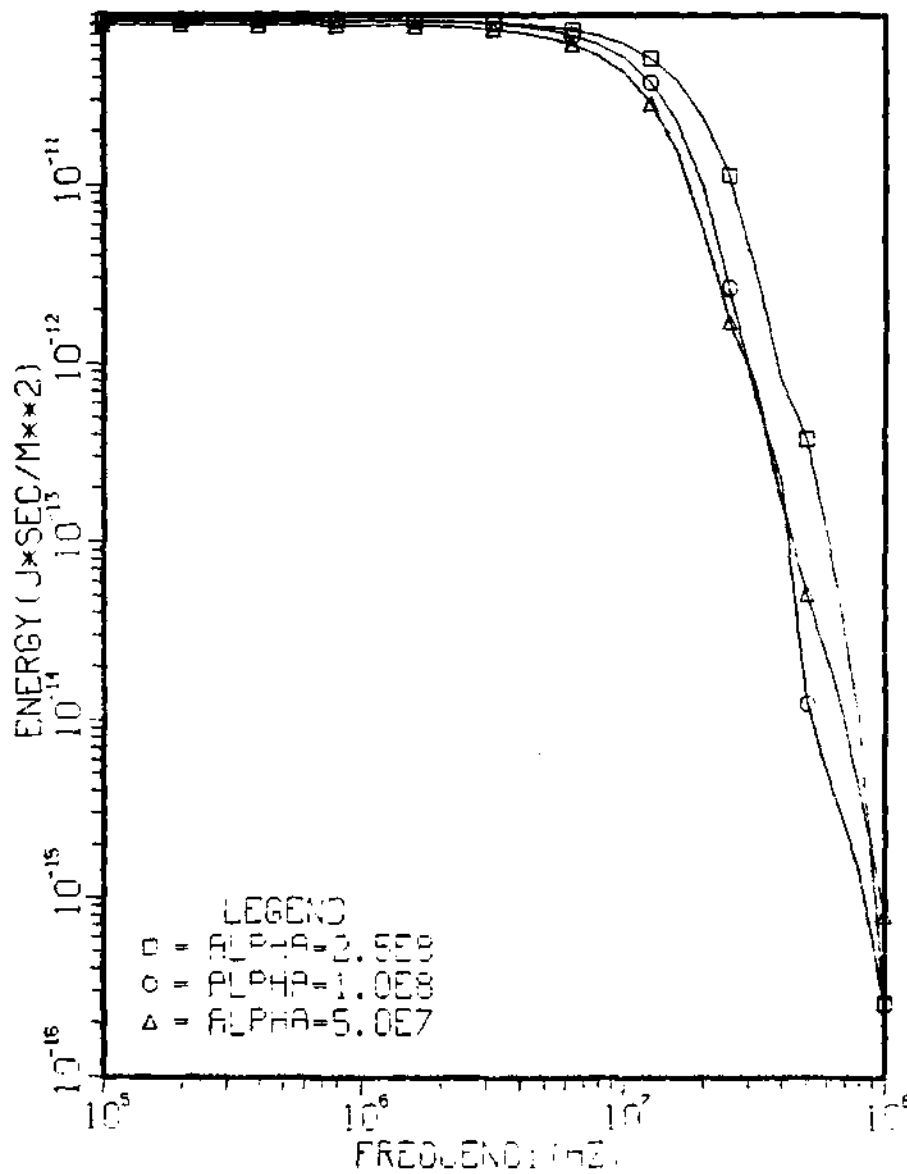


Figure 5.2 Frequency Profile, TP=2.0 Shake, Beta=1.5·Alpha  
Alpha=2.5x10<sup>7</sup>, 1.0x10<sup>8</sup> and 2.5x10<sup>8</sup> (sec<sup>-1</sup>)

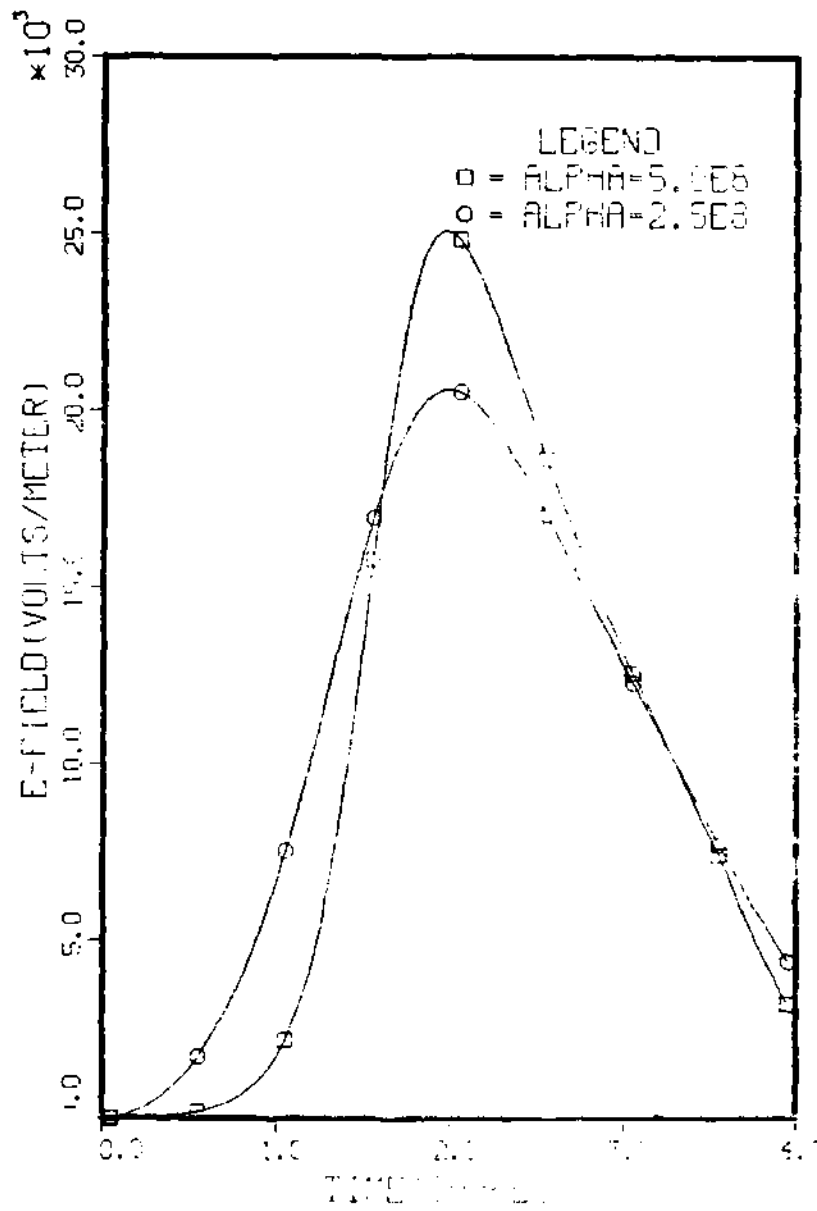


Figure 5.3 Electric Field, TP=1.5 Shake, Beta=1.5·Alpha  
 Alpha=2.5x10<sup>8</sup> and 5.0x10<sup>8</sup> (sec<sup>-1</sup>)

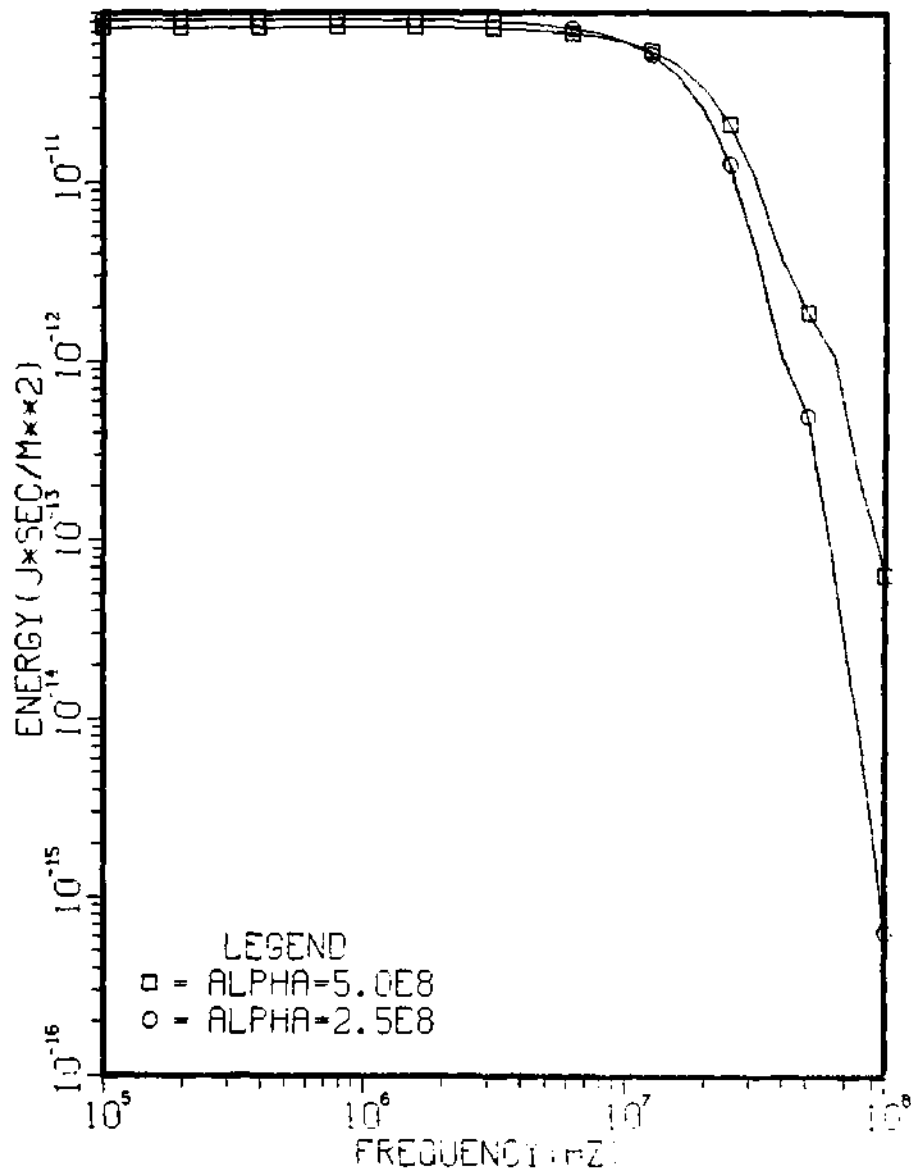


Figure 5.4 Frequency Profile, TP=1.5 Shake, Beta=1.5·Alpha  
 Alpha=2.5x10<sup>8</sup> and 5x10<sup>8</sup> (sec<sup>-1</sup>)

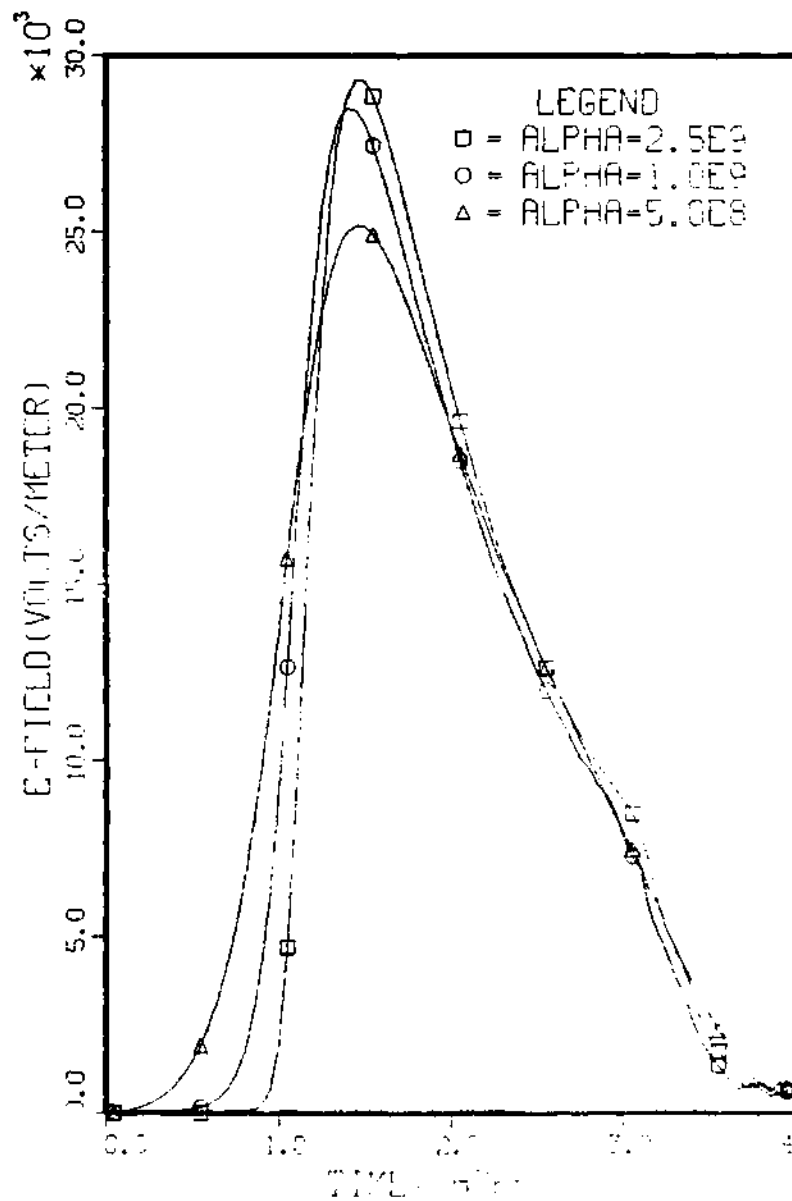


Figure 5.5 Electric Field, TP=1.0 Shake, Beta=1.5·Alpha  
 Alpha=5.0x10<sup>8</sup>, 1.0x10<sup>9</sup> and 2.5x10<sup>9</sup> (sec<sup>-1</sup>)

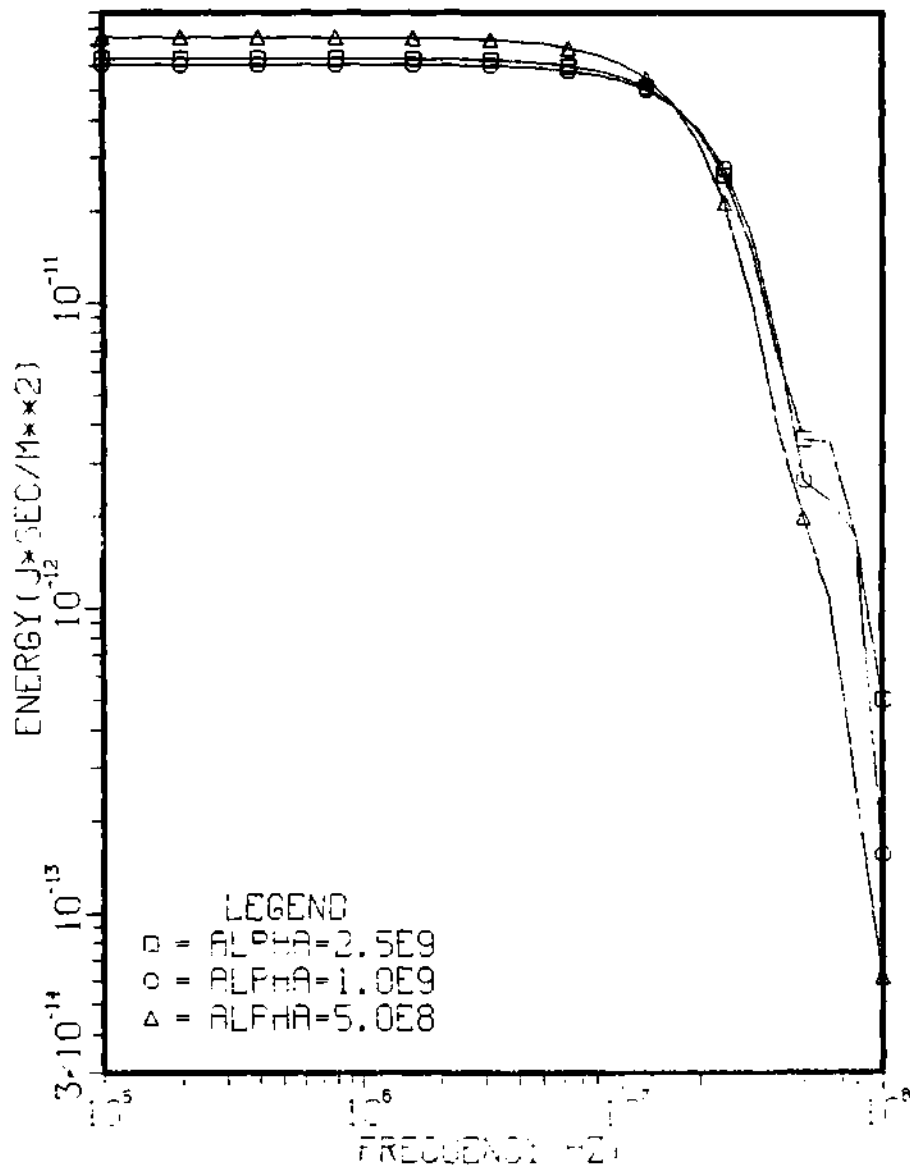


Figure 5.6 Frequency Profile, TP=1.0 Shake, Beta=1.5\*Alpha  
 Alpha=5.0x10<sup>8</sup>, 1.0x10<sup>9</sup> and 2.5x10<sup>9</sup> (sec<sup>-1</sup>)

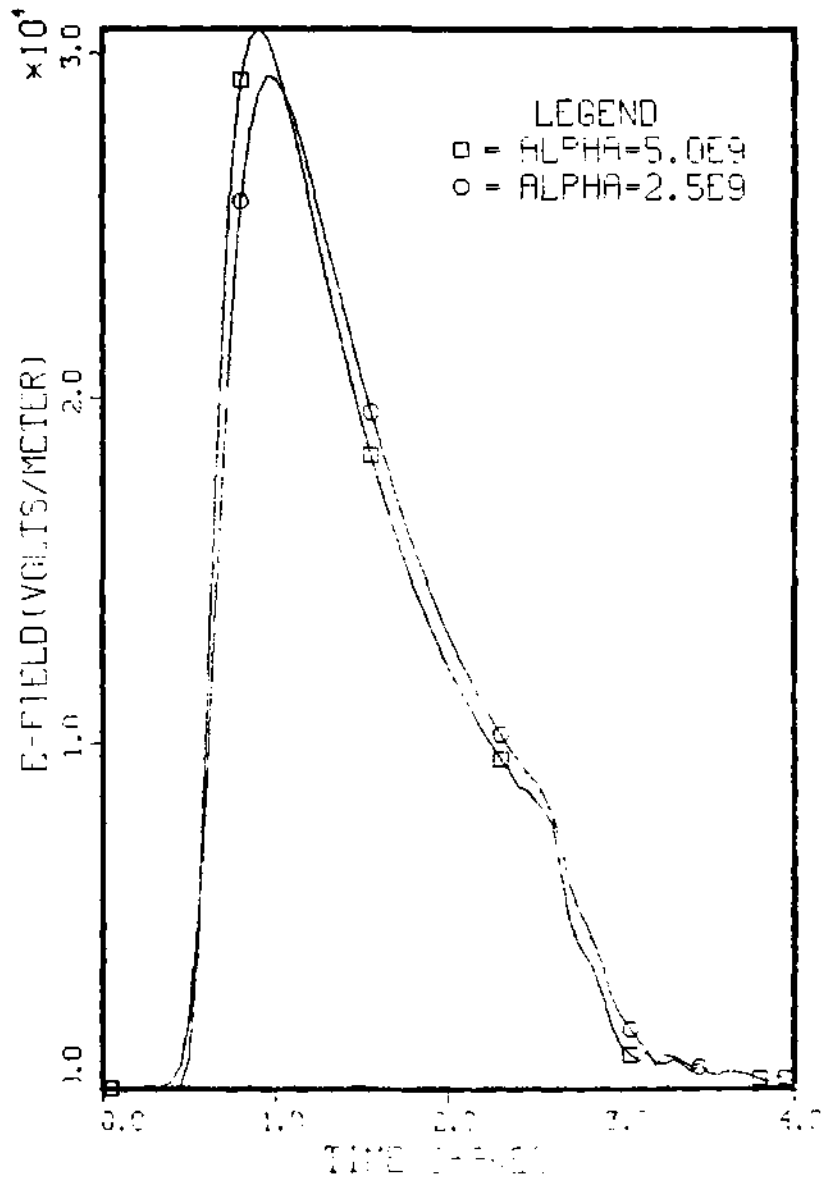


Figure 5.7 Electric Field, TP=0.5 Shake, Beta=1.2·Alpha  
 Alpha=2.5x10<sup>9</sup> and 5.0x10<sup>9</sup> (sec<sup>-1</sup>)

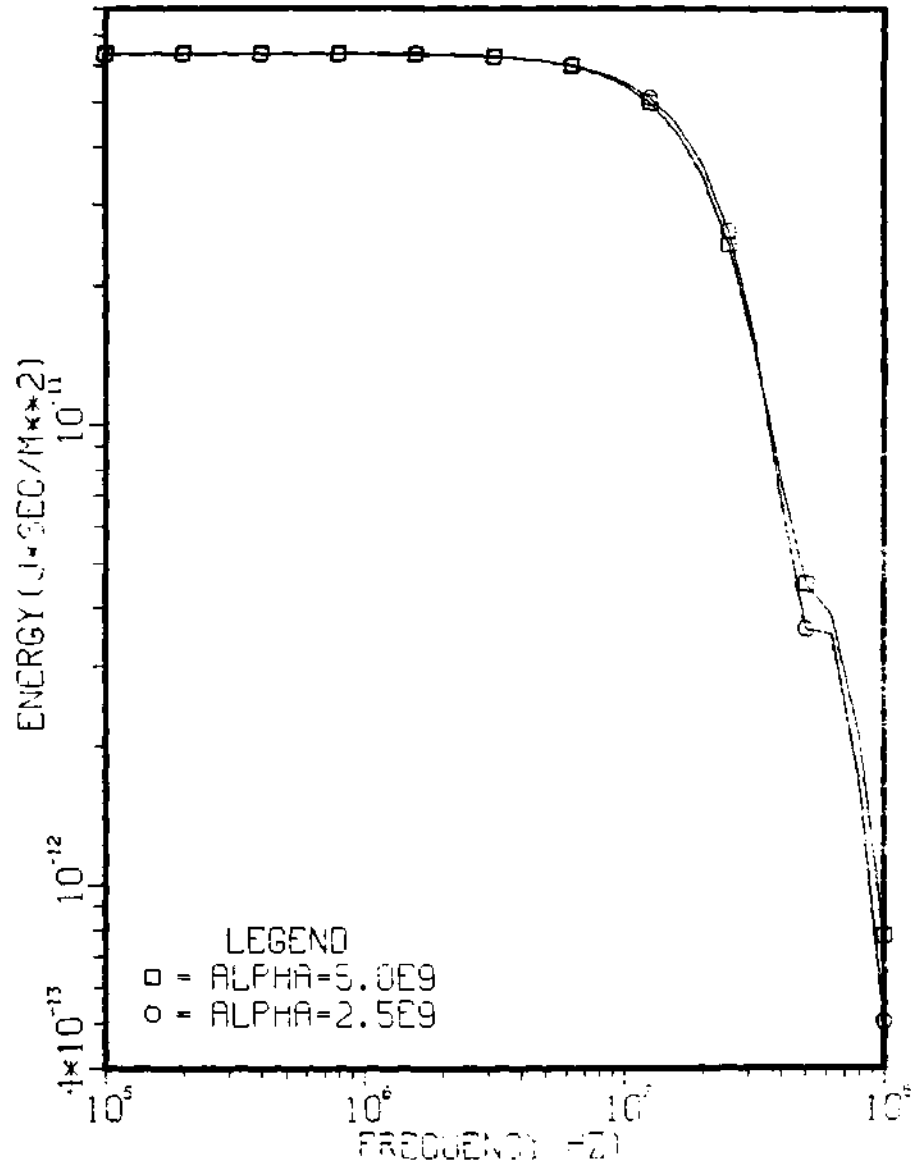


Figure 5.8 Frequency Profile, TP=0.5 Shake, Beta=1.2·Alpha  
Alpha=2.5x10<sup>9</sup> and 5.0x10<sup>9</sup> (sec<sup>-1</sup>)



### GAMMA RAY ENERGY

The gamma ray spectrum from a nuclear device will be a function of the mix of nuclear reactions and the composition of the device. The purpose is to demonstrate the relationship between mean gamma ray energy and the spectral characteristics of the EMP. No attempt is made to model the EMP from a spectrum of gamma rays. This would require a multi-group gamma ray calculation or a model to account for spectrum hardening. Spectrum hardening is the effect of having the mean energy of the gamma spectrum increase as the low energy gamma rays are filtered out faster than high energy gamma rays.

Changing the gamma ray energy changes the Compton electron density profile as discussed in Chapter II. Increasing the energy of the gamma rays causes the peak of the deposition region to shift to lower altitudes. The electron mobility is inversely proportional to pressure; therefore, the electron mobility is reduced at the peak of the deposition region. The resulting reduction in conductivity lead to larger electric fields.

The Compton electron dynamics are effected by the gamma ray energy. An increase in the gamma ray energy will cause increases in the Compton electron energy, initial velocity and range. The Compton electrons will generate secondary electrons faster which enhances the build-up of the secondary electron density. An increase in the gamma energy will decrease the mean deflection angle of the Compton electron (Table 3.2). This along with the higher intial velocity increases the Compton current. The net effect from Compton electron dynamics leads to faster rise times and higher peak electric fields.

The yield is set at 0.1 kilotons. This has the effect of reducing the number of gamma rays emitted from an increase in gamma ray energy. This will reduce the Compton currents. The impact from changing the energy of the gamma ray with this approach is demonstrated by Figure 5.9. The variation in the spectral characteristics is indicated in Figure 5.10.

Another way to see the effects of changing the mean energy is to fix the number of gamma rays emitted. The impact from changing the energy with this approach is demonstrated by Figure 11. The 10 MeV gamma ray pulse is largest but close to the 5 MeV pulse. The effects due to the Compton electron dynamics are being cancelled by gamma absorption from pair production. The number of gamma rays is based on 0.1 kiloton yield of 1.5 MeV gamma rays. The variation in the spectral characteristics is indicated in Figure 5.12.

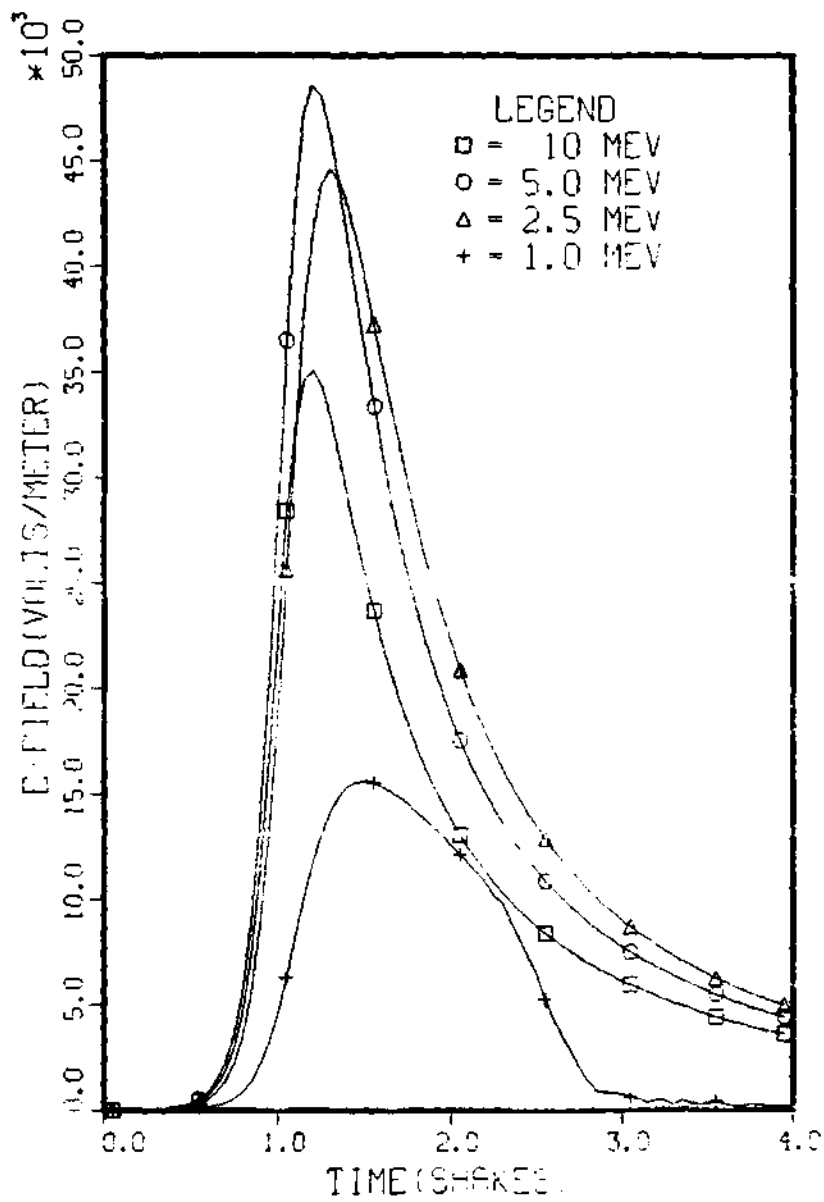


Figure 5.9 Electric Field, Gamma Ray Energy  
Yield=0.1 Kilotons

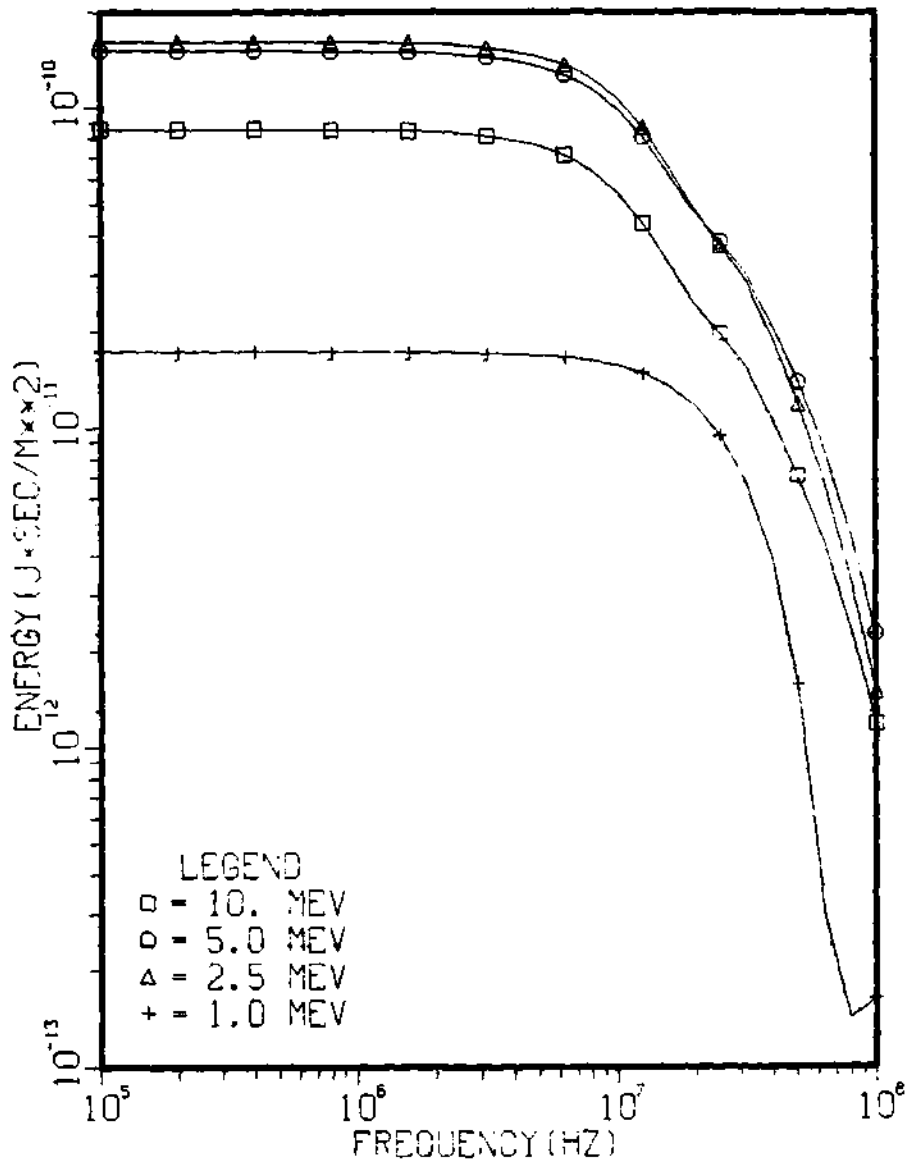


Figure 5.10 Frequency Profile, Gamma Ray Energy Yield=0.1 Kilotons

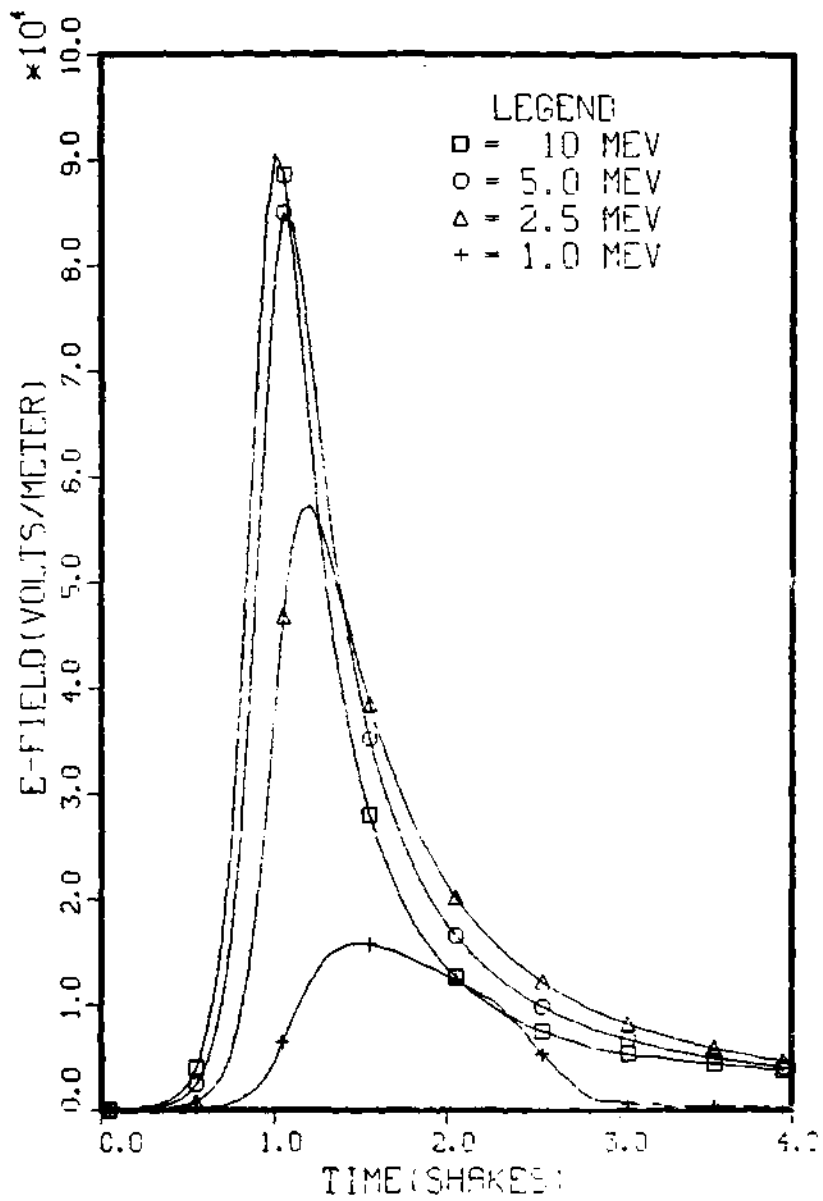


Figure 5.11 Electric Field, Gamma Ray Energy  
 $Yield = E_{\gamma} \text{ (MeV)} \cdot 0.0667 \text{ Kilotons}$

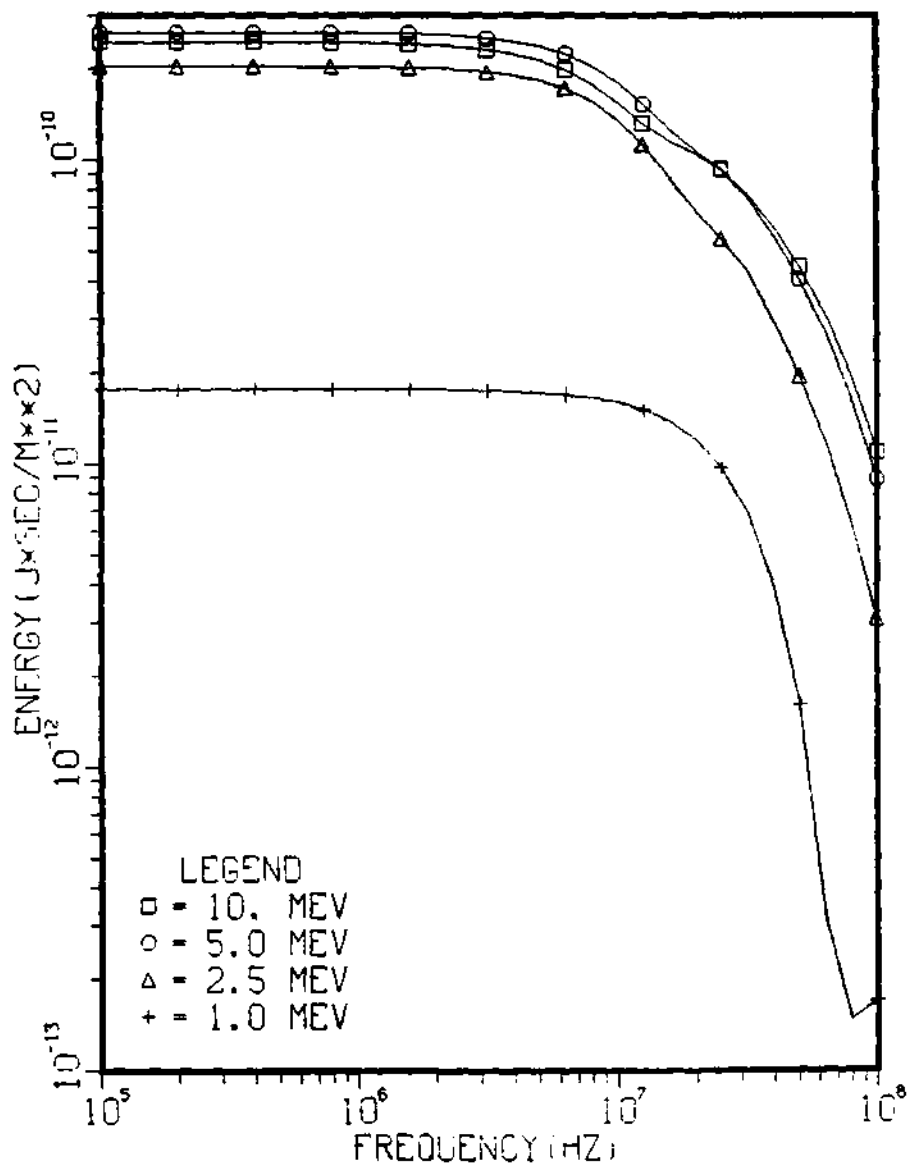


Figure 5.12 Frequency Profile, Gamma Ray Energy  
Yield=E (MeV)·0.0667 Kilotons

## YIELD

The yield impacts the Compton currents and the conductivity histories. Raising the yield by an order of magnitude (0.1 Kt 1.0 Kt) produced an increase of only 25% in the peak electric field. This is due to the effects of saturation. The concept of saturation can be understood by analyzing the differential equation for the transverse electric fields.

$$\frac{\delta E_T}{\delta r} = -\frac{E_T}{r} - \frac{\mu \cdot C}{2} \cdot (J_T + \sigma \cdot E_T) \quad (5.14)$$

For electric fields greater than the saturation field the conduction current ( $\sigma \cdot E$ ) would be larger than the Compton current. Ignoring the radial divergence, the electric field will remain less than the saturation field ( $-J/\sigma$ ). The air conductivity is increasing with the Compton currents to hold the peak field down. The increase in the electric field is due to a change in the saturation field.

At lower yields the electric field is not saturated and the conductivity remains low. The result is a lower peak electric field but higher electric fields for time greater than 3 shakes.

Increasing the yield to saturation leads to a shorter pulse with a faster rise and decay. This increases the energy associated with the high frequencies with little change in the low frequencies. A further increase in yield (to  $Y_\gamma = 1.0$  kiloton) increased the low frequencies with little change in the high frequencies. The impact of a change in yield on the electric field is demonstrated by Figure 5.13. The impact on the frequency profiles is in Figure 5.14.

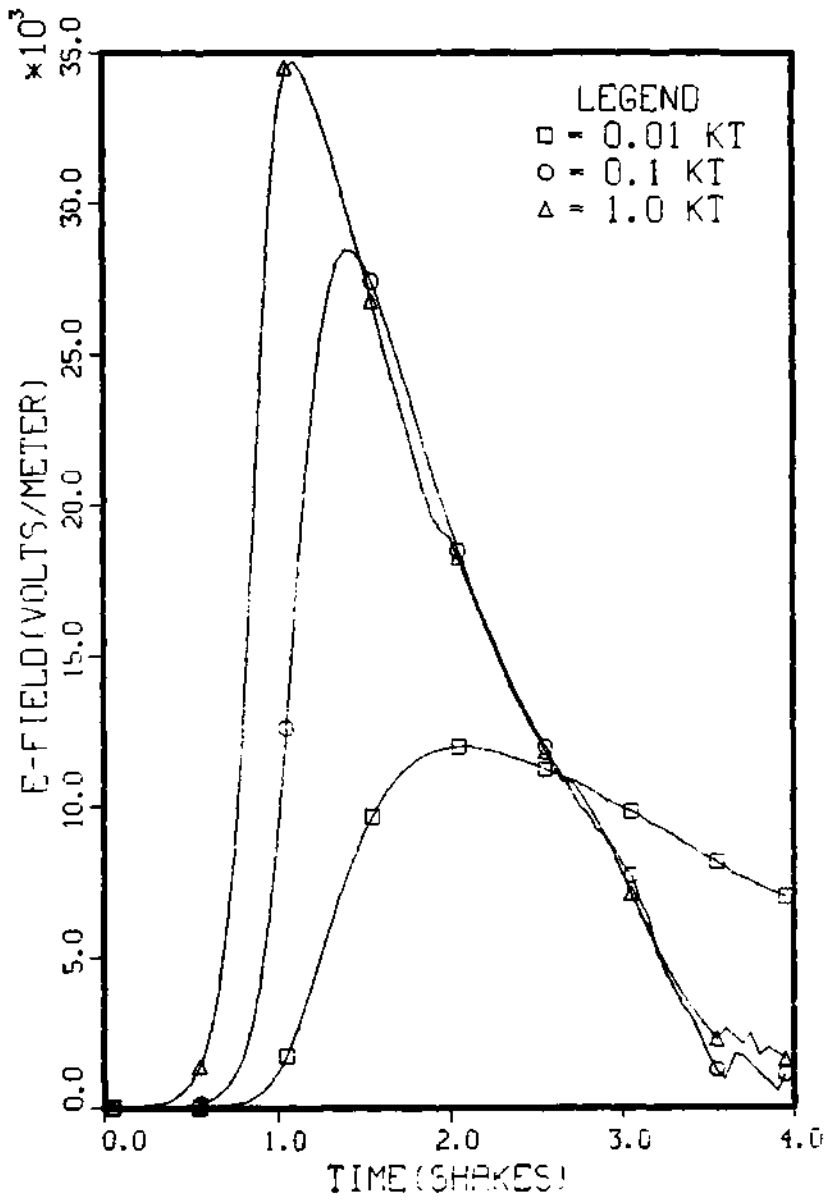


Figure 5.13 Electric Field, Gamma Ray Yield



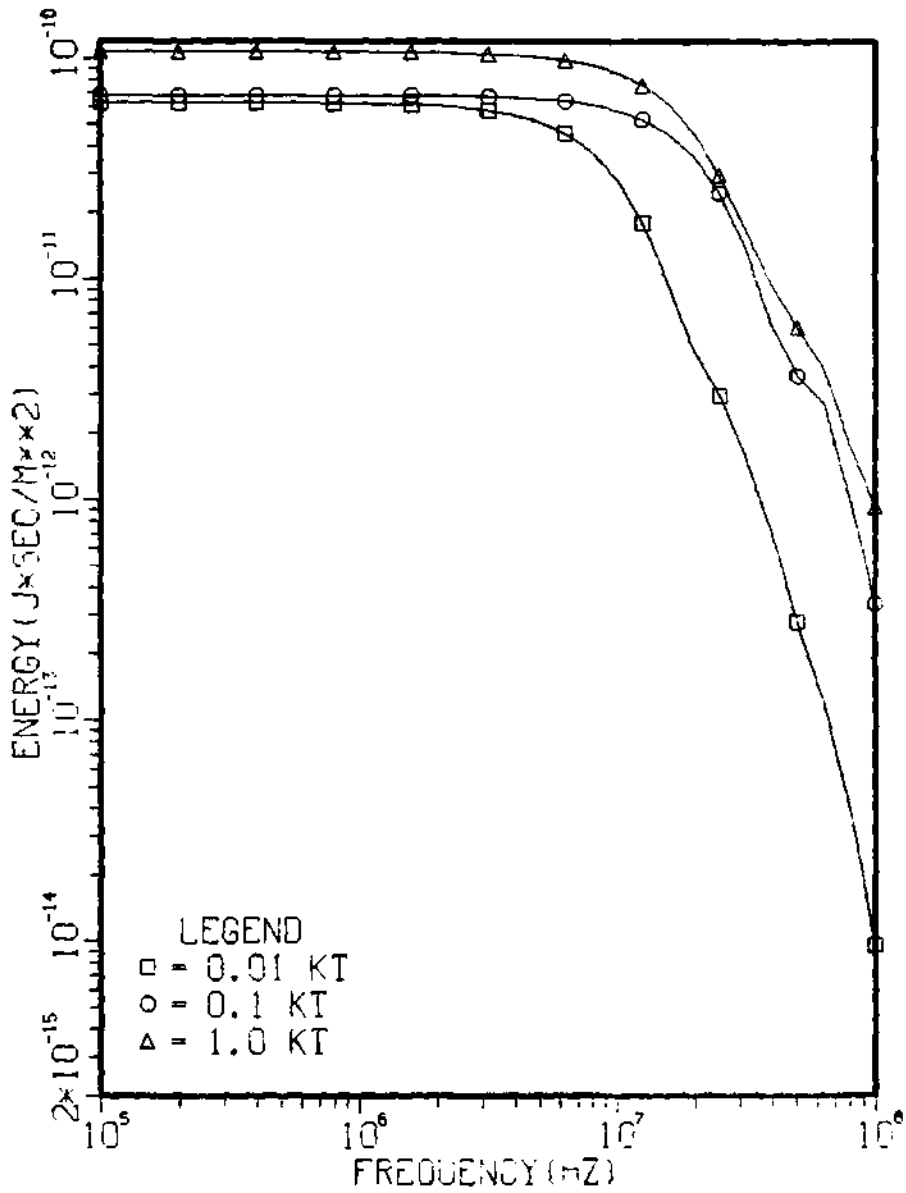


Figure 5.14 Frequency Profile, Gamma Ray Yield

### HEIGHT OF BURST

Changing the height of burst has an effect similar to changing the yield. The Compton current and conductivity are decreased for larger heights of burst. The deposition profiles for various HOBs are given in Chapter II. At low HOB (75 Km and 100 Km), the fields are limited by the saturation voltage; therefore, the peak voltage is relatively insensitive to decreasing HOB. For large HOB (200 Km), the conductivity remains low and the electric field doesn't saturate. As a result, the electric fields are larger for time greater than 3 shakes. Figure 3.15 demonstrates the impact on the electric fields. The frequency profiles are in Figure 3.16.

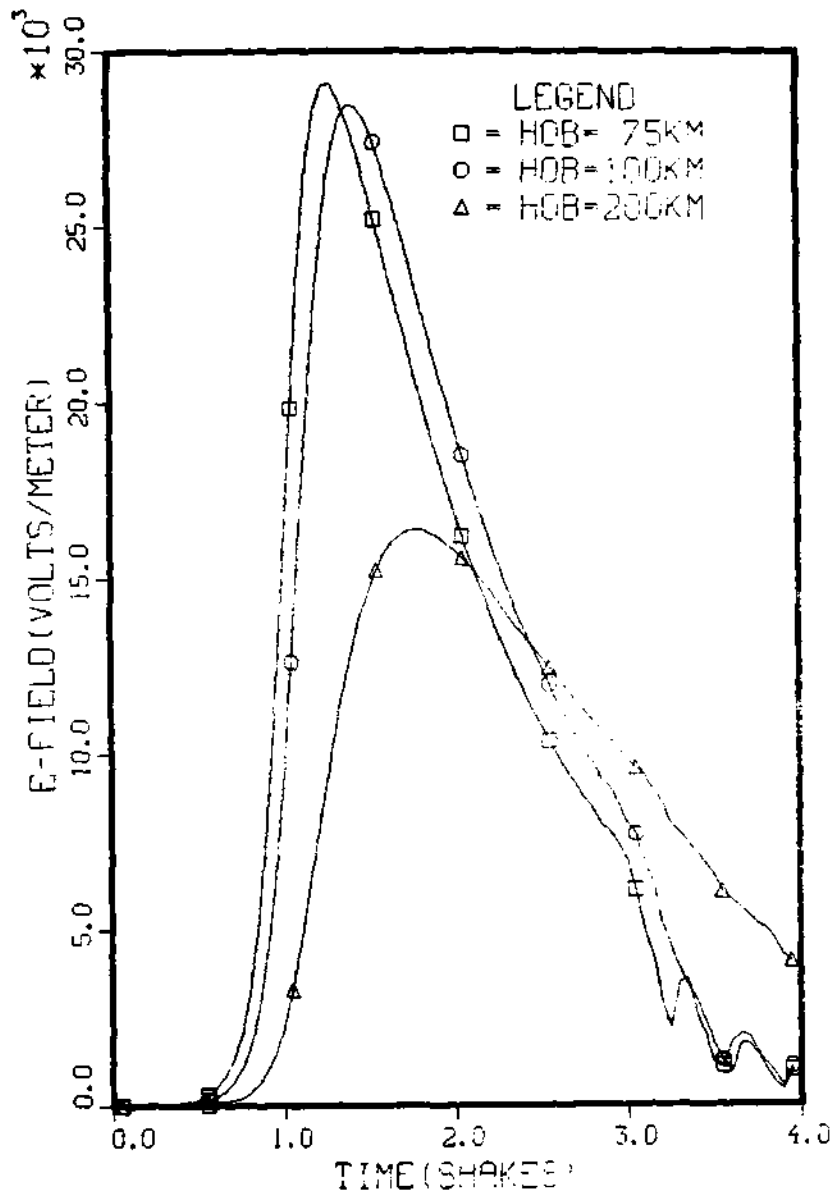


Figure 5.15 Electric Field, Height of Burst

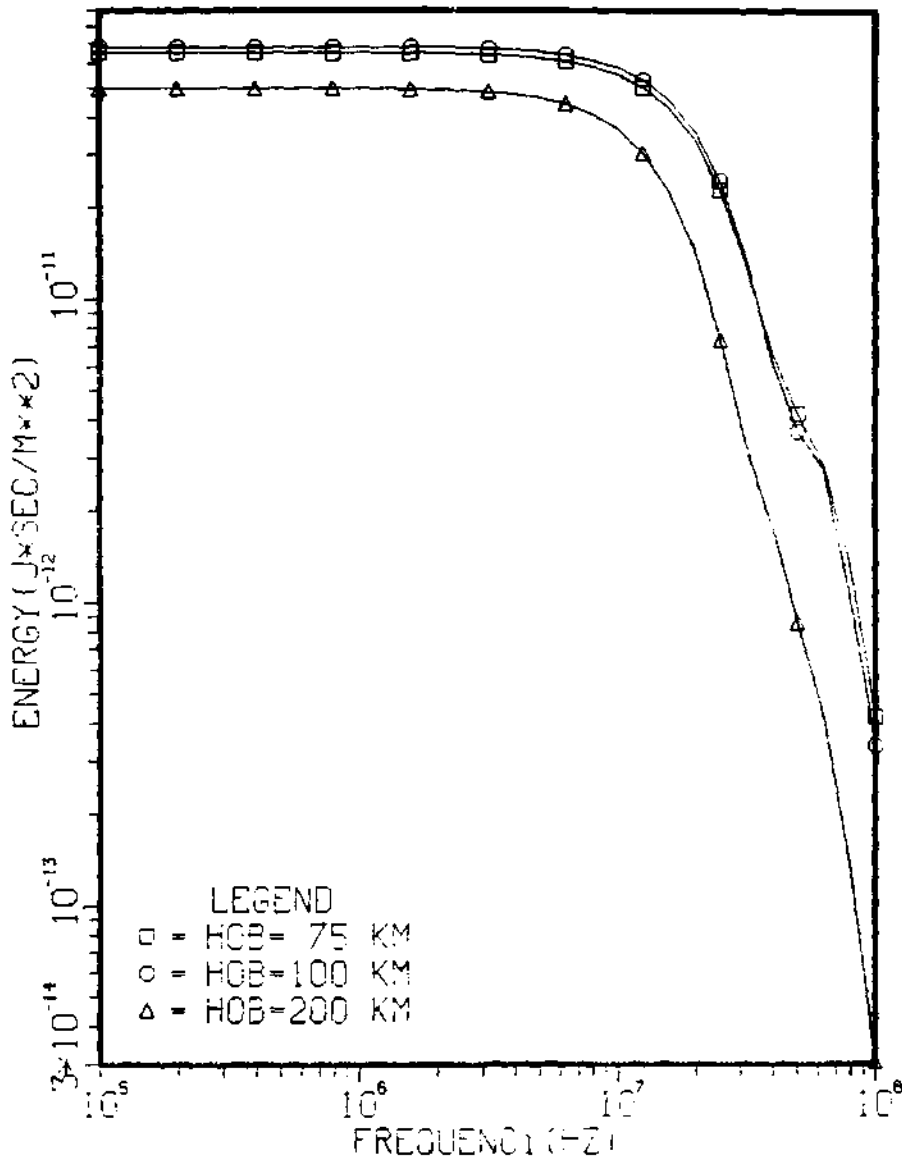


Figure 5.16 Frequency Profile, Height of Burst

### DIP ANGLE

The dip angle of the geomagnetic field will change the trajectory of the Compton electrons. The phi component of the Compton current is largest for the dip angle equal to zero. The phi component of the Compton current will go to zero as the dip angle goes to  $90^\circ$ . The theta component is zero when the dip angle equals zero. The theta component reaches a maximum when the dip angle is equal to  $45^\circ$ . Then the theta component goes to zero as the dip angle goes to  $90^\circ$ .

When the dip angle is at  $90^\circ$  (parallel to the gamma ray trajectory), there are no transverse currents generated. In this case, the Compton currents do not form a radiating magnetic dipole. The resulting EMP would be due to the electric dipole formed by the radial currents. The electric fields radiating from the electric dipole are small and are lower in frequency compared to those from the magnetic dipole for the case of high altitude EMP. The phi component of the Compton current makes the largest contribution to the magnetic dipole. The radiated electric fields go to zero as the dip angle goes to  $90^\circ$ .

The components of the Compton current are a function of dip angle but the conductivity profile will remain the same. As a result, the peak electric field does not shift with dip angle. The effect of dip angle on the electric field is demonstrated by Figure 5.17. The frequency profiles are in Figure 5.18.

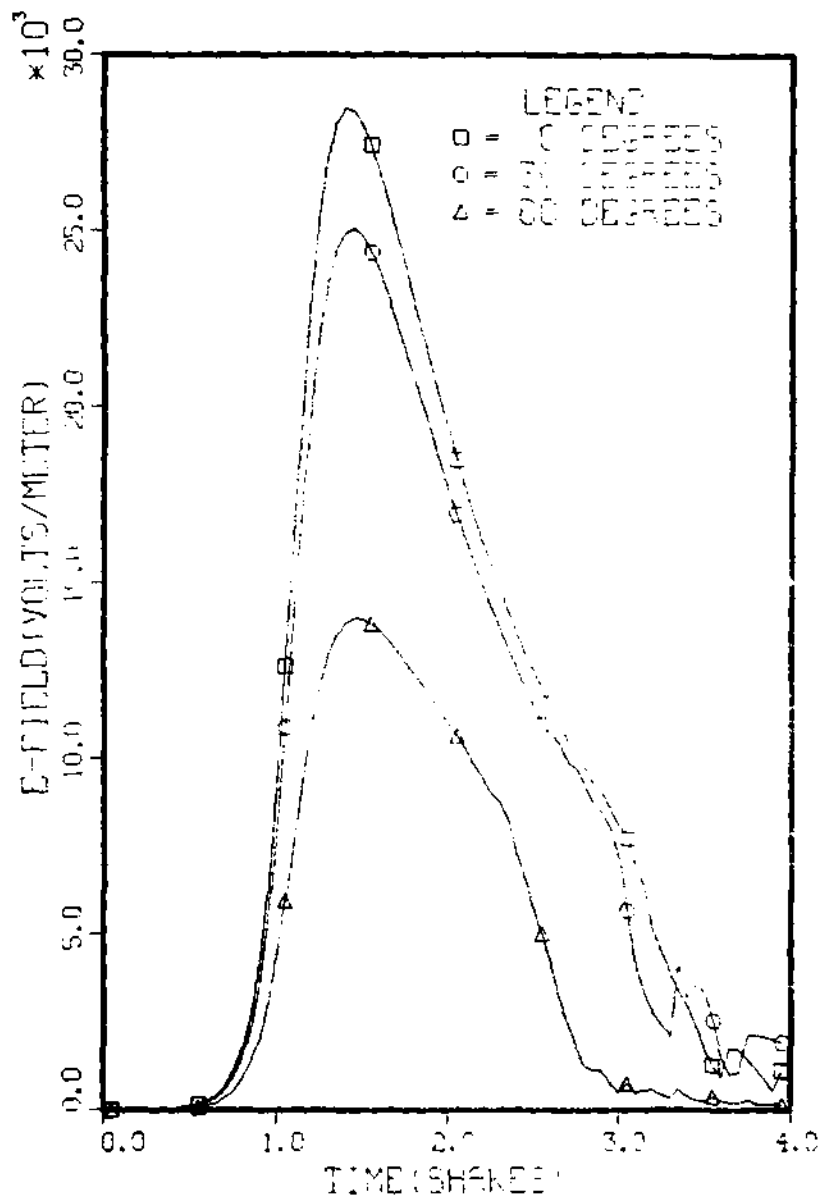


Figure 5.17 Electric Field, Geomagnetic Field Dip Angle

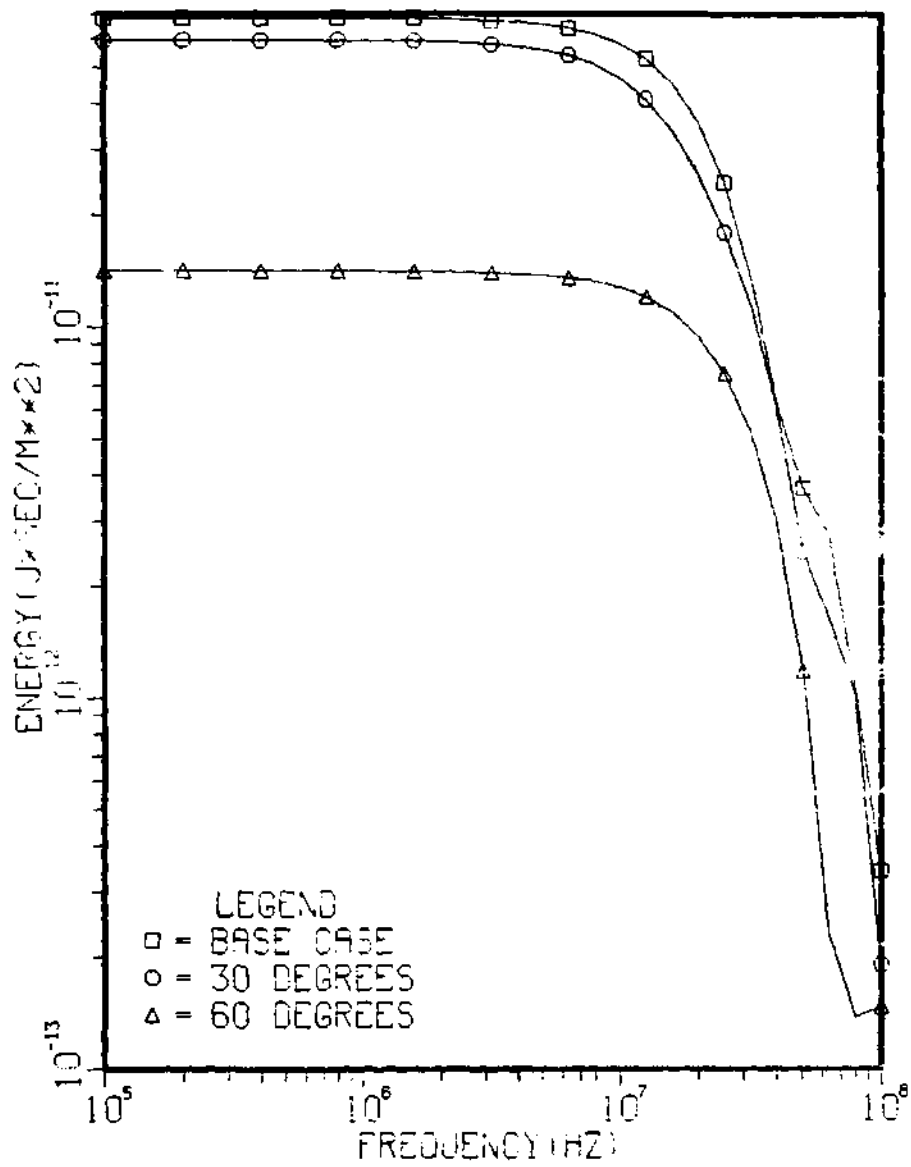


Figure 5.18 Frequency Profile, Geomagnetic Field Dip Angle

## VI. CONCLUSIONS AND RECOMMENDATIONS

### CONCLUSIONS

The EMP from high altitude nuclear detonations is modeled by EMPFRE. Constraints on the project made it impractical to refine the model or reduce the error by imposing finer steps for computations. These limitations do not invalidate the results of the parametric studies performed. This project documents basic relationships between burst parameters and the resulting EMP. The following conclusions are drawn for the parametric studies.

1) The energy in the EMP is enhanced by a large alpha. This is due to the phasing between the Compton current and conductivity. An increase in alpha allows the Compton currents to get larger before the conductivity gets large. The result is faster rise time and larger peak fields. The energy associated with 100 MHz is several orders of magnitude lower for  $\alpha=1.5 \times 10^8$ /second than for  $\alpha=2.5 \times 10^9$ /second.

2) The energy in the EMP is enhanced by higher gamma ray energies; however, a limit is reached where pair production counteracts the benefits due to Compton electron dynamics. The energy in the EMP is increased by more than an order of magnitude when the gamma ray energy is changed from 1 MeV to 2.5 MeV. Increases in the mean energy above 5 MeV results in a reduction of the energy.

3) The energy in the EMP is enhanced by an increase in yield. This is particularly true for frequencies above 10 MHz. The increase in yield produces faster rise times and decay times. Higher yields produce larger peak fields and narrower pulses. Increases in yield passed that needed to saturate the electric field produce limited changes in the



energy in the EMP.

4) Decreasing the angle of intersection between the geomagnetic field and the slant range decreases the energy associated with the electric field. Varying this angle between  $90^\circ$  and  $60^\circ$  has little effect on the resulting EMP. Varying this angle between  $60^\circ$  and  $30^\circ$  results in a large reduction in the EMP. This effect is due to a reduction of the phi component of the Compton current.

#### RECOMMENDATIONS

SPATIAL STEP REDUCTION. The behavior of the late time electric fields could be improved by increasing the number of spatial steps from 50 to at least 100. Figure 4.5 shows the improvement made for the base case. A larger number of steps may be required for some cases. The effects on the frequency profile were small for the base case but confidence would be increased in other results if this recommendation is implemented.

REFINEMENTS TO THE LORENTZ MODEL. The Lorentz model is an approximation used to model secondary electron behavior. The secondary electrons are assumed to be created at the equilibrium temperature of the electrons in the local electric field. The potential impact of this approximation is demonstrated by Figure 4.7.

At early times, the growth in the Compton current density is matched by a growth in the electromagnetic fields generated. The simultaneous growth of secondary electron density increases air conductivity and limits the growth of the electromagnetic field. The peak field strength and frequency profile are sensitive to the phasing of the Compton current density and conductivity growth.

Secondary electrons are born with temperatures above the equilibrium temperature. For dry air, the electron mobility is reduced by an increase in the temperature. A derivation of the relationship between electron temperature and mobility is presented by C. E. Baum (Ref 1). The Lorentz model overestimates the secondary electron mobility from birth to thermalization.

Two approaches are identified. The first approach is discussed by L. W. Seiler (Ref 15:24). The secondary electron collision frequency is assumed to be linear function of time between birth and thermalization. Another approach is used by Karzas and Latter (Ref 10). In the reference, Age Theory is used to find the average electron mobility for a given alpha. This is the same approach used to find single group cross sections for systems of neutrons. The last approach appears to be more flexible for application in EMPFRE.

SPECTRUM HARDENING. Incorporating a model to treat spectrum hardening is proposed as a follow-up thesis. The first step is the development of a method to determine an effective gamma ray energy for a given gamma ray spectrum. Important characteristics to consider are MFP, Compton electron energy and Compton electron deflection angle. The second step is to model the shift in effective gamma energy as the pulse propagates through the atmosphere. Lt A. Dooley (GNE-34M) worked on a thesis to model the impact on gamma ray spectral characteristics due to attenuation by the atmosphere. The results from this work may provide the data needed to develop a model for spectrum hardening.

## BIBLIOGRAPHY

1. Baum, C. E. "The Calculation of Conduction Electron Parameters in Ionized Air," Electromagnetic Pulse Theoretical Notes: Note 6, Kirtland AFB, New Mexico: Air Force Weapons Laboratory, (April 1967)
2. , "Electron Thermalization and Mobility in Air," Electromagnetic Pulse Theoretical Notes: Note 12, Kirtland AFB, New Mexico: Air Force Weapons Laboratory, (April 1967)
3. Broad, W. J. "Nuclear Pulse (I): Awakening to the Chaos Factor," Science: 1009-1012 (May 1981)
4. , "Nuclear Pulse (II): Ensuring Delivery of the Doomsday Signal," Science: 1116-1120 (June 1981)
5. Erkkila, J. H. "Calculations of the EMP From High Altitude Nuclear Detonations," Electromagnetic Pulse Theoretical Notes: Note 26. Kirtland AFB, New Mexico: Air Force Weapons Laboratory, (April 1967)
6. , "Prompt Gamma-Ray Fluxes and Energy Deposition in an Exponential Atmosphere," Electromagnetic Pulse Theoretical Notes: Note 17, Kirtland AFB, New Mexico: Air Force Weapons Laboratory, (April 1967)
7. , Lecture Materials distributed in NE-625. School of Engineering, Air Force Institute of Technology (AU), Wright-Patterson AFB OH, (1983)
8. Evans, R. D. The Atomic Nucleus. New York: McGraw Hill Book Co. (1966)
9. Karzas, W. J. and Richard Latter. "Detection of the Electromagnetic Radiation From Nuclear Explosions in Space," Physical Review, Vol 137, Number 5B (March 1965)
10. , Air Conductivity Produced by Nuclear Explosions. MEMORANDUM RM-3671-PR, RAND Corporation, (May 1963)
11. Longley, H. J. and Conrad L. Longmire. Electron Mobility and Attachment Rate in Moist Air. MRC-N-222, Mission Research Corporation, Santa Barbara, CA (December 1975)
12. Longmire, Conrad L. "On the Electromagnetic Pulse Produced by Nuclear Explosions," IEEE Transactions on Antennas and Propagation, AP-26: 3-13 (January 1978)

13. Milne, W. E. Numerical Solutions of Differential Equations. New York: Dover Publications Inc. (1970)
14. Pettus, E. and W. F. Crevier. Analytic Representation of Electron Mobility and Attachment Data in Dry and Moist Air from van Lint's HIFX Experiments. MRC-R-576 Santa Barbara, CA: Mission Research Corporation (July 1980)
15. Seiler, L. W. A Calculational Model for High Altitude EMP. MS thesis, School of Engineering, Air Force Institute of Technology (AU), Wright-Patterson AFB OH (March 1975)
16. U. S. Department of Health Education and Welfare. Radiological Health Handbook. Revised edition (January 1970)

## APPENDIX A

### VERIFICATION OF EMPFRE

FOURIER TRANSFORM. The numerical method used to compute the continuous Fourier transform is verified by applying it to a test case which is solved analytically in the class notes (Ref 7:122). The electric field is written as:

$$E(t) = E_0 \cdot [\text{EXP}(-\alpha t) - \text{EXP}(-\beta t)] \quad (\text{A.1})$$

where:  $E_0 = 1 \times 10^5$  volts/meter  
 $\alpha = 1 \times 10^7$  second<sup>-1</sup>  
 $\beta = 5 \times 10^7$  second<sup>-1</sup>

This model describes a pulse which rises to a peak in a few shakes and then decays in several shakes (Figure A.1). The analytic solution is written as:

$$\epsilon(\omega) = \frac{E_0}{\eta \sqrt{2\pi}} \frac{(\beta - \alpha)^2}{(\alpha^2 + \omega^2)(\beta^2 + \omega^2)} \quad (\text{A.2})$$

where:  $\epsilon(\omega)$  - energy (joule·second/meter<sup>2</sup>)  
 $\omega$  - angular frequency (radians/second)  
 $\eta = \mu_0 / \epsilon_0$

The method used to perform the Fourier transform is described in Chapter IV. The electric field is truncated at 4 shakes and the Fourier transform is performed on the resulting pulse. The truncated form of the pulse is shown in Figure A.1.

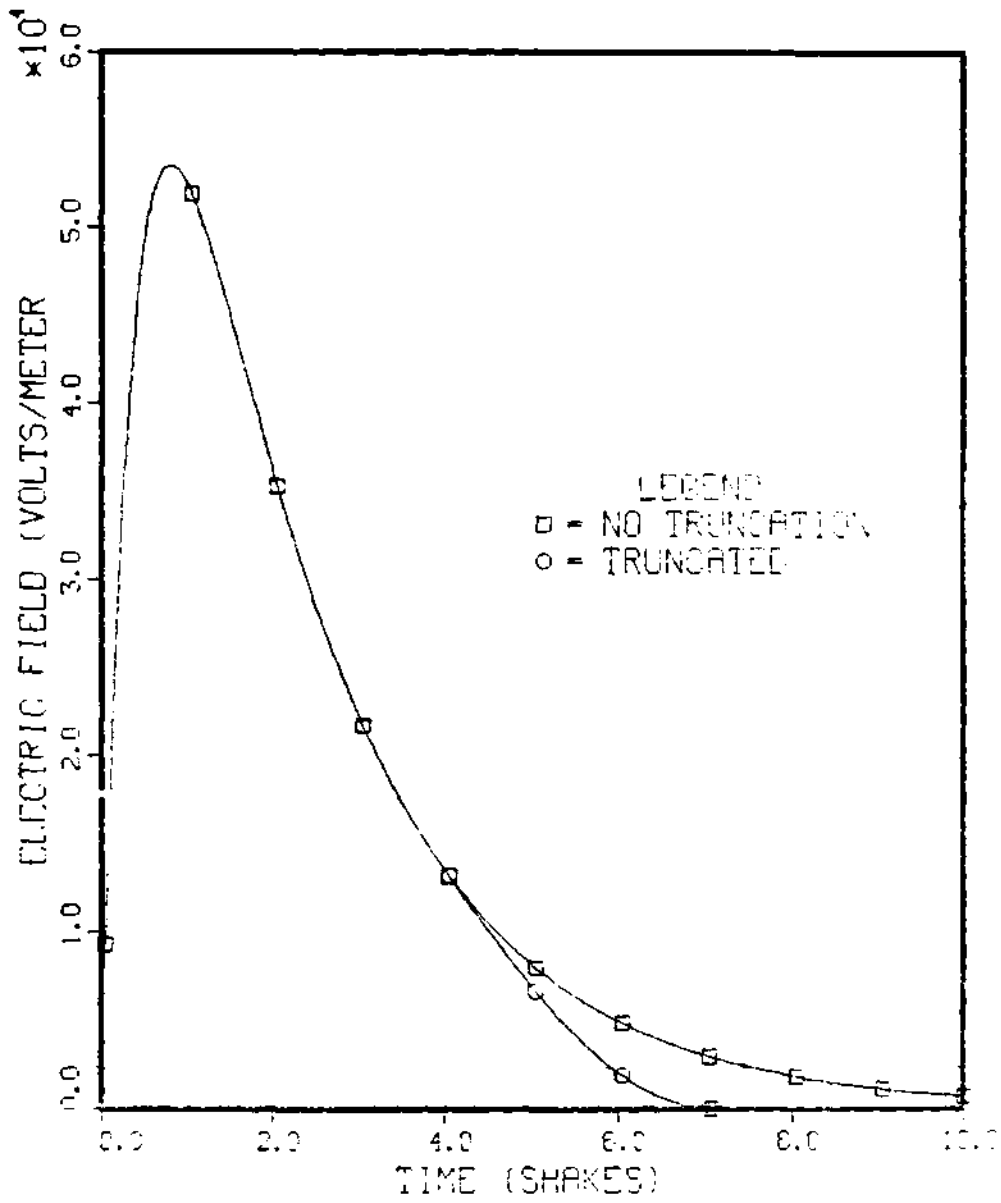


Figure A.1 Electric Field, Verification

The solution from EMPFRE is compared to the analytic solution in Figure A.2. At low frequencies, EMPFRE underestimates the energy because of the pulse truncation. At frequencies above 100 MHz, EMPFRE overestimates the energy because of the sampling frequency. The parametric studies deal with the frequency range between 100 KHz and 100 MHz. The sampling rate was chosen to provide accurate results up to 100 MHz. Accuracy beyond 100 MHz would require higher sampling rates.

ELECTRIC FIELDS. HEMPB is a computer code used at the Air Force Weapons Laboratory to model EMP. Lt D. Benzer provided HEMPB output for use as a test case. The burst parameters are provided below.

$$\text{HOB} = 100 \text{ Km} \quad (\text{A.3})$$

$$\text{Gamma Yield} = 0.01 \text{ Ktons} \quad (\text{A.4})$$

$$\text{Target Location: LONGITUDE } 5^{\circ}\text{W} \\ \text{LATITUDE } 50^{\circ}\text{N}$$

$$\text{Burst Location: West of Target}$$

$$\text{Slant Range} = 628 \text{ Km} \quad (\text{A.5})$$

$$\text{Geomagnetic field} = 5.6 \times 10^{-5} \text{ Weber s/m}^2 \quad (\text{A.6})$$

$$\text{Gamma Ray Energy} = 2.5 \text{ MeV} \quad (\text{A.7})$$

$$\text{Alpha} = 5.0 \times 10^5 \text{ second}^{-1} \quad (\text{A.8})$$

$$\text{Beta} = 0.55 \times 10^8 \text{ second}^{-1} \quad (\text{A.9})$$

$$\text{TP} = 3.0 \times 10^{-8} \text{ seconds} \quad (\text{A.10})$$

The peak electric and magnetic fields are computed for 26 ranges along the slant range (Table A.1). Computations start at a range of 257 Km from the burst and step toward the target. Computations end when the Compton current's effect on the EMP become small. The electric field is then calculated at the target allowing for  $1/r$  attenuation.

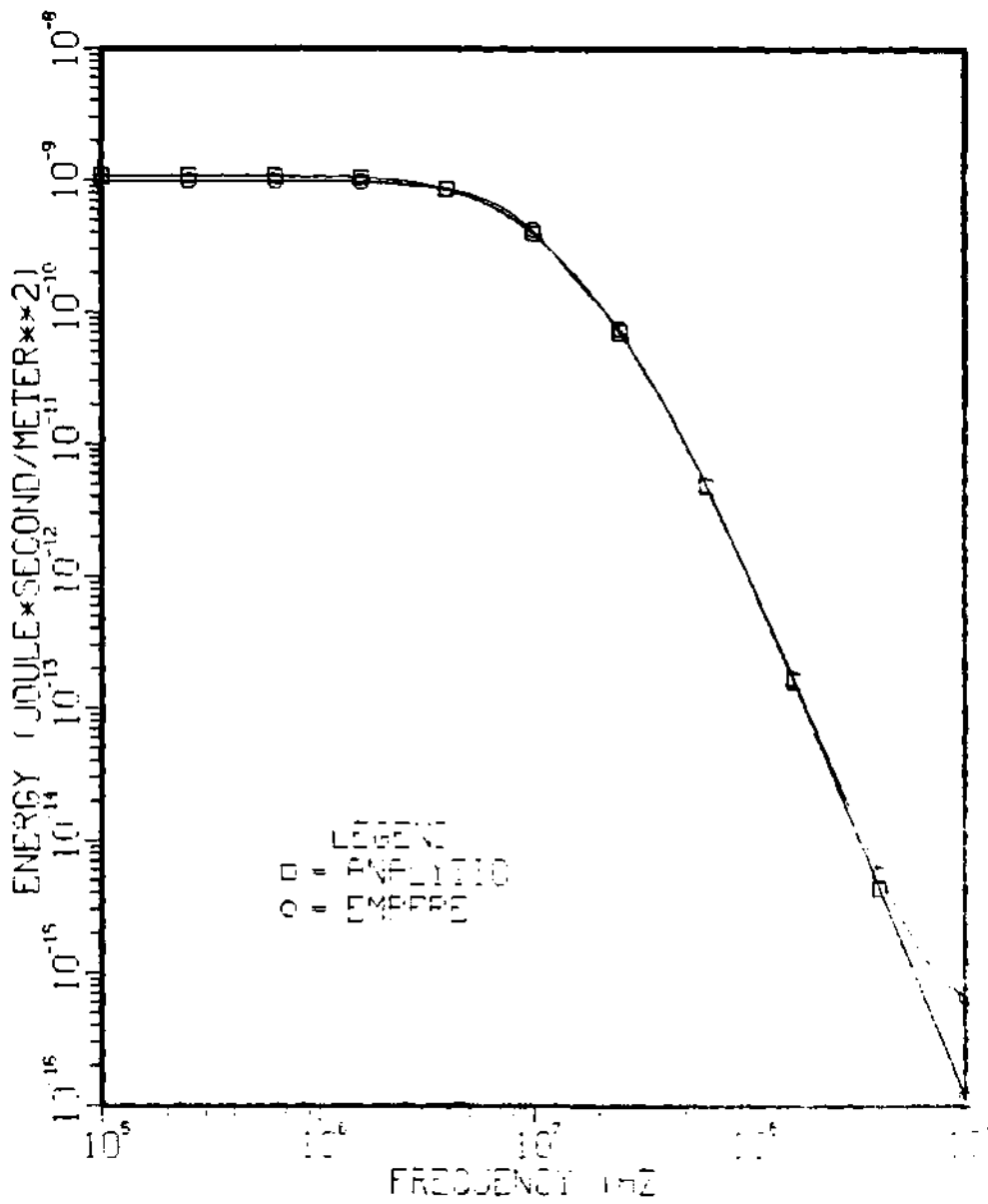


Figure A.2 Frequency Profile, Verification



The burst parameters for EMPFRE were generated to match the test scenario. Figures 3.2 and 3.3 are used to find the declination and dip angle of the geomagnetic field.

$$\text{Declination} = 15^\circ \text{ West} \quad (\text{A.11})$$

$$\text{Dip Angle} = 70^\circ \text{ North} \quad (\text{A.12})$$

$$X = (628 \text{ Km}) \cdot \text{COS}(15^\circ) = 6.06\text{E5 meters} \quad (\text{A.13})$$

$$Y = (628 \text{ Km}) \cdot \text{SIN}(15^\circ) = 1.63\text{E5 meters} \quad (\text{A.14})$$

$$Z = 1.0 \times 10^5 \text{ meters} \quad (\text{A.15})$$

$$\text{Beta} = 5.55 \times 10^8 \text{ seconds}^{-1} \quad (\text{A.16})$$

Other parameters follow directly from above.

The peak electric field predicted by EMPFRE is 285 volts/meter. The prediction from HEMPB is 198 volts/meter. The most likely cause for the error is due to the flat earth approximation and its effect on the atmosphere profile along the slant range. This source of error will have no impact on the results of the parametric studies because the targets are at ground zero.

	ALT(Km)	RANGE(Km)	E-MAX(V/M)
1	60.000	256.80	0
2	57.910	272.26	70.744
3	55.857	287.73	102.61
4	53.841	303.19	135.70
5	51.851	318.66	170.13
6	49.917	334.13	209.13
7	48.011	349.59	250.58
8	46.142	365.06	294.02
9	44.309	380.53	338.72
10	42.512	395.99	383.57
11	40.752	411.46	419.32
12	39.030	426.92	444.98
13	37.344	442.39	460.45
14	35.695	457.86	467.27
15	34.083	473.32	464.87
16	32.508	488.79	455.48
17	30.970	504.25	442.72
18	29.469	519.72	429.48
19	28.005	535.19	-----
20	26.578	550.65	-----
21	25.188	566.12	-----
	0	627.98	198.45

Table A.1 Maximum Electric Fields From HEMPB

## APPENDIX B

### PROGRAM DESCRIPTION AND LISTING

EMPFRE calculates the gamma ray induced EMP from a high altitude nuclear detonation. The program is written in FORTRAN IV. A listing of EMPFRE is provided along with comments to identify key variables and procedures. A detailed explanation of the methods employed is provided in Chapter III. Parameter variations are made by editing the code. The results are written to a tape. Another program accesses the tapes and generates a plot using DISSPLA8. EMPFRE generates the electric field and continuous Fourier transform for one scenario. Execution time on the CYBER-750 is roughly 5 seconds per electric field evaluation made.

Key flow diagrams are given in Figures B.1 and B.2.

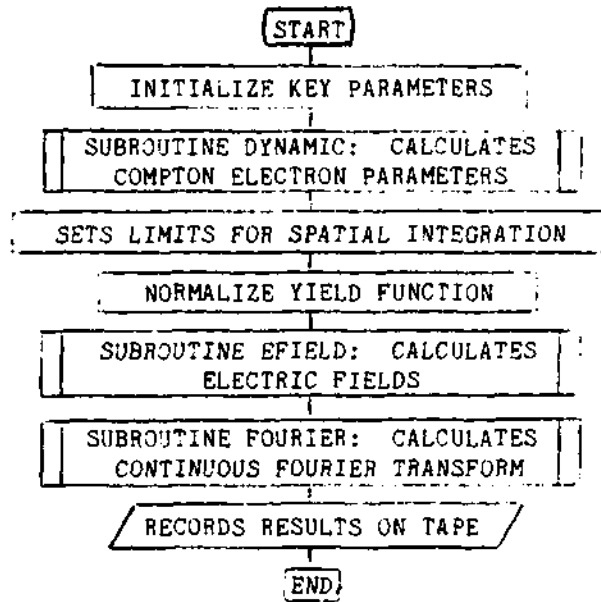


FIGURE B.1 Flow Diagram For Program EMPFRE

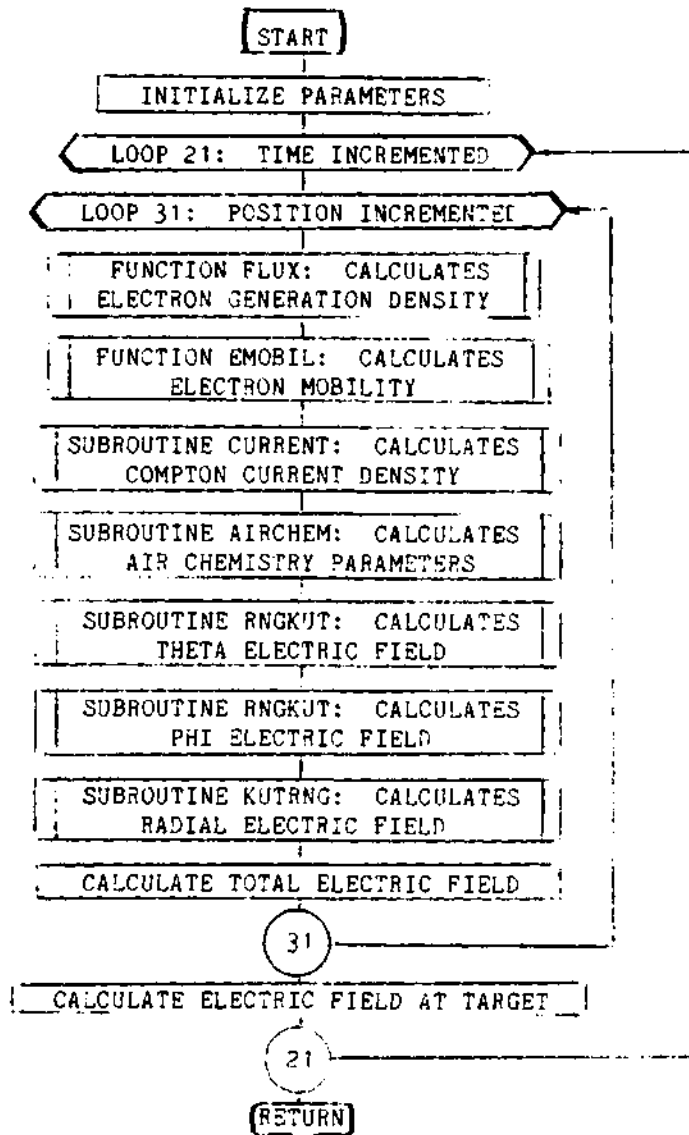


FIGURE B.2 Flow Diagram For Subroutine EFIELD

100 PROGRAM F001E9 (COMP1-DUPEUL,P1 FILE 0, IAH 16)  
 110 COMMON /AA/DEL TMS,DEL T  
 120 COMMON /BB/LOSA,SIN1,COS1,HOB  
 130 COMMON /BB/NUMBER  
 140 COMMON /EE/VELD,YINTEG  
 150 COMMON /EE/KMAX,NDEL,C,NDEL,R,Z,ZKMAX,ERMIN  
 150 COMMON /EE/RANGE  
 170 REAL I(100),TIME(100),HUMID,OMEGA,HOB,OMEGA,ENERGY(61)  
 180 REAL GAM(100),FIB(100)  
 190 INTEGER IIAK(100)  
 200 CALL COMPG3  
 210 C

220 C X,Y,Z IS THE TARGET LOCATION IN METERS

230 C FOR THE NORTHERN HEMISPHERE

240 C X IS MAGNETIC WEST

250 C Y IS MAGNETIC SOUTH

260 C Z IS ALTITUDE

270 C HOB IS HEIGHT OF BURST IN METERS

280 C X=0.0

290 C Y=0.0

300 C Z=0.0

310 C HOB=100000

320 C

330 C MAGNITUDE OF GEOMAGNETIC FIELD IN WEBER/ME<sup>2</sup> IS

340 C REFLD=5.5E-5

350 C

360 C DIP ANGLE OF THE GEOMAGNETIC FIELD

370 C RANGLE=0.0

380 C

390 C SIZE OF TIME STEP

400 C DELT=5E-10

```

410=C
420=C
430=C
440=C
450=C
460=C
470=C
480=C
490=C
500=C
510=C
520=C
530=C
540=C
550=C
560=C
570=C
580=C
590=C
600=C
610=C
620=C
630=C
640=C
650=C
660=C
670=C
680=C
690=C
700=C
710=C
720=C
730=C
740=C

NUMBER OF SPACIAL STEPS BETWEEN RMIN AND RMAX
NDEL R=50

GAMMA RAY ENERGY
EGAM=1.5

GAMMA RAY YIELD (KILOTONS)
YIELD=0.01

NUMBER OF TIME STEPS
NDEL T=80

INTEGRATION LIMITS FOR YIELD INTEGRAL
PULMID=1E-7

FRACTION OF WATER VAPOR IN ABSORPTION REGION
HUMID=0.0001

UNIT CONVERSIONS
YIELD =.616E25*YIELD/EGAM
RANGLE=0.01/45.3295**RANGLE

SUBROUTINE TO DETERMINE PARAMETERS FOR COMPTON DYNAMICS
CALL DYNAMIC(U,GAM,REFIELD)

BURST GEOMETRY CALCULATIONS
RANGE=SQRT((X*Y)**2+(HOR Z)**2)
A=ACOS((HOR-Z)/RANGE)
THE TA=ACOS(COS(RANGLE)*Y/RANGE+PSIN(RANGLE))*(Z-HOR)/RANGE)

CONSTANTS ARE COMPUTED HERE TO SAVE RUN TIME
LATEL IN THE LOOPS COMPUTING THE T-FIELD
COST=COS(THETA)

```

```

750= SIN(COS(DELTA))
760= COS(COS(A))
770=C
780=C
790=
800=
810=
820=
830=
840=
850=
860=
870=
880=
890=
900=
910=
920=
930=C
940=C
950=
960=
970=
980=
990=
1000= 2221
1010=
1020=C
1030=C
1040=
1050=C
1060=C
1070=
1080=C

SINE=COS(DELTA)
COS=COS(A)

      DETERMINE RMIN AND RMAX
ZRMIN=4.E4
IF(HOB,LI,ZRMIN) ZRMIN=HOB
IA=(ZRMIN-HOB)/(Z-HOB)
XRMIN=IA**X
YRMIN=IA**Y
RMIN=SQRT(XRMIN**2+YRMIN**2+(ZRMIN-HOB)**2)
ZRMAX=Z
IF(7,LI,2.E4) ZRMAX=2.E4
IF(HOB,LI,4E4) ZRMAX=Z
TR=(ZRMAX-HOB)/(Z-HOB)
XRMAX=TR**X
YRMAX=TR**Y
RMAX=SQRT(XRMAX**2+YRMAX**2+(ZRMAX-HOB)**2)
DELTA=-(RMAX-RMIN)/NOFLK

NORMALIZE YIELD FUNCTION
T=0.0 $ YIN=0.0 $ YINTEG=1.0
LL=PI*WIB/DELT*10
DO 2221 I=1,II
  T=I*DELT*0.1
  YIN=YIN+GAMYIUC(I)
CONTINUE
YINTEG=YIN/DELT*10

1020=C
1030=C
1040=
1050=C
1060=C
1070=
1080=C

SUBROUTINE TO CALCULATE ELECTRIC FIELDS
CALL FFIELD(F,TIME)

SUBROUTINE TO CALCULATE FOURIER TRANSFORM OF F-FIELD
CALL FOURFRCE,OMEGA,ENERGY)

```



```

1090=C FREQUENCY COORDINATES ARE GENERATED FOR PLOTTING
1100=C DD J I=1,41
1110=C XX (149)
1120=C FRE(I)=10**(XX/10)
1130=C CONTINUE
1140=C RESULTS ARE RECORDED ON TAPE16
1150=C I=0
1160=C DO 9 I=1,NDEL1
1170=C I=I+DEL1
1180=C TIME(I)=I/1E-8
1190=C WRITE(16,45)TIME(I),F(I),FRE(I),ENERGY(I)
1200=C CONTINUE
1210=C 9
1220=C 45
1230=C FORMAT(1F4E17.8)
1240=C PLOTTING WITH DISPLA8
1250=C CALL OPENPL1
1260=C CALL MKKPL1(I)
1270=C CALL XLABEL('FREQUENCY(HZ)',100)
1280=C CALL YLABEL('ENERGY (JOULE*SECOND/METER^2)',100)
1290=C CALL LOGPL1(FRQ,ENERGY,41)
1300=C CALL FRAM1
1310=C CALL LINES('0.05 SHAKES',1)PAK,1)
1320=C CALL LEGEND(IPAK,1,0.2,0.1)
1330=C CALL ENDF1(I)
1340=C CALL PONEFL
1350=C STOP
1360=C ENB
1370=C SUBROUTINE USED TO DRIVE FIELD CALCULATIONS
1380=C SUBROUTINE EFFLDCE,TIME)
1390=C REAT I(100),TIME(100),FR(100),ERNW(100),DIRK(100),OSIG(100)
1400=C
1410=C

```

```

1420= REAL JTB(1A),JBT(1B),JB,NF(100),NF(100),NN(100),ET(100),MU,GG
1430= REAL OLDS(100)
1440= COMMON /AA/DEL T AR,DEL T
1450= COMMON /BB/CDXA,SINT,COST,HOB
1460= COMMON /C1/RMAX,NDEL T,NDEL R,Z,ZRMAX,RMIN
1470= COMMON /HH/NE,NF,NN
1480= COMMON /JJ/RANGE
1490=C
1500=C
1510= DO 16 J=1,NDEL T
1520= E(J)=0.0
1530= 16
1540= DO 61 J=1,NDEL R
1550= E(J)=0.0 $ ERNW(J)=0.0
1560= ET(J)=0.0 $ OLEJR(J)=0.0 $ OSIG(J)=0.0 $ OLDS(J)=0.0
1570= NF(J)=0.0 $ NF(J)=0.0 $ NN(J)=0.0
1580= 61
1590=C
1600=C
1610=C
1620=C
1630= DO 21 I=1,NDEL T
1640= R=RMIN $ OLDSIG=0.0
1650= ETHENW=0.0 $ EPHINW=0.0
1660= OLEJPH=0.0 $ OLEJTB=0.0
1670= TIME(I)=I*DEL T
1680= DO 31 K=1,NDEL R
1690= R=R+DEL T AR
1700=C
1710=C
1720= GG=FLUX(R)
1730=C
1740=C
1750=

```

INITIALIZE ARRAYS AND CONSTANTS

START INTEGRATIONS  
 OUTSIDE LOOP IS FOR CALCULATION IN RETARDED TIME  
 INSIDE LOOP IS FOR INTEGRATION IN R AT EACH TIME STEP

COMPTON ELECTRON GENERATION DENSITY

ELECTRON MOBILITY  
 MU=EMOBIL(R,ET(K))

```

1760=C
1770=C
1780=
1790=C
1800=C
1810=C
1820=
1830=
1840=
1850=C
1860=C
1870=
1880=
1890=
1900=C
1910=C
1920=
1930=
1940=
1950=C
1960=C
1970=
1980=
1990=
2000=C
2010=C
2020=
2030= 31
2040=C
2050=C
2060=
2070=
2080= 21
2090=

SUBROUTINE TO CALCULATE COMPTON CURRENT DENSITY
CALL CURRENT(JTHETA, JPHI, JR, S, TIME(I), R, GG)

SUBROUTINE TO CALCULATE AIR CHEMISTRY PARAMETERS
AND CONDUCTIVITY
CALL AIRCHEM(K, R, TIME(I), S, MU, SIGMA, OLDS(K))
OLDS(K)=S
ETHE=ETHENW

SUBROUTINE PERFORMS RUNGE-KUTTA METHOD WITH THETA E-FIELD
CALL RKGKUT(ETHENW, ETHE, R, SIGMA, JTHETA, OLDJTH, OLDSIG)
OLDJTH=JTHETA
EPHI=EPHINW

SUBROUTINE PERFORMS RUNGE-KUTTA METHOD WITH PHI E-FIELD
CALL RKGKUT(EPHINW, EPHI, R, SIGMA, JPHI, OLDJPH, OLDSIG)
OLDJPH=JPHI
ER(K)=ERNW(K)

SUBROUTINE PERFORMS RUNGE-KUTTA METHOD WITH RADIAL E-FIELD
CALL KUTRNG(ERNW(K), ER(K), SIGMA, JR, OLDJR(K), OSIG(K))
OLDJR(K)=JR
OSIG(K)=SIGMA $ OLDSIU=SIGMA

TOTAL E-FIELD IS CALCULATED FOR ELECTRON MOBILITY
ET(N)=SQRT(ETHENW**2+EPHINW**2+ERNW(K)**2)
CONTINUE

FIND MAGNITUDE OF EFIELD AT TARGET
E(I)=SQRT(ETHENW**2+EPHINW**2)*RMAX/RANGE
IF(Z.EQ.ZRMAX) E(I)=SQRT(ETHENW**2+EPHINW**2+ERNW(K)**2)
CONTINUE
RETURN $ END

```

```

2100=C
2110=C
2120=C
2130=C
2140=C
2150=C
2160=C
2170=C
2180=C
2190=C
2200=C
2210=C
2220=C
2230=C
2240=C
2250=C
2260=C
2270=C
2280=C
2290=C
2300=C
2310=C
2320=C
2330=C
2340=C
2350=C
2360=C
2370=C
2380=C
2390=C
2400=C
2410=C
2420=C
2430=C

FUNCTION CALCULATES THE COMPTON ELECTRON GENERATION
DENSITY ASSUMING AN EXPONENTIAL ATMOSPHERE
REAL FUNCTION FLUX(R)
COMMON /BB/COSA,SINT,COST,HOR
COMMON /MM/COMMF,ARSMFF,COPH,COTH
REAL HOR
SOLVE=7E3/COSA/ABSMFF*(-1.+EXP(R*COSA/7E3))*EXP(-HOR/7E3)
DENOM=12.56637#R#R*COMMF*EXP((HOR-R*COSA)/7E3)
FLUX=EXP(-SOLVE)/DENOM
RETURN $ END

SUBROUTINE CALCULATES THE COMPTON ELECTRON TIME OF FLIGHT
ASSUMING A CONSTANT VELOCITY
REAL FUNCTION CLIFE(R)
COMMON /BR/COSA,SINT,COST,HOR
COMMON /CC/O,ERANGE,VZERO,VC,OMEGA
REAL HOR,OMEGA

COMPTON ELECTRON RANGE DIVIDED BY INITIAL VELOCITY
A=ERANGE*EXP((HOR-R*COSA)/7000.)/VZERO
CLIFE=A
RETURN $ END

SUBROUTINE EXECUTES THE RUNGE KUTTA METHOD
FOR THE TRANSVERSE E-FIELDS
SUBROUTINE RINGKUT(E1,E,R,SN,CN,C0,SD)
COMMON /AA/DELTA1,DEL1
REAL NJ,NS,K1,K2,K3,K4

U IS THE PERMEABILITY OF VACUUM TIMES THE SPEED OF LIGHT
D=DELTA1 $ U=375.73
N=1

```

2440=C DO LOOP PERFORMS THE STEP REDUCTION WHEN INSTABILITY  
2450=C IS FORECASTED

2460= 1 DO 2 K=1,N  
2470= S=K-1

2480=C STEP PARAMETERS ARE REDEFINED WHEN THE STEP SIZE  
2490=C IS REDUCED--ASSUMES LINEAR FUNCTION FOR PARAMETERS

2500=C OS=S0+(SN-S0)\*S/N

2510= NS=S0+(SN-S0)\*K/N

2520= R1=R-D+S\*D/N

2530= R2=R-D+(S+0.5)\*D/N

2540= R3=R-D+K\*D/N

2550= OJ=CO+(CN-CD)\*S/N

2560= NJ=CO+(CN-CD)\*K/N

2570=C

2580=C

2590=C

2600=C

2610=C

2620=C

2630=C

2640=C

2650=C

2660=C

2670=C

2680=C

2690=C

2700= 2

2710=

2720= 3

2730=

2740=C

2750=C

2760= 4

2770=

ESTIMATES OF THE CHANGE IN E-FIELD

K1=-D/N\*((1/R1+U\*DS/2)\*E+U\*DJ/2)

K2=-D/N\*((1/R2+U\*(OS+NS)/4)\*(E+K1/2)+U\*(OJ+NJ)/4)

K3=-D/N\*((1/R3+U\*(OS+NS)/4)\*(E+K2/2)+U\*(OJ+NJ)/4)

K4=-D/N\*((1/R3+U\*NS/2)\*(E+K3)+U\*NJ/2)

CHECKS FOR INSTABILITY

IF (K1\*\*2+K2\*\*2.LT.100) GO TO 2

IF (K1\*\*2.GT.2\*\*K2\*\*2) GO TO 3

IF (K2\*\*2.GT.2\*\*K1\*\*2) GO TO 3

IF (K1\*\*K4.LT.0.0) GO TO 3

CONTINUE

GO TO 4

N=N\*K2

GO TO 1

NEW E-FIELD

E1=E+(K1+2\*(K2+K3)+K4)/6

RETURN \$ END

```

2780=C SUBROUTINE EXECUTES THE RUNGE-KUTTA METHOD
2790=C FOR THE RADIAL E-FIELD
2800=C SURROUTINE KUTRNG(E1,E,SN,CN,CO,SO)
2810=C COMMON /AA/DELTA,DELT
2820=C REAL NJ,NS,K1,K2,K3,K4
2830=C
2840=C U IS THE PERMITTIVITY OF VACUUM
2850=C D=DELT * U=8.854E-12
2860=C N=1
2870=C
2880=C DO LOOP PERFORMS THE STEP REDUCTION WHEN INSTABILITY
2890=C IS FORECASTED
2900=C DO 2 K=1,N
2910=C 1
2920=C S=K-1
2930=C
2940=C STEP PARAMETERS ARE REDEFINED WHEN THE STEP SIZE
2950=C IS REDUCED---ASSUMES LINEAR FUNCTION FOR PARAMETERS
2960=C OS=SO+(SN-SO)*S/N
2970=C NS=SO+(SN-SO)*K/N
2980=C OJ=CO+(CN-CO)*S/N
2990=C NJ=CO+(CN-CO)*K/N
3000=C
3010=C ESTIMATES OF THE CHANGE IN I FIELD
3020=C K1= D/N*(OJ+OS*E)/U
3030=C K2=-D/N*((OJ+NJ)/2+(OS+NS)/2*(E+K1/2))/U
3040=C K3=-D/N*((OJ+NJ)/2+(OS+NS)/2*(E+K2/2))/U
3050=C K4=-D/N*(NJ+NS*(E+K3))/U
3060=C
3070=C CHECKS FOR INSTABILITY
3080=C IF(K1**2+K2**2.LT.100) GO TO 2
3090=C IF(K1**2.GT.2**K2**2) GO TO 3
3100=C IF(K2**2.GT.2**K1**2) GO TO 3
3110=C IF(K1**K4.LI.0.0) GO TO 3

```

```

3120= 2      CONTINUE
3130=       GO TO 4
3140= 3      N=NX2
3150=       GO TO 1
3160=C      NEW E-FIELD
3170=C      E1=E1(K1+2*(K2+K3)+K4)/6
3180= 4      RETURN $ END
3190=
3200=C
3210=C      SUBROUTINE CALCULATES THE COMPTON CURRENTS AND
3220=C      SECONDARY ELECTRON PRODUCTION RATE DENSITY
3230=C      SUBROUTINE CURRENT(JTH,JPH,JR,S,I,R,GG)
3240=C      COMMON /AA/DELTA,DELTA
3250=C      COMMON /RR/COSA,SINI,COSI,HOB
3260=C      COMMON /CC/R,ERANGE,VZERO,VC,OMEGA
3270=C      COMMON /MM/COMMP,ABSMFP,COPH,COTH
3280=C      REAL JR,JPH,JTH,I,OMEGA,GG,GAMYLID
3290=C      INTEGER STEP
3300=C      JR=0.0 $ JTH=0.0 $ JPH=0.0 $ S=0.0
3310=C      I=DELT/10
3320=C      CONST=1.6E-19*VZERO*GG*COth
3330=C      N=10*CLIFF(R)/DELTA
3340=C
3350=C      NUMERICAL INTEGRATION OF THE INTEGRALS
3360=C      DEVELOPED BY KARZAS AND LATTER
3370=C      DO 97 STFF=1,N
3380=C      TM=I-(I-VC*CONST**2)*STEP*I*VC*SINI**2*SIN(OMEGA*STEP*L)/OME
3390=
3400=
3410=C
3420=C      COMPTON CURRENT DENSITIES
3430=C      JR=JR*CONST**2*(COSI**2+SINI**2)*COS(OMEGA*STEP*L)*DELT**2
3440=C      JTH=JTH*CONST**2*(SINI*COSt*(SINI*COSt*(COS(OMEGA*STEP*L)-1))*DELT**2

```

HA

```

3450= JPH=JPH CONSTY*SNIN*(OMGASSTI*1)*HIT*(X,1
3460=C
3470=C
3480= S=SQ*ZERO/(CRANGE*EXP((HOB-R*COSA)/7000))*GG*Y*DELT*.1
3490= CONTINUE
3500= RETURN $ END
3510=C
3520=C
3530=C
3540= SUBROUTINE AIRCHEM(K,R,1,SNEM,MU,SIG,SOLID)
3550= INTEGER STEP
3560= REAL NE(100),NF(100),NN(100),K1,K2,K3,MU
3570= COMMON /AA/DELTAR,DELT
3580= COMMON /BB/COSA,SINT,COST,HOB
3590= COMMON /HH/NE,NF,NN
3600=C
3610=C
3620= RATE CONSTANTS
3630= K1=10*EXP(2*(R*COSA-HOB)/7000)
3640= K2=2E 13
3650= K3=1*EXP((R*COSA-HOB)/7000)
3660= DT=1011/100
3670=C
3680=C
3690=C
3700= S=SOLID*(SNEM-SOLID)*STEP/100
3710=C
3720=C
3730= NE(K)=NE(K)+S*K1*NE(K)-K2*NE(K)*NF(K))*DT
3740=C
3750=C
3760= NF(K)=NF(K)+S*K1*NE(K)*NF(K)-K3*NF(K)*NN(K))*DT
3770=C
3780=C
NEGATIVE ION DENSITY

```

SECONDARY ELECTRON SOURCE IS ASSUMED TO BE A LINEAR

FUNCTION FOR INTERMEDIATE STEPS

S=SOLID\*(SNEM-SOLID)\*STEP/100

SECONDARY ELECTRON DENSITY

NE(K)=NE(K)+S\*K1\*NE(K)-K2\*NE(K)\*NF(K))\*DT

POSITIVE ION DENSITY

NF(K)=NF(K)+S\*K1\*NE(K)\*NF(K)-K3\*NF(K)\*NN(K))\*DT

NEGATIVE ION DENSITY



```

3790= NN(K)-NN(K)+(K*ANE(K)-K.3*NF(K)*NN(K))*TI
3800=C
3810=C
3820= IF(NN(K).LT.0)NN(K)=0.0
3830= 23
3840=C
3850=C
3860= SIG=(NF(K)*MID(NN(K)+NF(K))*2.5E-4*EXP((HDB-R*COSA)/7000))*
1.6E-19
3870= RETURN $ END
3880=C
3890=C
3900=C
3910= FUNCTION CALCULATES THE ELECTRON MOBILITY
3920= METHOD IS OUTLINED IN SECTION 3.12
3930= REAL K,F,MUA,HUMID
3940= COMMON /DB/HUMID
3950= F=100*HUMID $ A=2.457 $ B=0.6884 $ C=1.195
3960= K=P**0.934
3970= FS=EXP((HDB-R*COSA)/7000)/6000 $ LS1=0.0/85.6*(110*K)
3980= FS2=3.015+DK
3990= IF(ES.GT.E51) GO TO 1
4000= ES0=ES/(1+A*K) $ GO TO 3
4010= 1
4020= IF(ES.GT.E52) GO TO 2
4030= 2
4040= 3
4050= ES0=(SQRT((B*K/2)**2+ES) R**2)**2 $ GO TO 3
4060= ES0=ES-D*K
4070=C
4080=C
4090= X=((16.8+ES0)/(1.63+36.7*ES0))**.5
4100= MUA=1E6/EXP((R*COSA-HDB)/7000)**X
4110=C
4120= RR=1.55+210/(1111.8*ES0+7.2*ES0**2)
4130=C
4140=C
4150= ELECTRON MOBILITY
4160= EMOBIL=MUA/(1-HUMID+HUMID*RR)/5.002E6
4170= RETURN $ END

```

```

4120=C      FUNCTION DEFINES THE GAMMA OUTPUT HISTORY OF THE BURST
4130=C      FUNCTION GAMYLD(T)
4140=C      COMMON /FE/YIELD, YINTEG
4150=C      GAMYLD=0.0
4160=C      IF (T.LF.O)GO TO 19
4170=C
4180=C      AL--RISE PARAMETER
4190=C      (RE-AL)--DECAY PARAMETER
4200=C      TIME OF PFAK
4210=C      AL=1E9 $ BE=1.5E9 $ TP=1E-8
4220=C      Y=EXP(AL*T)/(1+EXP(RE*(T-TP)))
4230=C
4240=C      YINTEG--NORMALIZATION FACTOR TO MAKE THE INTEGRAL EQUAL
4250=C      TO THE SPECIFIED YIELD
4260=C      GAMYLD=Y*YINTEG
4270=C      RETURN $ END
4280=C
4290=C      SUBROUTINE CALCULATES COMPTON REACTION PARAMETERS
4300=C      BASED ON THE GAMMA RAY ENERGY
4310=C      SUBROUTINE DYNAMIC (EGAM,BFIELD)
4320=C      COMMON /CC/Q,FRANGE,VZERO,VC,OMEGA
4330=C      COMMON /MM/COMMF,ABSMFP,COPH,CDTH
4340=C      IF (EGAM.GT.0.5)GO TO 1
4350=C
4360=C      COSINE OF GAMMA RAY REFLECTION ANGLE
4370=C      COPH=COS(.7854-(ALOG(EGAM)+1.609)*0.095277)
4380=C
4390=C      MEAN FREE PATH DUE TO COMPTON INTERACTION ALONE
4400=C      COMMF=1/(.0035+(ALOG(EGAM)+1.609)/3271)
4410=C
4420=C      MEAN FREE PATH DUE TO ALL INTERACTIONS
4430=C      ABSMFP=COMMF
4440=C
4450=C      COSINE OF COMPTON ELECTRON DEFLECTION ANGLE

```

```

4460= COTH COS(1.2488-(ALOG(EGAM)+1.6094)*0.18)
4470= GO TO 3
4480= 1 COPH=COS(0.6931-0.2097*(ALOG(EGAM)+0.6931))
4490= IF(EGAM.GT.1.5)GO TO 2
4500= COMMF=1/(0.00375-(ALOG(EGAM)+0.6931)/1927)
4510= ABSMFF=COMMF
4520= COTH=COS(1.0838-(ALOG(EGAM)+0.6931)*0.1422)
4530= GO TO 3
4540= 2 COMMF=1/(0.00333+(0.4055-ALOG(EGAM))/983)
4550= ABSMFF=1/(0.00333+(0.4055-ALOG(EGAM))/1423)
4560= COTH=COS(0.9163+(0.4055-ALOG(EGAM))*0.1371)
4570= 3 IF(EGAM.GT.4)GO TO 4
4580=C
4590=C
4600=C
4610= 4 ENERGY=EGAM*(0.695+(ALOG(EGAM)-1.386)/9.163)
4620= 4 VC=SQRT(1.0-(0.510976/(ENERGY+0.510976)))**2)
4630= 5
4640=C
4650=C
4660=C
4670=C
4680=C
N
4690= 0=ENERGY*1E6/34.
4700=C
4710=C
4720= CYCLOTRON FREQUENCY
4730=C OMEGA=1.602E-19*HFIELD*SQRT(1.0 VC**2)/9.108E-31
4740=C COMPTON ELECTRON RANGE
4750= IF(ENERGY.LT.2.5) ERANGE=3.19*ENERGY**(1.265-.0954*ALOG(ENERGY))
4760= IF(ENERGY.GE.2.5) ERANGE=4.10*ENERGY-0.82
4770= RETURN $ END

```

```

4780=C SUBROUTINE PERFORMS A FOURIER TRANSFORM ON THE EMP
4790=C TO DETERMINE THE SPECTRAL CHARACTERISTICS
4800=C SUBROUTINE FOURIER(E,OMEGAT,ENERGY)
4810=C REAL ENERGY(61),E(100),TIME(100)
4820=C COMMON /AA/DELTA,DELT
4830=C COMMON /FF/RMAX,NBELT,NDELR,Z,ZRMAX,RMIN
4840=C
4850=C SINE FUNCTION IS MERGED TO THE TRUNCATED PULSE
4860=C TO REDUCE THE IMPACT ON THE ENERGY SPECTRUM
4870=C A=E(NBELT)
4880=C
4890=C ANGULAR FREQUENCY OF SINE FUNCTION IS CHOSEN TO MATCH
4900=C THE SLOPE OF THE EMP
4910=C OMEGAT=(E(NBELT-1)-E(NBELT))/DELT/A
4920=C N*NBELT/13.1415926/OMEGAT/DELT/2
4930=C
4940=C 41 FREQUENCIES ARE SAMPLED
4950=C DO 11 K=50,90
4960=C X=K
4970=C XOMEGA=6.28319*10.0**(X/10.0)
4980=C SI=0.0 $ CO=0.0
4990=C
5000=C INTEGRATION TO FIND ENERGY DENSITY
5010=C DO 9 M=1,M
5020=C IF (M.LE.NBELT)DE=F(M)
5030=C IF (M.GT.NBELT)DE=A*(1-SIN(OMEGAT*DELT)*M*(M-NBELT))
5040=C SI=SI+DE*5IN(XOMEGA*DELT*M)*DELT/2.50663
5050=C CO=CO+DE*COS(XOMEGA*DELT*M)*DELT/2.50663
5060=C 9 CONTINUE
5070=C
5080=C ENERGY DENSITY
5090=C ENERGY(K-49)=(SI**2+CO**2)/376.75
5100=C 11 CONTINUE
5110=C RETURN $ END

```

VITA

Randy J. Lavigne was born [REDACTED] [REDACTED] [REDACTED] [REDACTED],  
[REDACTED] [REDACTED] [REDACTED] [REDACTED] [REDACTED] [REDACTED] [REDACTED] in 1975.  
He received a Bachelor of Science degree in Nuclear Engineering from  
University of Lowell in 1979. In May 1979, he was commissioned in the  
United States Air Force through the ROTC program. In July 1979, he  
entered active duty as a project officer for advanced plans at Space  
Division in the Defense Meteorological Satellite Program SPO. In August  
1982, he entered the Air Force Institute of Technology.

Permanent Address: [REDACTED]  
[REDACTED] [REDACTED]  
[REDACTED]

UNCLASSIFIED

SECURITY CLASSIFICATION OF THIS PAGE

REPORT DOCUMENTATION PAGE

1a. REPORT SECURITY CLASSIFICATION <b>UNCLASSIFIED</b>			1d. RESTRICTIVE MARKINGS			
2a. SECURITY CLASSIFICATION AUTHORITY			3. DISTRIBUTION/AVAILABILITY OF REPORT Approved for public release; distribution unlimited.			
2b. DECLASSIFICATION/DOWNGRADING SCHEDULE			5. MONITORING ORGANIZATION REPORT NUMBER(S)			
4. PERFORMING ORGANIZATION REPORT NUMBER(S) AFIT/GNE/PH/84M-10			7a. NAME OF MONITORING ORGANIZATION			
6a. NAME OF PERFORMING ORGANIZATION School of Engineering		6b. OFFICE SYMBOL (if applicable) AFIT/EN		7b. ADDRESS (City, State and ZIP Code)		
6c. ADDRESS (City, State and ZIP Code) Air Force Institute of Technology Wright-Patterson AFB, Ohio 45433			9. PROCUREMENT INSTRUMENT IDENTIFICATION NUMBER			
8a. NAME OF FUNDING/SPONSORING ORGANIZATION		8b. OFFICE SYMBOL (if applicable)		10. SOURCE OF FUNDING NOS.		
8c. ADDRESS (City, State and ZIP Code)		PROGRAM ELEMENT NO.	PROJECT NO.	TASK NO.	WORK UNIT NO.	
11. TITLE (Include Security Classification) See Box 19			12. PERSONAL AUTHOR(S) Randy J. Lavigne, B.S., Lt. USAF			
13a. TYPE OF REPORT MS Thesis		13b. TIME COVERED FROM _____ TO _____		14. DATE OF REPORT (Yr., Mo., Day) 1984 March		15. PAGE COUNT 141
16. SUPPLEMENTARY NOTATION						
17. COSATI CODES			18. SUBJECT TERMS (Continue on reverse if necessary and identify by block number)			
FIELD	GROUP	SUB. GR.	EMP, High Altitude Burst, Frequency Characteristics			
20	14					
19. ABSTRACT (Continue on reverse if necessary and identify by block number)						
Title: A PARAMETRIC STUDY OF HIGH ALTITUDE NUCLEAR EMP			<p>Approved for public release: IAW AFB 150-17.</p> <p><i>[Signature]</i> LYNN E. WOLAVER 8 Aug 84 Dean for Research and Professional Development Air Force Institute of Technology (AFIT) Wright-Patterson AFB OH 45433</p>			
Thesis Chairman: J. H. Erkkila, Lt.Col., USAF						
20. DISTRIBUTION/AVAILABILITY OF ABSTRACT UNCLASSIFIED/UNLIMITED <input checked="" type="checkbox"/> SAME AS RPT. <input type="checkbox"/> DTIC USERS <input type="checkbox"/>			21. ABSTRACT SECURITY CLASSIFICATION UNCLASSIFIED			
22a. NAME OF RESPONSIBLE INDIVIDUAL J. H. Erkkila, Lt.Col., USAF			22b. TELEPHONE NUMBER (include Area Code) 513-255-2012		22c. OFFICE SYMBOL AFIT/ENP	

DD FORM 1473, 83 APR

EDITION OF 1 JAN 73 IS OBSOLETE

UNCLASSIFIED  
SECURITY CLASSIFICATION OF THIS PAGE

UNCLASSIFIED

SECURITY CLASSIFICATION OF THIS PAGE

A program is developed to model the electromagnetic pulse from a high altitude nuclear detonation. A Runge-Kutta numerical technique is used to solve for the electric fields. A continuous Fourier Transform of the EMP is used to determine the frequency profile of the EMP. Parametric studies are performed to determine cause and effect relationships between burst parameters and the EMP frequency profile from 100 KHz to 100 MHz. Burst parameters studied are: gamma pulse time history, gamma ray energies from 1 MeV to 10 MeV, gamma ray yield, height of burst from 75 Km to 200 Km and intersection angle of the slant range with the geomagnetic field from 90 degrees to 30 degrees.

UNCLASSIFIED